X-646-73-111
PREPRINT

VLF-HISS FROM ELECTRONS IN THE EARTH'S MAGNETOSPHERE

KAICHI MAEDA

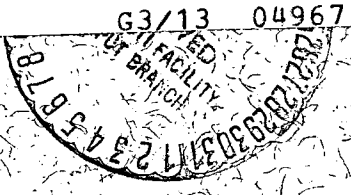

MAY 1973

GODDARD SPACE FLIGHT CENTER
GREENBELT, MARYLAND

VLF-HISS FROM ELECTRONS IN THE EARTH'S MAGNETOSPHERE

By

Kaichi Maeda
NASA-Goddard Space Flight Center
Greenbelt, Md. 20771

April 1973

ABSTRACT

Intensities of auroral and magnetospheric hiss generated by the Cherenkov radiation process of electrons in the lower magnetosphere are calculated with respect to a realistic model of the earth's magnetosphere. In this calculation, the magnetic field is expressed by the "Mead-Fairfield Model" (EOS, 53, 1099, 1972), and a static model of the iono-magnetospheric plasma distribution is constructed by accumulated data obtained by recent satellite observations (Alouette-I, -II, ISIS-I, OGO-4, -6 and Explorer 22). The energy range of hiss producing electrons and the frequency range of produced VLF in the computation are 100 eV to 200 keV, and 2 to 200 kHz, respectively. Intensities with a maximum around 10 kHz, of the order of 10^{-12} watts m^{-2} Hz^{-1} observed at satellite altitudes and of 10^{-14} watts m^{-2} Hz^{-1} at the ground seem to be ascribale to the incoherent Cherenkov emission from soft electrons with a differential energy spectrum E^{-2} having an intensity of the order of 10^{8} cm^{-2} sec^{-1} str^{-1} eV^{-1} at 100 eV. It is shown that the frequency of hiss spectral density peak at geomagnetic latitude 70^{o} night side is around 20 kHz for the soft spectrum ($\sim E^{-2}$) electrons, which shifts to 10 kHz for the hard spectrum ($\sim E^{-1.2}$) electrons. The maximum hiss intensity produced by soft electrons is more than one order higher than that of hard electron produced hiss. Higher rate of hiss occurrence in the daytime side, particularly in the soft electron precipitation zone in the morning sector, and less association of auroral hiss in nighttime sectors must be, therefore, due to the local time dependence of the energy spectra of precipitating electrons rather than the difference in the geomagnetic field and in the geoplasma distributions.

1. INTRODUCTION

Estimations of hiss intensity associated with auroras have been made recently by Lim and Laaspere (1972), in which the contribution of the relatively low energy electrons below 1 KeV is taken into consideration. Their calculation has shown the importance of low energy electrons on auroral hiss generation which has been disregarded in previous theoretical works, mainly due to the lack of observational information of low energy electrons and of reliability of theoretical formula (McKenzie, 1963, 1967; Mansfield, 1964, 1967; Liemohn, 1965; Jørgensen, 1968). Measurements of low energy auroral electrons by means of rockets (Evans, 1968; Ogilvie, 1968; Feldman et al., 1971) and of satellites (Frank and Ackerson, 1972, Hoffman, 1969; Burch, 1968) have provided abundant information. Comparisons of low energy electron spectra observed by satellites and rockets as well as their variations with latitude and time have been shown recently in great detail, indicating the dynamics of these electrons in the earth's magnetosphere (Rees, 1969; Hones et al. 1971). Furthermore, the better correlation of auroral hiss occurrence with precipitations of low energy electrons rather than those of high energy electrons has been shown by the latest analyses of simultaneous satellite observations of auroral VLF-hiss and of electron precipitation events (Hoffman and Laaspere, 1972, Gurnett and Frank, 1972).

On the other hand, the calculation by Lim and Laaspere (1972) is limited for the daytime polar region (78° geomagnetic latitude) where the plasma distribution is derived from the theoretical model of Banks and Holzer (1969) and the magnetic field is assumed to be that of the centered dipole. Obviously the earth's magnetic field differs significantly

from that of the centered dipole particularly near the so-called cusp region where most auroral daytime events including VLF-hiss take place.

Owing to numerous satellite observations, the distribution of plasma, i.e., densities of thermal electrons, protons and ions, in the earth's ionosphere and magnetosphere has been known in fair detail. Since these plasma data are essential for the estimation of hiss-generation and the propagation through these media a more realistic model of the earth's plasma distribution than that used by Lim-Laaspere (1972) is worth constructing, with indications of its variation with latitude, altitude and local time.

The purpose of this paper is, therefore, to recalculate the auroral hiss intensity and intensities of VLF-hiss in the magnetosphere produced from magnetospheric low energy electrons, by making use of a realistic model of the earth's magnetic field and of plasma distributions. The latter is constructed by making use of the accumulated satellite data of electron, proton and ion density distributions obtained by Alouette I, II, ISIS-I, OGO-4 and 5. The geomagnetic field is expressed by the "Mead-Fairfield 1972 model " (EOS, 53, 1097, 1972).

2. FORMULATIONS OF THE CALCULATION

A charged particle moving along its helical trajectory in the tenuous magnetoplasma emits Cherenkov radiation in addition to the synchrotron radiation, if its velocity parallel to the static magnetic field is larger than the local phase velocity of the wave in the plasma. In contrast to

synchrotron radiation which is emitted as a result of decelerating gyromotion of the particle due to the static magnetic field imbedded in the plasma, Cherenkov radiation is emitted from the polarized wake produced in the medium a fast moving electric charge.

The frequency range of the wave associated with these polarized wakes of plasma medium is wide but limited below a certain frequency characterized by the plasma and magnetic field, as shown in the next section. Propagations of these waves in the earth's magnetosphere are very slow, dispersive and mostly along the field line until their frequencies approach another characteristic frequency of the magnetoplasma, called the lower hybrid resonance (LHR) frequency, f_{LH}. Since the propagation of the wave in the magnetoplasma above the LHR is essentially due to the mobility of electrons in the medium, which is far larger than that of ions, the polarization of the wave is the same sense as that of electron-gyration, i.e., right-handed with respect to the direction of the magnetic field. This mode of wave propagation is called the whistler mode (R-mode VLF).

The phase velocity of waves propagating in a magnetoplasma is shown in Figure 1, as a function of wave angular frequency $\omega(=2\pi f)$ for the case when the electron gyrofrequency f_H and the plasma frequency f_N are 10 kHz and 30 kHz, respectively. As can be seen from this figure, phase velocities of waves in the whistler mode are far slower than the light velocity c, and decrease with wave frequency, approaching that of Alfvén waves below the ion-gyrofrequency, Ω_i, of the plasma.

It should be noted that the upper limit of whistler mode frequency is f_H if $f_H < f_N$, in contrast to the case shown in Figure 1.

2.1. The Formula of Cherenkov Radiation in Magnetoplasma

The Cherenkov emission from an electron moving along its helical trajectory in the magnetic field imbedded in a cold, collisionless plasma has been described in many theoretical papers. Although the final expressions are more or less the same, the derivation of the formula of Cherenkov radiation from an incident spiraling electron in plasma is not unique.

Eidman (1958) has applied the so-called Hamiltonian method known in the field theory of quantum electrodynamics (Heither, 1944) for the estimate of emission rate from the polarized anisotropic plasma medium. This is further extended to the relativistic form by Liemohn (1965).

McKenzie (1963, 1967) and Mansfield (1964, 1967) have used classic forms of the solution of Maxwell's equations for the polarized electric field and the current in the anisotropic plasma induced by a spiraling incident electron by means of Fourier transforms. According to Trulsen and Fejer (1970), Eidman's results are more accurate in general than Liemohn's, even though his derivation is based on the non-dispersive medium with non-relativistic formulation.

The present calculation follows essentially the Mansfield method as has been used by Jørgensen (1968) and by Lim-Laaspere (1972). Since Mansfield's notations and definitions of plasma parameters are different from those commonly used in the physics of plasmas and of the ionosphere,

the basic formulae are rewritten in the Appendix B: notations, definitions and constants are listed in Appendix A, which are mostly taken from books by Stix (1962) and by Ratcliffe (1962).

As shown in Appendix B, by (B-50), the intensity of Cherenkov emission per unit time, i.e., the power of Cherenkov radiation, $\bar{P}_o$ (in watt/cm^2) from an electron with kinetic energy, E (in keV) averaged over the spiraling period $\tau_H(=2\pi/\Omega_e)$ is expressed as functions of the radiated wave frequency $f(=\omega/2\pi)$, of the magnetic field intensity, B (in gauss) and of plasma parameters. The plasma parameters are represented by a plasma frequency $f_N(=2\pi/\Pi_o)$ and the magnetic field is expressed by the gyrofrequency of electron, f_H $(=\Omega_e/2\pi)$.

The dependence of $\bar{P}_o$ on τ_H and τ_N is expressed by the inverse dielectric tensor $\mathbf{T}^{-1}(\cos\theta)$ shown by (B-39), where the analytic expressions of S, P and D as functions of τ_H and of τ_N can be seen from (B-13).

Most VLF measurements are made not on the total intensity over the whole observable frequency range but rather on the differential intensity, i.e., on intensities at different frequencies. Therefore, the power per frequency, $d\bar{P}_o/df$ (in watts/Hz el.) is a more useful presentation for the comparison with experimental results. This can be written from (B-52) as follows:

$$\frac{d\bar{P}_o}{df} = \frac{q^2\pi}{\varepsilon_o c} \cdot f \sum_{j=1}^{2} \frac{\beta_\parallel}{\Delta_o} t_{33}(n_j^2) \left[J_o^2(\xi_j) + \left(\frac{\beta_\perp}{\beta_\parallel}\right)^2 J_1^2(\xi_j) \frac{t_{11}(n_j^2)}{t_{33}(n_j^2)} + 2\left(\frac{\beta_\perp}{\beta_\parallel}\right) J_o(\xi_j) J_1(\xi_j) \frac{t_{13}(n_j^2)}{t_{33}(n_j^2)} \right] \tag{2.1}$$

where J_o, J_1 are the Bessel functions of the zero-th and the first order, respectively with the argument

$$\xi_j = \frac{\omega\beta_\perp}{\Omega_e} \gamma\, n_j \sin\theta_o \tag{2.2}$$

The so-called Cherenkov angle θ_o, in (2.2) is given by the following relativistic formula;

$$\cos\theta_o = \frac{1}{\beta_\parallel\, n_j} \tag{2.3}$$

where $\beta_\perp = \beta\cos\alpha, \qquad \beta_\parallel = \beta\sin\alpha$

and

$$\beta = \frac{\sqrt{E(E + 2\, m_e c^2)}}{E + m_e c^2} \tag{2.4}$$

E and $m_e c^2$ are the kinetic energy (in KeV), and the rest mass of electron $m_e c^2 = 510.98$ (in KeV), respectively. α is the pitch angle of helical trajectory of the electron with respect to the static magnetic field direction.

The two values of the refractive index of a plasma medium stand for

$$n_j^2 = \frac{-b_o - (-1)^j \Delta_o}{2S} \tag{2.5}$$

with

$$\Delta_o = \sqrt{b_o^2 - 4S\, c_o} \tag{2.6}$$

$$b_o = \frac{P - S}{\beta_\parallel^{\,2}} + D^2 - S^2 - PS$$

and

$$c_o = \frac{1}{\beta_\parallel^{\,2}} (S^2 - D^2 - PS) + P\ (S^2 - D^2) \tag{2.8}$$

2.2. The Dispersion Relation of Waves in the Plasma

As shown in Figure 1, the propagation velocity of waves in the magnetoplasma changes with the angle (θ) of propagation vector $\mathbb{k}$ of the wave from the direction of magnetic field $\mathbb{B}$. The directional dependence of propagation velocity further changes with wave frequency. These angular and frequency dependences of wave propagation in a plasma can be found by calculating the dispersion relation of the wave in the plasma.

Since the Cherenkov radiation occurs only when the velocity of an impinging electron along the field line, $V_{\parallel}$, is larger than the phase velocity, V_{ph}, of the wave in the plasma, the refractive index n ($=c/V_{ph}$) is one of the essential parameters in the present calculation. The ratio of the critical velocity of the electron, V_c (below which no Cherenkov emission takes place in the plasma) to the velocity of light in vacuum, $\beta_c = V_c/c$, is therefore equal to the inverse of the refractive index of the medium. This can be seen from the Cherenkov condition (B-28) with $\theta=0$. The β-value of the electron is shown in Figure 2 as a function of the kinetic energy of the electron E. The right side scale of ordinates indicates the value of the refractive index n corresponding to the critical value of β_c and the kinetic energy E of the electron. It should be noted that in the energy range below around 100 keV, β is proportional to the square-root of E as can be expressed by the non-relativistic expression of kinetic energy, i.e.

$$E \cong \frac{m_e v^2}{2} \quad (= \frac{m_e c^2}{2} \beta^2)$$

On the other hand, in the energy range above roughly 2 MeV, the velocity of the electron can be regarded as almost the velocity of light in vacuum, where the approximation called "the extreme relativistic, $\beta \simeq 1$." can be used. It is in this energy domain where the Cherenkov radiation has been used for the detection of charged particle in high energy physics (Oostens et. al, 1967; Yuang et al., 1969).

In plasma, however, the propagation of the polarization in the medium, which is the electromagnetic wave propagation in the medium, is so slow that the Cherenkov emission is important rather in the non-relativistic energies than in the extreme relativistic energy domains. As shown in the following sections, the rate of Cherenkov emission in the plasma is larger at lower energies than at higher energies, as long as the velocity of incident electrons is larger than that of plasma electrons. However, if the energy of the incident electron approaches the thermal energy of the medium, the formula of Cherenkov emission based on the cold plasma is no longer correct. The correction is, however, very small as long as the energy of the incident electron is above the thermal energy of the plasma as shown recently by Trulsen and Fejer (1970) and by Trulsen (1971).

The dispersion relation of cold plasma is derived from the determinant of the dielectric tensor of the plasma, i.e.,

$$|\mathbf{T}(\cos\theta)| = 0$$

where $\mathbb{T}(\cos\theta)$ is given by (B-16)*. As can be seen from (B-17) with (B-18), this leads to the fourth order equation of n. Therefore, there are two solutions for the real values of n^2. Using the matrix elements shown in (B-16), the solution of (B-17) can be written in the following

form

$$n^2 = \frac{B \pm F}{2A} \tag{2.9}$$

where

$$F^2 = (RL - PS)\sin^4\theta + 4P^2D^2\cos^2\theta \tag{2.10}$$

A, B, S, P, D, R and L are given by (B-18).

Equation (2.9) presents one of the dispersion relations of the plasma and is shown in Figure 3, by plotting n^2 against ω/Ω_e.

Substitution of (B-18) into (2.9), brings the following form of the dispersion relation

$$tg^2\theta = \frac{-P(n^2-R)\ (n^2-L)}{(Sn^2-RL)\ (n^2-P)} \tag{2.11}$$

From (2.11) we find the following propagating wave modes in the plasma;

(i) Propagation along the magnetic field, by setting $\theta=0$, we get

$$P=0,\ n^2 = R \text{ and } n^2 = L \tag{2.12}$$

---

*Footnote: Since the propagation vector $\mathbb{k}$ is taken in ZY-plane, the matrix elements in $\mathbb{T}(\cos\theta)$ are different from those of Stix (Eq. 20 in p. 11, 1962), in which $\mathbb{k}$ is taken in ZX-plane while the direction $\mathbb{B}$ is the same in Z-axis. Because of the axial symmetry of the plasma characteristics around Z-axis, the dispersion relation (2.9) is the same as that of Stix (Eq. 21 in p. 11, 1962).

(ii) Propagation across the magnetic field, by setting $\theta = \frac{\pi}{2}$,

$$n^2 = \frac{RL}{S} \quad \text{and} \quad n^2 = P \tag{2.13}$$

S, P, R and L are analytic functions of ω, Ω_j, Π_j and θ as shown in (B-13), where suffix j stands for electron (j=1), proton (j=2) and other ions in the plasma (j = 3, 4 .....).

In the actual earth's ionosphere and magnetosphere, the gyrofrequency Ω_e is not necessarily smaller than the plasma frequency Π_e as shown in Figure 1. In Figure 3, therefore, the dispersion relations are shown for three cases i.e. (a) $\Omega_e < \Pi_e$, (b) $\Omega_e = \Pi_e$ and (c) $\Omega_e > \Pi_e$, assuming Ω_e = 836 kHz. One of the common features in these figures which will be called the "dispersion diagram" of the plasma, is that wave modes in the diagrams consist of two basic domains, distinguished by the refraction index (n) of the plasma, i.e., the one (A) with $n^2 \leq 1$ and the other (B) with $n^2 \geq 1$.

In the domain (A), there are three cutoff frequencies which are given by setting $n^2 = 0$ in (B-17). Since C=RPL, these cutoff frequencies correspond to R=0, P=0 and L=0 modes, respectively. The mode R=0, which is right-handed in circular polarization, corresponds to X-mode in Figure 1. P=0 and L=0 modes are left-handed in circular polarization and correspond to the O- and Z-modes, respectively. The nomenclature X-, O- and Z-modes are made for the classification of radio waves in the ionosphere, based on the so-called Appleton-Hartree dispersion formula (Ratcliffe, 1962). The Appleton-Hartrie formula can be obtained from Equation (2.9) by making an approximation

$$\Omega_j \ll \omega \lesssim \Omega_e$$

In the domain (B), there are at least four resonant frequencies in which the index of refraction diverges, i.e., $n^2 \to \infty$, and the phase velocity of the wave approaches to zero, $V_{ph} = 0$. As shown in Appendix C, these resonant frequencies are the upper hybrid frequency, ω_{UH}, the electron gyrofrequency Ω_e, the plasma frequency Π_e and the lower hybrid frequency ω_{LH}. For the case of only an electron plasma, as used for drawing Figure 3, $\omega_{LH} \to 0$. In the multi-component plasma, Ω_j and Π_j appear also as resonance frequencies. In Figure 3, the right-handed and left-handed modes are indicated by dotted and hatched domains respectively.

As can be seen from these figures (Fig. 1, 2 and 3) the waves produced by the Cherenkov process are limited in this domain, (i.e., $n^2 > 1$ or $V_{ph} < c$). The propagation modes and the directional phase velocities of the wave, particularly those around the resonance frequencies are discussed in detail in Appendix C.

2.3 The Plasma Data

Since the rotation of the electric field vector of a right-handed circular polarized wave (R-mode wave) is the same as the gyration of an electron in a magnetic field, the waves produced by the motion of electrons in the magnetoplasma are R-mode waves (in brief, R-waves).

As shown in Figure 1, the frequency range of R-waves is limited between two resonance frequencies, ω_{UH} and ω_{LH}. Due to other resonance frequencies, Ω_e and Π_e, which exist between ω_{UH} and ω_{LH}, these waves are divided into two modes, i.e., the one is called the whistler mode and

the other is the R-mode EM wave in a narrow frequency band. If $\Omega_e < \Pi_e$, as shown in Figure 1 and Figure 3(a), the whistler mode is limited between Ω_e (where the propagation is parallel to B, i.e., $\theta=0$) and ω_{LH} (where the propagation is perpendicular to B, i.e., $\theta=\pi/2$). The other R-mode wave frequency ω is limited in $\Pi_e \leq \omega \leq \omega_{UH}$, where the propagation is parallel to B at $\omega = \Pi_e$ and perpendicular to B (i.e., $\theta = \frac{\pi}{2}$) at $\omega = \omega_{UH}$. The changes of propagation direction with wave frequency at a given point in the magnetosphere are shown by calculating the refractive index surface as a function of frequency, f (for example, Jørgensen, 1968, Fig. 9).

If $\Omega_e > \Pi_e$, then as shown in Figure 3(c), the frequency range of the whistler mode is $\omega_{LH} \leq \omega \leq \Pi_e$, where the propagation is longitudinal* ($\theta \cong 0$) at $\omega \cong \Pi_e$ and transversal* ($\theta \cong \pi/2$) near $\omega \equiv \omega_{LH}$ as before. The other R-mode wave is in a narrow band of $\Pi_e \leq \omega \leq \omega_{UH}$ with transverse propagation near ω_{UH} and longitudinal near Π_e. The band shrinks further into the narrow band $\Omega_e \lesssim \omega < \omega_{UH}$ at larger values of the refractive index, $n^2 \gtrsim 50$ or for slower phase velocities, $V_{ph} \lesssim 10^5$ km/sec. ($V_{ph} \lesssim 0.3c$). This narrow band of R-mode is connected to the whistler mode, if $\Pi_e = \Omega_e$ where the propagation is longitudinal ($\theta \cong 0$ propagation) in both modes. This case is shown in Figure 3(b).

It should be noted that the most part of auroral hiss is in the whistler mode with $\omega \lesssim \Omega_e$ (if $\Omega_e < \Pi_e$) or $\omega \lesssim \Pi_e$ (if $\Pi_e < \Omega_e$).

---

* Footnote: Here the words longitudinal and transverse are used for parallel and perpendicular to the imposed magnetic field, as commonly used in the ionosphere physics (Ratcliffe, 1962). In plasma physics, however, they are used for $k \parallel E_o$ and $k \perp E_o$ while parallel, perpendicular are used for $k \parallel B_o$ and $k \perp B_o$, respectively (Stix, 1962, p.39).

Due to the increasing magnetic field intensity B with decreasing altitudes, the whistler mode VLF produced at high altitudes in the earth's magnetosphere approaches the local lower hybrid frequency ω_{LH} as it propagates toward the ionosphere. Correspondingly, the direction of propagation becomes more transversal as the wave approaches the ionosphere from its original longitudinal propagation at large distances. Consequently, some of the lower frequency VLF-waves are reflected back into the magnetosphere where the propagation becomes more longitudinal again until the wave enters into the other hemisphere. Repeating these process, VLF-waves of whistler mode can be trapped between two hemispheres and in the earth's magnetosphere. An important role of these trapped VLF-waves in reducing the lifetime of electrons in the radiation belt, i.e., the formation of the "slot" around $L \cong 3$, has been discussed recently by Russel and Thorne (1970).

In this respect, the calculation of Ω_e, Π_o, ω_{UH} and ω_{LH} as functions of the altitude, of the latitude and of the local time are rather important not only for the calculation of VLF-production and its propagation in the magnetosphere but also for the study of dynamics of trapped charged particles in the earth's radiation belts.

2.3 The Model of the Geomagnetic Field

As discussed in the introduction, the earth's magnetic field has been assumed to be that of the centered dipole in the previous theoretical works on VLF emission and its propagation in the magnetosphere (Helliwell, 1965; Jørgensen, 1968; Lim-Laaspere, 1972). The deviation of the actual

field configuration from the centered dipole field can be seen from Figure 4, in which several magnetic field lines are drawn for comparison. The dipole field is shown by thin lines and the field calculated by a model of the earth's magnetic field called "MF-72 (Mead-Fairfield 1972 model)" is indicated by heavy lines. The field lines starting from the daytime side of the earth's surface and from the nighttime side are distinguished by full lines and dashed lines, respectively. The MF-72 is constructed by least squares fitting to magnetic field measurements obtained by latest available satellites, Explorer 33, 34, 41 and 43 (Mead and Fairfield, 1972). This model has been elaborated by separating the data and the corresponding parameters in the model into two cases of geomagnetic conditions, i.e., for quiet times ($Kp < 2$) and the other for disturbed periods ($Kp \geq 2$). Since the auroral hiss occurs during polar and magnetospheric substorms, MF-72 model for $Kp \geq 2$ conditions should be the logical choice for the purpose of the present calculation. The difference between the two cases is, however, a small affect on the result of the present calculation, although the difference of these models from the centered dipole field is significant as can be seen from the comparison shown in Figure 4. The difference between the two cases (quiet and disturbed) of MF-72 is significant at large distances from the earth (larger than 10 R_E) while most of the VLF-hiss production takes place within the domain of distance less than 10 R_E. Furthermore, the magnetospheric model should depend on the solar wind and on the interplanetary magnetic field (IMF). The effects of these variations are rather complex functions of time and space to be considered in the present subject. This

requires a wide range of parameters hard to fit into a single model. In Figure 5, the field lines and corresponding iso-gyrofrequency lines of electrons in the Kp < 2 model used in the present calculation are shown, where (a) is for geocentric distances less than 15 R_E and (b) for distances less than 5 R_E, respectively. The units between the marks shown along field lines are 1.0 R_E and 0.2 R_E, respectively. The unit of gyrofrequency is kHz. These figures correspond to Helliwell's dipole field charts (Helliwell, 1965, pp. 316-319).

2.5. The Distributions of Magnetospheric Plasma

As discussed Appendix C, the upper and the lower hybrid resonance frequencies, ω_{UH} and ω_{LH} are functions of gyro- and plasma - frequencies of charged particles in the earth's magnetoplasma. In order to compute these characteristic frequencies, a model of the spatial distributions of electrons, protons and O^+ - ions in the magnetosphere (including the ionosphere) has been built by using the latest available data obtained by the following satellites and investigators (indicated in the parenthesis); Alouette-I and II (Chan and Colin, 1969; Norton, 1969; Jackson, 1967, 1969; Rycroft and Thomas, 1970), OGO-4 and 6 (Mayr et al., 1970; Brinton et al., 1971; Taylor, 1972; Taylor and Walsh, 1972) and Explorer 22 (Brace et al., 1970).

Since these data do not cover whole domains of the magnetosphere, extrapolations as well as interpolations of the data have been made in several parts in the model, by utilizing the theoretical works on the plasma transport in the polar-magnetosphere (Banks and Holzer, 1969 a,b; Banks et al., 1971). Some parts of the results are shown in Figures 6,

and 7 by plotting the number densities of electrons, protons and O^+ ions against geomagnetic latitudes for the daytime and nighttime sides, respectively*. Since the extremely disturbed periods are not included in these data, this geoplasma distribution can be regarded as a model for $Kp \lesssim 2$.

2.6. Characteristic Frequencies in the Magnetosphere.

Based on the model of the MF-72 geomagnetic field and that of the iono-magnetospheric plasma distributions described in the previous sections, the upper and the lower hybrid resonance frequencies, f_{UH} and f_{LH} are calculated as functions of the altitude, latitude and local time. These are shown in Figures 8 and 9, together with the electron gyrofrequency, f_H, and the plasma frequency, f_N, plotting them against the distance from the ground measured along the magnetic field lines (in km) for different geomagnetic latitudes; (a) 60^o, (b) 70^o and (c) 80^o for daytime, and for (a) 60^o, (b) 70^o, (c) 75^o and (d) 80^o for night time, respectively, where the electron gyrofrequency $f_H = \Omega_e/2\pi$, the

*Footnote: Most of original data below 1000 km level are given as a function of geographic latitude, while most magnetospheric data are given against dip or geomagnetic latitudes. Since the difference, particularly the longitudinal dependence due to the difference of these coordinate system is not critical to the present calculations in which only midday and midnight conditions are considered, all parameters are shown against geomagnetic latitudes. The difference between dip and geomagnetic latitude is important only near the polar lower ionospheric regions.

plasma frequency $f_N = \Pi_o/2\pi$, the upper hybrid resonance frequency $f_{UH} = \omega_{UH}/2\pi$ and the lower hybrid resonance frequency $f_{LH} = \omega_{LH}/2\pi$ are calculated by the equations (A-1), (A-3), (C-15) and (C-16), respectively.

Some significant aspects of these figures are; (i) there is an altitude range at each latitude both in the day side and in the night side, where the plasma frequency is smaller than the electron gyrofrequency, i.e., $f_N < f_H$, corresponding to the dispersion diagram Figure 3(c), while outside of this altitude range, the dispersion relation corresponds to the diagrams of Figure 3(a) and Figure 1 ($f_N > f_H$). (ii) There is a minimum of f_{LH} around the latitude of 70^o λ for each altitude, corresponding to the so-called ion-trough (Taylor, 1972; Taylor and Walsh, 1972), although f_{LH} decreases with the latitude in general (Brice and Smith, 1965). (iii) There is a maximum of f_{LH} along each field line on both the day side and night side, forming a barrier for the propagation of VLF of frequencies lower than 10 kHz from the outer magnetosphere to the lower ionosphere. (iv) In the night, due to the low electron density below the altitudes around F-maximum, (below 350 km level) there is another barrier for high frequency side of VLF above several hundreds kHz as can be seen from Figure 9.

It would be worth noting that the physical meaning of f_{UH} and f_{LH} can be described as follows; under the high frequency waves, the motion of positive ions is negligible as compared to that of electrons. The electrons, on the other hand, undergo oscillatory motion by the periodic force of the wave which resonate at the plasma frequency. In

the magnetoplasma, the motion of electrons becomes circular due to the static field and their gyrating motions are imposed on the plasma oscillation. The resulting frequency is therefore $\omega_{UH} = (\Omega_e^2 + \Pi_o^2)^{\frac{1}{2}}$ which approaches the plasma frequency as the magnetic field is reduced to zero, i.e., $\omega_{UH} \rightarrow \Pi_o$ as $B \rightarrow 0$.

Contrary to the high frequency disturbance, at the very low frequencies, electrons can be regarded as a quasi-homogeneous background tightly bound to the static magnetic field, while oscillatory motions of ions under slow periodic field variations will resonate at a certain frequency that is ω_{LH}, in a manner that electrons oscillate at ω_{UH}.

3. CALCULATIONS AND THE RESULTS

3.1. Energy Dependence of Hiss-Production

With respect to the plasma distribution described in the previous sections, the power of Cherenkov emissions per frequency (watts/Hz) by an electron are calculated by the equation (2.1) along the field lines in the magnetosphere. These powers are shown in Figures 10 and 11 for the daytime side and for the nighttime side, respectively. Since these differential powers (watts/Hz) of Cherenkov emission depend on the energy, of the hiss-producing electrons, figures are shown for (a) E = 100 keV, (b) E = 1 keV for dayside (Figure 10), and (a) E = 100 keV, (b) E = 10 keV, (c) E = 1 keV and (d) E = 0.1 keV for nightside (Figure 11), respectively. These results correspond to those shown in Figure 10 of Jørgensen's paper (Jørgensen, 1968). The present results indicate the following; (i) As shown in the calculation by Lim and Laaspere (1972),

the power of Cherenkov emission, contributing the VLF-hiss in the magnetosphere increases with decreasing energy of electrons. (ii) The power of emission per electron is larger for higher frequencies for a given energy of electron, but (iii) this increase is not monotonic, particularly when the total emission per frequency in the magnetosphere is considered. This will be discussed in the next section.

3.2. Distributions of Hiss-Production in the Magnetosphere

The differential intensity of hiss production by electrons per unit volume in the magnetosphere, DP/Df (in watts Hz cm^3) can be shown as a function of s, the arc-length from the earth's surface along the geomagnetic field line (in km), by integrating (2.1) with respect to the pitch angle, α, of electrons and to their energy, E. Assuming the isotropic pitch angle distribution, this is given by

$$\frac{DP}{Df} = \int_{E_c}^{\infty} 2\pi \int_0^{\pi/2} N_e(E) \cdot \sin\alpha \, d\alpha \, dE \, \left(\frac{dP}{df}\right) \quad . \tag{3.1}$$

where dP/df (in watts/Hz.el.) is given by (2.1), $N_e(E) = j_e(E)/v_e$ is the number density of electrons (cm^{-3} str^{-1} keV^{-1}). The velocity $v_e = \beta_e$ c (in cm sec^{-1}) of the electron with kinetic energy, E (in keV) is given by (2.4) and is shown in Fig. 2.

Using the energy spectrum of electrons observed by Hoffman and Laaspere (1972), i.e. $j_e(E) = 4 \times 10^8 \cdot E^{-2}$ (cm^{-2} sec^{-1} str^{-1} keV^{-1}), the integration of (3.1) with respect to the electron-energy E is performed numerically. This energy spectrum of electron has been also applied by Lim and Laaspere (1972) in their calculation. The results

for nightside are shown in Figure 12, (a) for f = 100, 10 kHz and (b) for f = 50, 20 and 5 kHz, respectively, where the lower limit of the energy integral, E_c is assumed to be 0.1 keV.

3.3. Variation of Hiss Production with Energy Spectrum of Electrons

The total intensity of auroral hiss per frequency produced by electrons in the magnetosphere can be estimated by integrating (3.1) with respect to the effective volume of production. Assuming the perfect ducting of hiss propagation between the magnetosphere and the ground level for the frequency range shown in Figures 8 (day side) and 9 (night side), this is given by

$$D(P/f) = \int_{s_o}^{s} \left(\frac{DP}{Df}\right) \cdot S(s) \cdot ds \qquad (3.2)$$

where DP/Df is given by (3.1) and shown in Figures 12 (a) and (b), the cross-sectional area S(s), (in m^2) at the distance s, which corresponds to the unit area S_o at the ground, s_o, is given by the magnetic flux conservation, i.e.,

$$S(s) = \left(\frac{B_o}{B(s)}\right) S_o \; . \qquad (3.3)$$

B_o and B(s) are the total intensity of geomagnetic field at s_o and s, respectively, and $S_o = 1\ m^2$.

In order to see the effect of the energy spectrum of electrons on the rate of hiss production, the similar calculation with a harder spectrum $j_e(E) = 8.10^7\ E^{-1.2}$ ($cm^{-2}\ sec^{-1}\ str^{-1}\ keV^{-1}$) is made with respect to the same geomagnetoplasma model. The total intensity of electron is normalized at E_c = 1. keV for both spectra, i.e., the total intensity above 1 keV

is the same for both cases, $J(E_c)=4 \times 10^8$ (els/cm^2 sec str). The results are shown in Figure 13 (a,b) with a full line and a dashed line for the hard and soft spectra of electrons, where (a) stands for 80° λ dayside and (b) for 70° λ nightside respectively. Notice that the vertical scale for the hard spectrum case (full line) is shown in the right side.

This figure indicates the following: (1) The peak intensity of hiss produced by electrons of soft energy spectrum is more than one order higher for the hiss produced by soft spectrum electrons. (2) The wave frequency of peak intensity is also higher for the hiss generated by soft spectrum electrons than the one by hard spectrum electrons.

These results agree qualitatively with those obtained by the recent calculation by Lim and Laaspere (1972). However, the spectral density has a peak intensity around 20 kHz, in contrast to 70 kHz in Lim-Laaspere's calculation, although the spectrum of electron energy is the same. The peak intensity of the present result for the soft electrons is roughly half that of Lim-Laaspere. This difference seems to be reasonable because of the shift of the peak toward lower frequency where the power of Cherenkov emission per electron is generally less than at higher frequency as shown in Figures 10 and 11.

As mentioned in the Introduction, the geomagneto-plasma model used by Lim and Laaspere (1972) is less accurate than the one used in the present calculation, especially at great distances from the earth where most of the low frequency hiss below 30 kHz is produced. Since in these calculations, the perfect ducting along the field line is assumed for

the propagation of VLF-hiss in the magnetosphere, the peak intensity corresponds roughly to the maximum volume of hiss production in the magnetosphere. As can be seen from Figures 8 and 9, therefore, the frequency of peak intensity should be around 20 kHz for both dayside and nightside.

The frequency of the peak intensity of hiss produced by hard spectrum electrons, 10 kHz, is rather in good agreement with Jørgensen's calculation (1968), although the energy spectrum of electrons is not exactly the same. The shift of the peak intensity to lower frequency with the harder energy spectrum of hiss producing electrons has been also stated in Lim-Laaspere's paper (1972). As can be seen from Figures 10 and 11, the increasing rate of VLF-emission with decreasing energy of electrons is larger at higher frequency. The surpressing effect of the harder spectrum on hiss production is, therefore, relatively dominant at higher frequencies. The shift of peak frequency of VLF hiss toward lower frequency by the harder energy spectrum of source electrons can be explained by this effect.

3.4. Discussions

As presented in Jørgensen's paper (1968), the peak intensity of auroral hiss observed at the ground (Byrd station, Antarctica) and by the OGO-2 satellite is both around 10 kHz (which is by no means constant but mostly below 30 kHz). In this respect, the models of the geomagnetic field and of the geoplasma distribution used in the present calculation seem to be very close to reality, giving proper values of the frequency for the peak intensity and of spectral density of auroral hiss.

On the other hand, as in the previous work by Jørgensen (1968) and by Lim and Laaspere (1972), the perfect ducting is also assumed in the present calculation for the propagation of all VLF with frequencies between the upper limit (electron gyrofrequency or plasma-frequency) and the lower limit (lower hybrid frequency). The conditions and the effect of the ducting for the magnetospheric hiss propagation have been discussed recently by Manoranjan Rao et al. (1973), who pointed out that near LHR-frequencies, the propagation of hiss requires large density enhancements along the field line instead of the previously assumed a few percent deviation for the ducting. These will be investigated further at well as the contribution of low energy electrons below 100 eV. It is known that the first effect reduces the intensity near LHR and the latter effect increases the peak intensity and the frequency of maximum intensities at all latitudes.

ACKNOWLEDGMENTS

I wish to express my appreciation to the following colleagues at Goddard Space Flight Center: Dr. Gilbert Mead for providing the geomagnetic field model (FM-72) and its computer program; Eric Victor for assisting in several parts of the calculation on the IBM-360-91; Harry A. Taylor, Jr., John E. Jackson and Dr. Larry H. Brace for providing important information about plasma distributions in the earth's magnetosphere and ionosphere. The initiation of the present work is due to Dr. Robert Hoffman and Prof. Thomas Laaspere at Dartmouth College, whose stimulating discussions are most helpful and greatly appreciated.

APPENDIX A

(a) Notations and Definitions

α: pitch angle of electrons

$\beta(=\mathbb{V}/c)$, where $\mathbb{V}$ is the velocity of electrons, km/sec.

$\beta_\perp$, $\beta_\parallel$, are normal and parallel component of β with respect to the magnetic field line $\mathbb{B}$.

$\mathbb{B}$: magnetic induction, gauss

ϵ_o: dielectric permittivity of plasma

E: kinetic energy of electron, keV

f: frequency of wave, sec^{-1}

$n(=V_{ph}/c)$, refractive index of the plasma, where V_{ph} is the phase velocity of the wave.

$\tau(=1/f)$ period of the wave, sec.

$f_H(=\Omega_e/2\pi)$, gyrofrequency of electron, sec^{-1}.

$f_N(=\Pi_o/2\pi)$, plasma frequency, sec^{-1}.

$\Omega_e(=\frac{eB}{m_e c})$; $\simeq 1.78 \times 10^7$ B, the angular gyrofrequency of electron, sec^{-1} where B is in gauss. (A-1)

$\Pi_e(=\sqrt{\frac{N_e e^2}{\epsilon_o m_e}})$ $\simeq 5.65 \times 10^4 \sqrt{N_e}$, electron plasma angular frequency, sec^{-1} where N_e is the electron density, cm^{-3}. (A-2)

$\Pi_o = (\Pi_e^2 + \Pi_p^2 + \Pi_i^2)^{\frac{1}{2}}$, angular plasma frequency, sec^{-1}. (A-3)

$\Pi_i = \sqrt{\frac{e^2 N_i Z_i}{\epsilon_o m_i}}$, angular plasma frequency of i-th ion, sec^{-1} where N_i Z_i and m_i are the number density, atomic number and the rest mass of the i-th ion. (A-4)

$\Omega_i = \frac{Z_i e B}{m_i c}$, angular gyrofrequency of the i-th ion, sec^{-1}.

s: length of the geomagnetic field-line from the earth's surface, km.

$S(s)$: cross section of the geomagnetic tube at a distance s, corresponding to the unit area at s=o, m^2.

j_p: plasma current, coulomb/cm^2 sec

$j_e(E)$: differential energy spectrum of electrons, cm^{-2} sec^{-1} str^{-1} keV^{-1}.

$\bar{P}_o$: time-average of radiated power over a gyro-period of electron, watts per electron.

$\frac{d\bar{P}_o}{df}$: radiated power averaged over a period of gyration, per electron per radiation-frequency, watts/Hz - electron.

$\frac{DP}{df}$: differential intensity of hiss radiated from unit volume of the earth's magnetosphere (Cherenkov emissivity of the magnetosphere per radiation frequency), watts/Hz cm^3.

$D(P/f)$: the total intensity of hiss per unit frequency produced by electrons in the magnetosphere, watts/Hz.

(b) Physical constants

Light velocity in vacuum,	$c = 2.997_3 \times 10^5$	km/sec
Rest mass of the electron,	$m_e = 5.110_1 \times 10^2$	keV/c^2
Rest mass of the proton,	$m_p = 9.3826 \times 10^5$	keV/c^2
Electronic charge,	$e = 1.602_1 \times 10^{-19}$	coulomb

APPENDIX B

Electric field E in the plasma is related to the source current, j_s, produced by incident particles through Maxwell's equation (in MKS units) as follows;

$$\nabla \times B = \frac{\partial D}{\partial t} + j_s \tag{B-1}$$

$$\frac{\partial D}{\partial t} = \epsilon_o \frac{\partial B}{\partial t} + j_p \tag{B-2}$$

and

$$\nabla \times E = - \frac{\partial B}{\partial t} \tag{B-3}$$

where ϵ_o is the dielectric permittivity of the plasma, j_p is the plasma current, which arises from polarization of the plasma by j_s, and can be expressed by the summation of individual currents, j_j of each species of the plasma, i.e.,

$$j_p = \sum_j j_j \quad , \quad j_j = \sigma_j E \tag{B-4}$$

where σ_j is the conductivity tensor of the plasma which is obtained by solving the Lorentz force equation for individual species of the plasma,

$$q_j(E (r,t) + V_j (r,t) \times B) = m_j \frac{\partial V_j (r,t)}{\partial t} \tag{B-5}$$

where m_j, q_j, V_j and B are the rest mass, the electric charge, the velocity of the j-th specie and the static magnetic field in the plasma, respectively.

Since the current j_j can be written as

$$j_j = q_j N_j V_j$$

where N_j is the number density of the j-th specie of the plasma, Fourier transform of (B-5) gives

$$- i \omega \tilde{j}_j + \epsilon_j \Omega_j \times \tilde{j}_j = \epsilon_o \Pi_j^2 \cdot \tilde{E} \tag{B-6}$$

where Ω_j and Π_j are the angular gyro-frequency and the angular plasma-frequency given by

$$\epsilon_j \Omega_j = \frac{q_j B}{m_j} \quad \text{and} \quad \Pi_j = \sqrt{\frac{q_j^2 N_j}{\epsilon_o m_j}} \tag{B-7}$$

respectively.

Comparison of (B-6) with $j_j = \sigma_j \cdot E_j$, we get the following expression for the conductivity tensor as a function of Ω_j, π_j, and ω,

$$\sigma_j = \frac{\epsilon_o \Pi_j^2}{\omega^2 - \Omega_j^2} \cdot \begin{pmatrix} i\omega & -\epsilon_j \Omega_j & 0 \\ \epsilon_j \Omega_j & i\omega & 0 \\ 0 & 0 & \frac{\omega^2 - \Omega_j^2}{-i\omega} \end{pmatrix} \tag{B-8}$$

Fourier transform of (B-1), (B-2) and (B-3) yields

$$k \times \tilde{B} = - \omega \epsilon_o K \cdot \tilde{E} + i \tilde{j}_s \tag{B-9}$$

where

$$K = I - \frac{\sigma_T}{i\omega \epsilon_o} \tag{B10}$$

with

$$\sigma_T = \sum_j \sigma_j$$

and $\mathbb{I}$ is the unit tensor,

$$\mathbb{I} \equiv \begin{pmatrix} 1 & 0 & 0 \\ 0 & 1 & 0 \\ 0 & 0 & 1 \end{pmatrix}$$

Introducing the propagation vector $\mathbb{n} = \mathbb{k} \frac{c}{\omega}$,

(B-9) can be written

$$[(\mathbb{nn} - n^2\mathbb{I}) + \mathbb{K}] \cdot \tilde{\mathbb{E}} = \frac{i}{\omega p_o} \tilde{\mathbb{j}}_s \qquad \text{(B-11)}$$

where

$$\mathbb{K} = \begin{pmatrix} S & -iD & 0 \\ iD & S & 0 \\ 0 & 0 & P \end{pmatrix} \qquad \text{(B-12)}$$

is called the dielectric tensor of the plasma (Stix, 1962), and the elements are given as functions of wave-frequency, ω, gyro-frequency, Ω_j, and plasma-frequency Π_j, i.e.

$$S \equiv 1 - \sum_j \frac{\Pi_j^2}{\omega^2 - \Omega_j^2}$$

$$D \equiv \sum_j \frac{\epsilon_j \Omega_j \Pi_j^2}{\omega(\omega^2 - \Omega_j^2)} \qquad \epsilon_j = \pm 1 \qquad \text{(B-13)}$$

and

$$P \equiv 1 - \Sigma_j \frac{\Pi_j^2}{\omega^2}$$

If the direction of the static magnetic field, $\mathbb{B}$, is taken in z-axis, the character of the plasma has the axial symmetry around the z-axis. Without losing the generality, the propagation vector of a wave, $\mathbb{k}$, can be taken in yz-plane, then

$$k_x = 0, \text{ and } \mathbb{k} = a_y k \sin\theta + a_z k \cos\theta \qquad \text{(B-14)}$$

where θ is the angle between $\mathbb{B}$ and $\mathbb{k}$,

a_x, a_y, a_z and k_x, k_y, k_z are unit vectors and wave numbers in x, y, z directions, respectively.

Substitution of (B-12) into (B-10) yields

$$\mathbb{T}\tilde{\mathbb{E}} = \frac{i}{\omega \epsilon_o} \cdot \tilde{\mathbb{j}}_s \tag{B-15}$$

where

$$\mathbb{T}(\cos\theta) = \begin{pmatrix} S-n^2 & -iD & 0 \\ iD & S-n^2\cos^2\theta & n^2 \sin\theta\cos\theta \\ 0 & n^2 \sin\theta\cos\theta & P-n^2\sin^2\theta \end{pmatrix} \tag{B-16}$$

and

$$|\mathbb{T}| = A\, n^4 - B\, n^2 + C \tag{B-17}$$

where

$$\begin{aligned} A &= S \sin^2\theta + P\cos^2\theta \\ B &= PS(1+\cos^2\theta) + RL\sin^2\theta \\ C &= PRL,\ R = S + D \text{ and } L = S - D \end{aligned} \tag{B-18}$$

$\mathbb{T} = 0$ gives the dispersion relation of waves in the collisionless, cold plasma.

From (B-15), we get

$$\tilde{\mathbb{E}}(\mathbb{k},\omega) = \frac{i}{\omega \epsilon_o} \mathbb{T}^{-1}(\cos\theta)\, \tilde{\mathbb{J}}_s\,(\mathbb{k},\omega) \tag{B-19}$$

By the Fourier integral theorem (Fourier's inversion formula for (B-19)),

$$\mathbb{E}(\mathbf{r},t) = \int_{-\infty}^{\infty} \int_{-\infty}^{\infty} \tilde{\mathbb{E}}(\mathbf{k},\omega) \cdot e^{i(\omega t - \mathbf{k}\cdot\mathbf{r})} d\mathbf{k}\, d\omega$$

we get

$$E(\mathbf{r},t) = \frac{i}{\epsilon_o} \iint_{-\infty}^{\infty} \mathbb{T}^{-1} (\cos\theta)\, \tilde{j}_s(\mathbf{k},\omega) \cdot e^{i(\omega t - \mathbf{k}\cdot\mathbf{r})}\, d\mathbf{k}\, \frac{d\omega}{\omega} \qquad \text{(B-20)}$$

The source current j_s can be expressed by

$$j_s(\mathbf{r}) = q_s \cdot \mathbb{V}_s(t) \cdot \delta(\mathbf{r} - \mathbf{r}_s(t)) \qquad \text{(B-21)}$$

The Fourier transform of this yields

$$\tilde{j}_s(\mathbf{k},\omega) = \frac{q_s}{(2\pi)^4} \int_{-\infty}^{\infty} \mathbb{V}_s(t) \cdot \exp[i(\mathbf{k}\cdot\mathbf{r}_s - \omega t)]\, dt \qquad \text{(B-22)}$$

Since a particle spirals around z-axis, moving along $\mathbb{B}$ direction with the velocity, $\mathbb{V}_s$, the radial vector of the particle, $\mathbf{r}_s(t)$, is given by

$$\mathbf{r}_s(t) = a_x r_o \cos\Omega' t + a_y r_o \sin\Omega' t + a_z V_{\parallel} t \qquad \text{(B-23)}$$

and

$$\mathbb{V}_s(t) = -a_x V_{\perp} \sin\Omega' t + a_y V_{\perp} \cos\Omega' t + a_z V_{\parallel} \qquad \text{(B-24)}$$

where $r_o = \frac{V_{\perp}}{\Omega'}$ is the gyro-radius of spiraling particle

$\Omega' = \Omega_s/\gamma$ and γ is the Lorentz factor of the particle, i.e.,

Since $\mathbb{k} = n\frac{\omega}{c}$, $\mathbb{V} = \beta c$, the product of (B-14) and (B-23) can be written as

$$\mathbb{k}\cdot\mathbf{r}_s - \omega t = \xi \sin\Omega' t + (n\beta_{\parallel}\cos\theta - 1)\,\omega t$$

where

$$\xi = \frac{\omega\beta_{\perp}}{\Omega'} n \cdot \sin\theta$$

The integrand of (B-22) is therefore written in the following form

$$\tilde{j}_s(\mathbb{k},\omega) = \frac{q}{(2\pi)^4}\int_{-\infty}^{\infty}(-a_x V_{\perp}\sin\Omega' t + a_y V_{\perp}\cos\Omega' t + a_z V_{\parallel} t) \cdot \exp\,[i(\xi\sin\Omega' t + (n\beta\cos\theta - 1)\,\omega t]\cdot dt \qquad \text{(B-25)}$$

$$= \frac{q}{(2\pi)^4}\sum_{s=-\infty}^{\infty}\int_{-\infty}^{\infty}(ia_x V_{\perp} J_s'(\xi) + a_y V\frac{s}{\xi}J_s(\xi) + a_z V_{\parallel} J_s(\xi)) \times \exp\,[i(s\,\Omega' + \omega n\,\beta_{\parallel}\cos\theta - \omega)t]\cdot dt$$

The second expression of (B-25) is derived by using the following formula of Bessel function;

$$\sin\Omega' t\cdot e^{i\,\xi\sin\Omega' t} = i\sum_{s=-\infty}^{\infty} J_s'(\xi)\cdot e^{is\Omega' t}$$

$$\cos\Omega' t\cdot e^{i\,\xi\sin\Omega' t} = \sum_{s=-\infty}^{\infty}\frac{s}{\xi}J_s(\xi)\cdot e^{is\Omega' t}$$

and

$$e^{i\,\xi\sin\Omega' t} = \sum_{s=-\infty}^{\infty} J_s(\xi)\cdot e^{is\Omega' t}$$

Using the Fourier integral representation of delta function, i.e.,

$$\delta(\omega) = \frac{1}{2\pi} \int_{-\infty}^{\infty} e^{i\,\omega t}\, dt$$

(B-25) can be written in the following form

$$\mathbb{J}_s(\mathbb{k},\omega) = \frac{q_s}{(2\pi)^3} \sum_{s=-\infty}^{\infty} (i a_x V_\perp \cdot J_s'(\xi) + a_y V_\perp \frac{s}{\xi} J_s(\xi) + a_z V_\parallel J_s(\xi)) \times \delta(s\,\Omega' + \omega n\,\beta_\parallel \cos\theta - \omega) \qquad \text{(B-26)}$$

This expression indicates that the radiation occurs only when the source current is in the following condition,

$$s\,\Omega' + \omega\, n\, \beta_\parallel \cos\theta - \omega = 0 \qquad \text{(B-27)}$$

In the case of s=0, this gives the Cherenkov condition,

$$\cos\theta = \frac{1}{\beta_\parallel n} \qquad \text{(B-28)}$$

The total instantaneous radiation from a spiraling particle is given by

$$\begin{aligned} P(\mathbb{r}_s;t) &= \mathbb{F} \cdot \frac{d\,\mathbb{r}_s}{d_t} \\ &= q_s\,(\mathbb{E} + \mathbb{V}_s \times \mathbb{B}) \cdot \mathbb{V}_s \\ &= q_s\,\mathbb{E}(\mathbb{r}_s,t) \cdot \mathbb{V}_s(t) \end{aligned} \qquad \text{(B-29)}$$

Since

$$d\,\mathbb{k} = k^2 dk\, d\Omega = \left(\frac{n^2\,\omega^3}{c^3}\right) dn\, d\Omega, \qquad d\Omega = d\varphi \cdot d\,(\cos\theta)$$

and

$$\delta(n\omega\beta_{\parallel}\cos\theta + s\Omega' - \omega) = \frac{1}{|\omega n \beta_{\parallel}|} \cdot \delta\left(\cos\theta - \frac{\omega - s\Omega'}{\omega n\, \beta_{\parallel}}\right)$$

By substituting (B-26) into (B-20), (B-29) can be written in the following expression,

$$P(\mathbf{r}_s,t) = \frac{iq^2}{\epsilon_o(2\pi)^3} \int_o^{\infty} n\, dn \int_{-\infty}^{\infty} \frac{\omega}{c^3}\, d\omega \cdot Q_s\,(\mathbf{r}_s,t)\, d\Omega \qquad \text{(B-30)}$$

where

$$Q_s\,(\mathbf{r}_s,t) = \mathbb{T}^{-1}(\cos\theta) \sum_{s=-\infty}^{\infty} \mathbb{V}_s\,(\xi) \cdot \delta\left(\cos\theta - \frac{\omega - s\Omega'}{\omega n\beta_{\parallel}}\right)$$

$$\text{x} \cdot e^{-i\,\xi\,\sin\Omega' t + i(1-n\beta_{\parallel}\cos\theta)\,\omega t}\; \mathbb{V}_s(\mathbf{r}_s,t) \qquad \text{(B-31)}$$

and

$$\mathbb{V}_s(\xi) = ia_x V_{\perp} J_s'(\xi) + a_y V_{\perp} \frac{s}{\xi} J_s(\xi) + a_z V_{\parallel} J_s(\xi) \qquad \text{(B-32)}$$

Due to the δ-function in the integrand, the result of integration of (B-30) by $d\Omega$ can be obtained by replacing ξ and $\cos\theta$ by ξ_s and $\cos\theta_s$, respectively, where

$$\xi_s = \frac{\omega\beta_{\perp}}{\Omega'} n \cdot \sin\theta_s \quad \text{and} \quad \cos\theta_s = \frac{1 - \frac{s}{\varpi}}{n\beta_{\parallel}} \qquad \text{(B-33)}$$

The instantaneous radiation power from a spiraling charged particle is therefore given by,

$$P(\mathbf{r}_s,t) = \frac{iq^2}{\epsilon_o(2\pi c)^3} \int_0^\infty n\, dn \int_{-\infty}^{\infty} \omega d\omega \quad 2\pi \sum_{s=-\infty}^{\infty} Q_s'(\mathbf{r}_s,n^2,t) \quad \text{(B-34)}$$

where

$$Q_s'(\mathbf{r}_s,n^2,t) = \mathbb{T}^{-1}(\cos\theta_s) \sum_{m=-\infty}^{\infty} \mathbb{V}_s^*(\xi) \cdot e^{-i(m-s)\,\Omega' t} \cdot \mathbb{V}_s(\xi) \quad \text{(B-35)}$$

The time-dependence of (B-34) can be eliminated by taking the time-average of $P(\mathbf{r}_s,t)$ over a revolution-period of the particle, $2\pi/\Omega'$,

$$\overline{P(\mathbf{r}_s)} = \frac{\Omega'}{2\pi} \int_0^{2\pi/\Omega'} P(\mathbf{r}_s,t)\, dt$$

As can be seen by (B-35), the integration of $P(\mathbf{r}_s,t)$ by t over a period $2\pi/\Omega'$ vanishes except for m = s, due to the term exp $[-i(m-s)\,\Omega' t]$. Thus we get

$$\overline{P(\mathbf{r}_s)} = \frac{iq^2}{\epsilon_o(2\pi c)^3} \int_0^\infty dn^2 \int_{-\infty}^{\infty} \omega d\omega 2\pi \sum_{s=-\infty}^{\infty} \overline{Q_s'(\mathbf{r}_s,\, n^2)} \quad \text{(B-36)}$$

where

$$\overline{Q_s'(\mathbf{r}_s,\, n^2)} = \mathbb{V}_s^*(\xi) \cdot \mathbb{T}^{-1}(\cos\theta_s) \cdot \mathbb{V}_s(\xi) \quad \text{(B-37)}$$

$$\mathbb{V}_s^*(\xi_s) = (-ia_x V_\perp J_s'(\xi),\ a_y V_\perp \frac{s}{\xi} J_s(\xi),\ a_z V_\parallel J_s(\xi)) \quad \text{(B-38)}$$

$$\mathbb{T}^{-1}(\cos\theta) = \frac{1}{|\mathbb{T}(\cos\theta)|} \begin{pmatrix} t_{11} & it_{12} & -it_{13} \\ -it_{21} & t_{22} & t_{23} \\ it_{31} & t_{32} & t_{33} \end{pmatrix} \tag{B-39}$$

and

$$V_s(\xi) = \begin{pmatrix} ia_x V_\perp J_s'(\xi) \\ a_y V_\perp \frac{s}{\xi_s} J_s(\xi) \\ a_z V_\parallel J_s(\xi) \end{pmatrix} \tag{B-40}$$

Elements of $\mathbb{T}^{-1}(\cos\theta_s)$ in (B-39), t_{ij}'s are calculated from the inverse matrix of (B-16). The result is as follows:

$$\begin{aligned}
t_{11} &= SP - An^2, \qquad A = S\sin^2\theta + P\cos^2\theta \\
t_{12} &= D(P - n^2\sin^2\theta) \\
t_{13} &= Dn^2 \sin\theta \cdot \cos\theta \\
t_{21} &= -t_{12} \\
t_{22} &= n^4\sin^2\theta - n^2(P + S\cdot\sin^2\theta) + SP \\
t_{23} &= (n^2 - S)\cdot n^2 \cdot \sin\theta\cdot\cos\theta \\
t_{31} &= -t_{13} \\
t_{32} &= t_{23}, \text{ and} \\
t_{33} &= n^4\cos^2\theta - n^2 S\cdot(1 + \cos^2\theta) + (D^2 - S^2)
\end{aligned} \tag{B-41}$$

From (B-16), the determinant of $\mathbb{T}(\cos\theta_s)$ can be written into the following form,

$$|\mathbb{T}(\cos\theta_s)| = S\cdot n^4 + b_s\cdot n^2 + c_s$$
$$= S\cdot(n^2 - n_1^2)\cdot(n^2 - n_2^2) \qquad \text{(B-42)}$$

where

$$n_1^2 = \frac{-b_s + \Delta_s}{2\cdot S}\ , \qquad n_2^2 = \frac{-b_s - \Delta_s}{2\cdot S} \qquad \text{(B-43)}$$

$$\Delta_s = (b_s^2 - 4\cdot S\cdot c_s)^{\frac{1}{2}} \qquad \text{(B-44)}$$

$$b_s = \frac{1}{\beta_\parallel^2}\cdot\left(1 - \frac{s}{\omega}\Omega'\right)^2\cdot(P - S) + D^2 - S^2 - PS \qquad \text{(B-45)}$$

and

$$c_s = \frac{1}{\beta_\parallel^2}\cdot\left(1 - \frac{s}{\omega}\Omega'\right)^2\cdot(S^2 - D^2 - PS) + P\cdot(S^2 - D^2) \qquad \text{(B-46)}$$

These expressions indicate that the integrand of (B-36) is regular except at four roots of (B-42), $n = \pm n_1$ and $\pm n_2$. The integration of (B-36) by n^2 can be therefore done by means of the residue theorem with respect to two poles of n^2, i.e., $n^2=n^2_j$, (j=1 and 2). With manipulations of three matrixes products, n^2-integration of (B-36) yields,

$$\overline{P(\mathbf{r}_s)} = \sum_{j=1}^{2}\frac{q^2}{4\pi\varepsilon_o c^2 V_\parallel}\int_{-\infty}^{\infty}|\omega|\cdot d\omega\cdot\sum_{s=-\infty}^{\infty}\overline{Q_s'(\mathbf{r}_s, n_j^2)} \qquad \text{(B-47)}$$

where

$$\overline{Q_s'(r_s,\ n_j^2)} = [t_{11}V_\perp^2(J_s')^2 + t_{22}V_\perp^2(\frac{s}{\xi})^2\ J_s^2 + t_{33}V_\parallel^2 J_s^2$$
$$+ t_{12}V_\perp^2 \cdot \frac{2s}{\xi} \cdot J_s' J_s - t_{13}V_\perp V_\parallel \cdot 2J_s' J_s \qquad \text{(B-48)}$$
$$+ t_{23}V_\perp V_\parallel \cdot \frac{2s}{\xi} \cdot J_s^2] \Big/ S\cdot(-1)^j(n_2^2 - n_1^2)$$

As can be seen from (B-33), the argument of Bessel function depends on two parameters s and j, i.e.,

$$\xi = \xi_{s,j} \qquad \xi_{s,j} = \frac{\omega\beta_\perp}{\Omega'} \cdot n_j \cdot \sin\theta_s$$

where the angle of wave propagation with respect to a static magnetic field, θ_s, is given instead of (B-27) by discrete values of s and j,

$$\cos\theta_{s,j} = (1 - \frac{s}{\omega})/n_j\ \beta_\parallel \qquad \text{(B-49)}$$

The result for s=0 in the above expressions, corresponds to Cherenkov radiation as shown by (B-28). The total power of Cherenkov radiation from a spiraling particle in the plasma is, therefore, given by setting s=0 in the above expressions.

$$\overline{P}_o = \frac{q^2}{4\pi\epsilon_o V_\parallel} \sum_{j=1}^{2} \int_{-\infty}^{\infty} \omega \, d\omega \, [\beta_\parallel^2 t_{33}(n_j^2) \, J_o^2(\xi_j) + \beta_\perp^2 \cdot t_{11}(n_j^2) \, J_1^2(\xi_j)$$

$$+ 2\beta_\perp \beta_\parallel t_{13}(n_j^2) J_o(\xi_j) J_1(\xi_j)]/S(-1)^j (n_2^2 - n_1^2) \qquad \text{(B-50)}$$

where $J_o'(\xi_j)$'s are replaced by $J_1(\xi_j)$, using the relation $J_o'(x) = -J_1(x)$, and

$$\xi_j = \frac{\omega\beta_\perp}{\Omega'} \, n_j \sin\theta_o, \quad \cos\theta_o = \frac{1}{\beta_\parallel n_j} \qquad \text{(B-51)}$$

The power per frequency, $\overline{dP_o}/df$, is more convenient for comparisons with the experimental results than the total power of emission over whole frequency range. Thus, from (B-51), we obtain the following expression of Cherenkov radiation per emission frequency,

$$\frac{\overline{dP_o}}{df} = \frac{q^2\pi}{\epsilon_o c} \cdot f \cdot \sum_{j=1}^{2} \frac{\beta_\parallel}{\Delta_o} t_{33}(n_j^2) \left[J_o^2(\xi_j) + \left(\frac{\beta_\perp}{\beta_\parallel}\right)^2 J_1^2(\xi_j) \frac{t_{11}(n_j^2)}{t_{33}(n_j^2)}\right.$$

$$\left. + 2\left(\frac{\beta_\perp}{\beta_\parallel}\right) J_o(\xi_j) J_1(\xi_j) \frac{t_{13}(n_j^2)}{t_{33}(n_j^2)}\right] \qquad \text{(B-52)}$$

where

$$\Delta_o = (b_o^2 - 4Sc_o)^{\frac{1}{2}}$$

$$b_o = \frac{P - S}{\beta_\parallel^2} + D^2 - S^2 - PS \qquad \text{(B-53)}$$

(B-54)

$$c_o = \frac{S^2-D^2-PS}{\beta_\parallel^2} + P(S^2 - D^2) \tag{B-55}$$

$$t_{11}(n_j^2) = -n_j^2 \cdot S + SP + \frac{S - P}{\beta_\parallel^2}$$

$$t_{33}(n_j^2) = n_j^2\left(\frac{1}{\beta_\parallel^2} - S\right) - \frac{S}{\beta_\parallel^2} + (D^2 - S^2) \tag{B-56}$$

$$t_{13}(n_j^2) = \frac{D}{\beta_\parallel^2}\sqrt{n_j^2\beta_\parallel^2 - 1}$$

In these expressions, S, P, and D are the function of angular frequency of the wave in a plasma, which are given by (B-41).

APPENDIX C

First, let us consider the case of a two component plasma which consists of equal numbers of electrons and protons.

Putting j=e for electrons and j=p for protons in (B-13) and $\theta=0$ in (B-18), we get the following expression which corresponds to (2.12),

$$n_{\parallel}^2 \simeq \frac{\omega^2 - \omega\Omega_e - \Omega_e\,\Omega_p - \Pi_o^2}{(\omega - \Omega_e)(\omega + \Omega_p)} \quad \text{, for } n^2=R \qquad \text{(C-1)}$$

and

$$n_{\parallel}^2 \simeq \frac{\omega^2 + \omega\Omega_e - \Omega_e\,\Omega_p - \Pi_o^2}{(\omega + \Omega_e)(\omega - \Omega_p)} \quad \text{, for } n^2=L \qquad \text{(C-2)}$$

where

$$\Pi_o^2 = \Pi_e^2 + \Pi_p^2 \qquad \text{(C-3)}$$

In these derivations, terms of Ω_p^2 are neglected as compared to those of ω^2 and Ω_e^2.

Solutions of numerators of (C-1), and (C-2), give the cutoff frequencies

$$\omega_R \simeq \Omega_e + \frac{\Pi_o^2}{\Omega_e} \quad \text{, for R-mode} \qquad \text{(C-4)}$$

and

$$\omega_L \simeq \frac{\Pi_o^2}{\Omega_e} \quad \text{, for L-mode} \qquad \text{(C-5)}$$

For the P-mode, P=0 gives $\omega_P = \Pi_e$ (C-6)

Equations (C-1) and (C-2) indicate also that $\omega=\Omega_e$ and $\omega=\Omega_p$ are resonant frequencies of the wave propagating parallel to the magnetic field, i.e.

$$n_{\parallel}^2 \to \infty$$

For the wave propagating perpendicular to the field, the resonance frequencies are obtained from (2.13), with $\theta = \frac{\pi}{2}$

$$n_\perp^2 = \frac{(\omega^2 - \omega_R^2)(\omega^2 - \omega_L^2)}{(\omega^2 - \omega_{LH}^2)(\omega^2 - \omega_{UH}^2)} \qquad \text{for } n^2 = \frac{RL}{S} \quad \text{(C-7)}$$

and

$$n_\perp^2 = \frac{\omega^2 - \Pi_o^2}{\omega^2} \qquad \text{for } n^2 = P \quad \text{(C-8)}$$

where ω_R and ω_L are cutoff frequencies of R and L-modes, given by (C-4) and (C-5), respectively.

(C-7) indicates ω_{UH} and ω_{LH} are the resonance frequencies of the wave propagating perpendicular to the magnetic field and called the upper and the lower hybrid frequencies, respectively.

As can be seen from Eq. (2.9), these are given by A=0, which is written further by (B-18)

$$tg^2\theta = -\frac{P}{S} \qquad \text{(C-9)}$$

For $\theta = \frac{\pi}{2}$, this requires S=0, from which we get

$$\omega^4 - \omega^2(\Omega_e^2 + \Omega_p^2 + \Pi_o^2) + [\Omega_e^2\Omega_p^2 + \Pi_e^2(\Omega_p^2 + \Omega_e\Omega_p)] = 0$$

The solution gives,

$$\omega^2 = \frac{\Omega_e^2 + \Omega_p^2 + \Pi_o^2}{2} \left[1 \pm \sqrt{1 - \frac{4(\Omega_e^2\Omega_p^2 + \Pi_e^2\Omega_p^2 + \Pi_e^2\Omega_e\Omega_p)}{(\Omega_e^2 + \Omega_p^2 + \Pi_o^2)^2}}\right]$$

$$\cong \frac{\Omega_e^2 + \Pi_o^2}{2} \left[1 \pm \left(1 - 2\,\frac{\Omega_e^2\Omega_p^2 + \Pi_e^2\Omega_p^2 + \Pi_e^2\Omega_e\Omega_p}{(\Omega_e^2 + \Pi_o^2)^2}\right)\right]$$

Taking the plus sign in the bracket, we get

$$\omega_{UH}^2 \cong \Omega_e^2 + \Pi_o^2 \tag{C-10}$$

and, for the minus sign in the bracket, we get

$$\omega_{LH}^2 \cong \frac{\Omega_e^2\Omega_p^2 + \Pi_e^2\,\Omega_p^2 + \Pi_e^2\Omega_e\Omega_p}{\Omega_e^2 + \Pi_o^2}$$

By making use of $\Pi_e^2\Omega_p = \Pi_p^2\Omega_e$, this can be written as,

$$\omega_{LH}^2 \cong \left(\frac{1}{\Omega_p^2 + \Pi_p^2} + \frac{1}{\Omega_e\,\Omega_p}\right)^{-1} \tag{C-11}$$

In the case of the multi-component plasma, S=0 gives the following formula,

$$\frac{\Pi_e^2}{\omega^2 - \Omega_e^2} + \frac{\Pi_p^2}{\omega^2 - \Omega_p^2} + \frac{\Pi_j^2}{\omega^2 - \Omega_j^2} + \ldots = 1 \tag{C-12}$$

Since $\Omega_p^2 = \Omega_e^2 \left(\frac{m_e}{m_p}\right)^2$ where $\frac{m_e}{m_p} = \frac{1}{1836} \sim 5.10^{-4}$

(C-12) can be approximated by

$$\frac{\Pi_e^2}{\omega^2 - \Omega_e^2} + \frac{1}{\omega^2}\left(\Pi_p^2 + \Pi_j^2 + \ldots\right) = 1 \tag{C-13}$$

$$\omega^4 - \omega^2(\Pi^2 + \Omega_e^2) + \Omega_e^2\,(\Pi^2 - \Pi_e^2) = 0$$

where

$$\Pi^2 = \Pi_e^2 + \Pi_p^2 + \Pi_j^2 + \ldots. \tag{C-14}$$

Similarly to (C-10) and (C-11), from (C-13), we get

$$\omega_{UH}^2 \cong \Omega_e^2 + \Pi^2 \tag{C-15}$$

and

$$\omega_{LH}^2 \cong \frac{\Omega_e^2 \ (\Pi^2 - \Pi_e^2)}{\Pi^2 + \Omega_e^2} \tag{C-16}$$

By defining

$$\frac{1}{M_{eff}} = \sum_i \alpha_i \ \frac{m_e \ Z_i}{m_i} \tag{C-17}$$

where α_i is the fraction of i-th ion species in the total position ion.

(C-16) can be approximated by (Brice and Smith 1964)

$$\frac{1}{\omega_{LH}^2} = M_{eff} \left(\frac{1}{\Pi_e^2} + \frac{1}{\Omega_e^2} \right) \tag{C-18}$$

REFERENCES

(1) Lim, T. L., and Thomas Laaspere, An Evaluation of the Intensity of Čerenkov Radiation from Auroral Electrons with Energies down to 100 eV, J. Geophys. Res., 77, 4145-4157, 1972.

(2) Jørgensen, T. S., Interpretation of Auroral Hiss Measured on OGO-2 and at Byrd Station in Terms of Incoherent Cerenkov Radiation, J. Geophys. Res., 73, 1055-1069, 1968.

(3) Mansfield, V. N., Čerenkov and Cyclotron Radiation as VLF Emission Sources, Scientific Report, Oct. 1964.

(4) Mansfield, V. N., Radiation from a Charged Particle Spiraling in a Cold Magnetopause, Astrophys. J., 147, 672-680, 1967.

(5) Liemohn, H. B., Radiation from Electrons in Magnetoplasma, Radio Sci., 69D, 741-766, 1965.

(6) Trulsen, J., and J. A. Fejer, Radiation from a Charged Particle in a Magnetoplasma, J. Plasma Phys., 4, 825-841, 1970.

(7) Trulsen, J., Cyclotron Radiation in Hot Magnetoplasmas, J. Plasma Phys., 6, 367-400, 1971.

(8) Hoffman, R. A., and T. Laaspere, Comparison of Very-Low-Frequency Auroral Hiss with Precipitating Low-Energy Electrons by the Use of Simultaneous Data from Two OGO-4 Experiments, J. Geophys. Res., 77, 640-650, 1972.

(9) Eidman, V. I., The Radiation from an Electron Moving in a Magneto-active Plasma, Soviet Phys. J.E.T.P., 34, 91-95, 1958.

(10) McKenzie, J. F., Čerenkov Radiation in a Magneto-Ionic Medium (With Application to the Generation of Low-Frequency Electro-Magnetic Radiation in the Exosphere by the Passage of Charged Corpuscular Streams), Phil. Trans. Roy. Soc., Lond. A255, 585-606, 1963.

(11) McKenzie, J. F., Radiation from a Test Particle in a Plasma, Phys. Fluids, 10, 2680-2694, 1967.

(12) K. Sakurai, Gyrosynchrotron Radiation and Its Transfer in a Magnetoactive Plasma, Astrophys. J., 174, 135-149, 1972.

(13) Sakurai, K. and T. Ogawa, Radiation Fields of Energetic Electrons in Helical Orbits within a Magnetoactive Plasma, Planet. Space Sci., 17, 1449-1458, 1969.

(14) Gurnett, D. A., and L. A. Frank, VLF Hiss and Related Plasma Observations in the Polar Magnetosphere, J. Geophys. Res., 77, 172-190, 1972.

(15) Bekefi, G., Radiation Processes in Plasmas, John-Wiley & Sons, N.Y., 1966.

(16) Ginzburg, V. L., The Propagation of Electromagnetic Waves in Plasma, Pergamon Press, N. Y., 1964.

(17) Stix, T. H., Theory of Plasma Waves, McGraw-Hill, N. Y., 1962.

(18) Schwinger, J., On the Classical Radiation of Accelerated Electrons, Phys. Rev., 75, 1912-1925, 1949.

(19) Helliwell, R. A., Whistlers and Related Ionospheric Phenomena, Stanford Univ. Press, Palo Alto, Calif., 1965.

(20) Banks, P. M., and T. E. Holzer, High-Latitudes Plasma Transport: The Polar Wind, J. Geophys. Res., 74, 6317-6332, 1969.

(21) Banks, P. M., and T. E. Holzer, Features of Plasma Transport in the Upper Atmosphere, J. Geophys. Res., 74, 6304-6316, 1969.

(22) Chan, K. L., and L. Colin, Global Electron Density Distributions from Topside Soundings, Proc. IEEE, 57, 990-1004, 1969.

(23) Norton, P. B., The Middle-Latitude F-Region During Some Severe Ionospheric Storms, Proc. IEEE, 57, 1147-1149, 1969.

(24) Jackson, J. E., Comparison between topside and ground-based soundings, Proc. IEEE, 57, 976-985, 1969.

(25) Taylor, H. A., The light ion trough, NASA Rept. X-621-72-44, 1972.

(26) Taylor, H. A. and W. J. Walsh, The light-ion trough, the main trough and the plasmapause, J. Geophys. Res., 77, 6716 - 6723, 1972.

(27) Brinton, H. C., J. M. Grebowsky and H. G. Mayr, Trough wind, J. Geophys. Res., 76, 3738-3745, 1971.;

(28) Bank, P. M. and T. E. Holzer, The polar wind, J. Geophys. Res., 73, 6846 - 6854, 1968.

(29) Rycroft, M. J. and J. O. Thomas, Plasmapause and electron density trough at the Alouette I orbit, Planet. Space Sci., 18, 65-80, 1970.

(30) Mayr, H. G., J. M. Grebowsky and H. A. Taylor, Study of the thermal plasma on closed field lines outside the plasmasphere, Planet Space Sci., 18, 1123 - 1135, 1970.

(31) Laaspere, T., and H. A. Taylor, Jr., Comparison of certain VLF noise phenomena with the lower hybrid resonance frequency calculated from simultaneous ion composition measurements, J. Geophys. Res., 75, 97 - 106, 1970.

(32) Evans, D. S., The observations of a near monoenergetic flux of auroral electrons, J. Geophys. Res., 73, 2315 - 2323, 1968.

(33) Ogilvie, K. W., Auroral electron energy spectra, J. Geophys. Res., 73, 2325 - 2332, 1968.

(34) Hoffman, R. A. and D. S. Evans, Field-Aligned electron bursts at high latitudes observed by OGO-4, J. Geophys. Res., 73, 6207 - 6214, 1968.

(35) Feldman, P. D., J. P. Doering and J. H. Moore, Rocket Measurement of the secondary electron spectrum in an aurora, J. Geophys. Res., 76, 1738 - 1745, 1971.

(36) Hoffman, R. A., Low energy electron precipitation at high latitudes, J. Geophys. Res., 74, 2425 - 2432, 1969.

(37) Frank, L. A., and K. L. Ackerson, Local-time survey of plasma at low altitudes over the auroral zones, J. Geophys. Res., 77, 4116, 1972.

(38) O'Brien, B. J., Direct observations of dumping of electrons at 1000 - kilometer altitudes and high latitudes, J. Geophys. Res., 67, 1227 - 1233, 1962.

(39) Rees, M. H., Auroral electrons, Space Sci. Rev., 10, 413-441, 1969.

(40) Burch, J. L., Low-energy electron fluxes at latitudes above the auroral zone, J. Geophys. Res., 73, 3585 - 3591, 1968.

(41) Mead, G. D., Deformation of the geomagnetic field by the solar wind, J. Geophys. Res., 69, 1181 -1195, 1964.

(42) Mead, G. D., and D. H. Fairfield, Two quantitative magnetosphere models derived from satellite magnetometer data, EOS, 53, 1099, 1972.

(43) Alfvén, H., Cosmical electrodynamics, Oxford Univ. Press. London, 1950.

(44) Heitler, W., The Quantum theory of radiation, Clarendon Press, Oxford, 1944.

(45) Jackson, J. E., The analysis of topside ionograms, NASA-Rpt. X-615-67-452, 1967.

(46) Ratcliffe, J. A., The magneto-ionic theory and its applications to the ionosphere, A Monograph, Cambridge Univ. Press, Cambridge, 1962.

(47) Oostens, J., S. Prünster, C. L. Wang and L. C. L. Yuan, Transition radiation from relativistic charged particles and its energy dependence, Phys. Rev. Letters, 19, 541-543, 1967.

(48) Yuang, L. C. L., C. L. Wang and S. Prunster, X-ray transition radiation applied to the detection of superhigh-energy particles, Phys. Rev. Letters, 23, 496 - 498, 1969.

(49) Smith, R. L. and N. Brice, Propagation in multicomponent plasmas, J. Geophys. Res., 69, 5029-5040, 1964.

(50) Mead, G., and D. H. Fairfield, Two quantitative magnetospheric models derived from satellite magnetometer data, Transactions AGU, 53, 1099, 1972.

(51) Russel, C. T. and R. M. Thorne, On the structure of the inner magnetosphere, Cosmic Electrodynamics 1, 67-89, 1970.

(52) Brace, L. H., H. G. Mayr and K. K. Mahajan, A polar maximum of electron concentration at 1000 km altitude, J. Atmos. Terr. Phys. 32, 1945-1957, 1970.

(53) Banks, P. M., A. F. Nagy and W. I. Axford, Dynamical behavior of thermal protons in the mid-latitude ionosphere and magnetosphere, Planet. Sp. Sci., 19, 1053-1067, 1971.

(54) Brice, N. M. and R. L. Smith, Lower hybrid resonance emissions, 70, 71-80, 1965.

(55) Manoranjan, Rao, S. K. Dikshit, and B. A. P. Tantry, Incoherent Cerenkov radiation in the magnetosphere and the ground observations of VLF hiss, J. Geophys. Res., 78, 191-196, 1973.

FIGURE CAPTIONS

Figure 1. The phase velocity, V_{ph} in km/sec of waves in plasma as a function of angular frequency of the wave, ω in sec^{-1} in various propagation modes in the plasma, where the gyrofrequency of electron, f_H and the electron-plasma frequency f_N are assumed to be 10 kHz and 30 kHz, respectively. Other notations are described in the list of Appendix A.

Figure 2. The critical velocity of electron $\beta=V/c$ as a function of kinetic energy E (in KeV), and the refractive index $n=c/V_{ph}$, of medium, corresponding to the critical velocity. The value of n is indicated in the right side of ordinates. The top scale of abscissa is the kinetic energy in eV for given β.

Figure 3. Square of refractive index n^2 of the plasma given by (2.9) versus ω/Ω_e where $\Omega_e=836$ kHz is assumed for computation. The dotted and hatched domains indicate possible propagation modes of waves for the right-handed and left-handed polarization, respectively. The numbers attached to boundaries of each domain are angle of propagation direction from the direction of magnetic field in degree. Dashed lines in each domains indicate 45^o propagation from the field line. ω_{UH} stands for the upper hybrid frequency given by (C-10). (a), (b) and (c) in Figure 3 correspond for the cases of $\Pi_e=2\Omega_e$, $\Pi_e=\Omega_e$ and $\Pi_e=0.5\ \Omega_e$, respectively.

Figure 4. Comparison of the Mead-Fairfield model-1972 (MF-72, Kp $\leq$ 2) earth's magnetic field (heavy lines) with the centered dipole field (thin lines). The field lines are shown in the noon-midnight meridional plane where the field lines of MF-72 starting from the daytime side of the surface and from the nighttime side are drawn by full lines and dashed lines, respectively.

Figure 5. Field lines, arc length and electron gyrofrequency of the Mead-Fairfield 1972 (MF-72, Kp $\lesssim$ 2) model of the earth's magnetic field. The units of gyrofrequency is kHz. The interval between marks along field lines are 1.0 R_E in (a) and 0.2 R_E in (b), respectively.

Figure 6. Spatial distributions of the plasma constituents in the daytime side of the ionosphere and magnetosphere. The number density (in cm^{-3}) of electrons (e^-), protons (H^+) and oxygen ions (O^+) are plotted against geomagnetic latitude by dashed lines, by full lines and by dash-dotted lines, respectively. Figures are shown for the altitudes of (a) 500 km, (b) 4000 km above the earth's surface and (c) 5 R_E geocentric distance (1.9×10^4 km above the surface).

Figure 7. Spatial distribution of the geoplasma in nighttime side. Notations of lines are the same as those in Figure 6, and the altitudes are (a) 300 km, (b) 600 km, (c) 1000 km, (d) 4000 km, (e) 3 R_E and (f) 10 R_E, respectively.

Figure 8. The altitude dependence of the characteristic frequencies of magnetoplasma in the daytime side of the earth's ionosphere and magnetosphere, i.e., the upper hybrid resonance frequency (UHR), f_{UH}, the gyrofrequency of electron, f_H, the plasma frequency, f_N and the lower hybrid resonance frequency (LHR), f_{LH}. The altitude is measured along the field line from the earth's surface, s (in km) for the geomagnetic latitude at the surface (a) 80^o, (b) 70^o and (c) 60^o, respectively.

Figure 9. The same as Figure 8 for the nighttime side, along the field line from the geomagnetic latitude (a) 80^o, (b) 75^o, (c) 70^o and (d) 60^o, respectively.

Figure 10. The power generated at Cherenkov radiation by an electron with energy E (in keV) and pitch angle 0^o at frequencies between 1 kHz and 1 MHz as a function of distance from the ground along the field line of geomagnetic latitude 80^o in daytime side. Two figures correspond to the energy of electron (a) 100 keV and (b) 1 keV.

Figure 11. The same as Figure 10 except for different energies of electrons along the field line of 70^o geomagnetic latitude from the ground in the nighttime side. Each figure corresponds to the energy of electrons, (a) 100 keV, (b) 10 keV, (c) 1. keV, and (d) 0.1 keV, respectively.

Figure 12. The power of Cherenkov emission per unit volume in the magnetosphere along 70^{o} field line by the electrons with an energy spectrum $j_e(E) = 4 \times 10^8 E^{-2}$ (cm^{-2} sec^{-1} str^{-1} keV^{-1}). (a) for f=100 and 10 kHz, and (b) for f=50, 20, 5 and 2 kHz, respectively.

Figure 13. The variation of Cherenkov hiss intensity with frequency of the emitted wave and its dependence on the energy spectrum of the hiss producing electrons in night side magnetosphere along field line (a) from 80^{o} geomagnetic latitude dayside and (b) from 70^{o} geomagnetic latitude nightside, respectively. The vertical scale for the soft spectrum electrons, E^{-2} (dashed line) and for the hard spectrum electrons, $E^{-1.2}$ (full line) are in left side and right side, respectively.

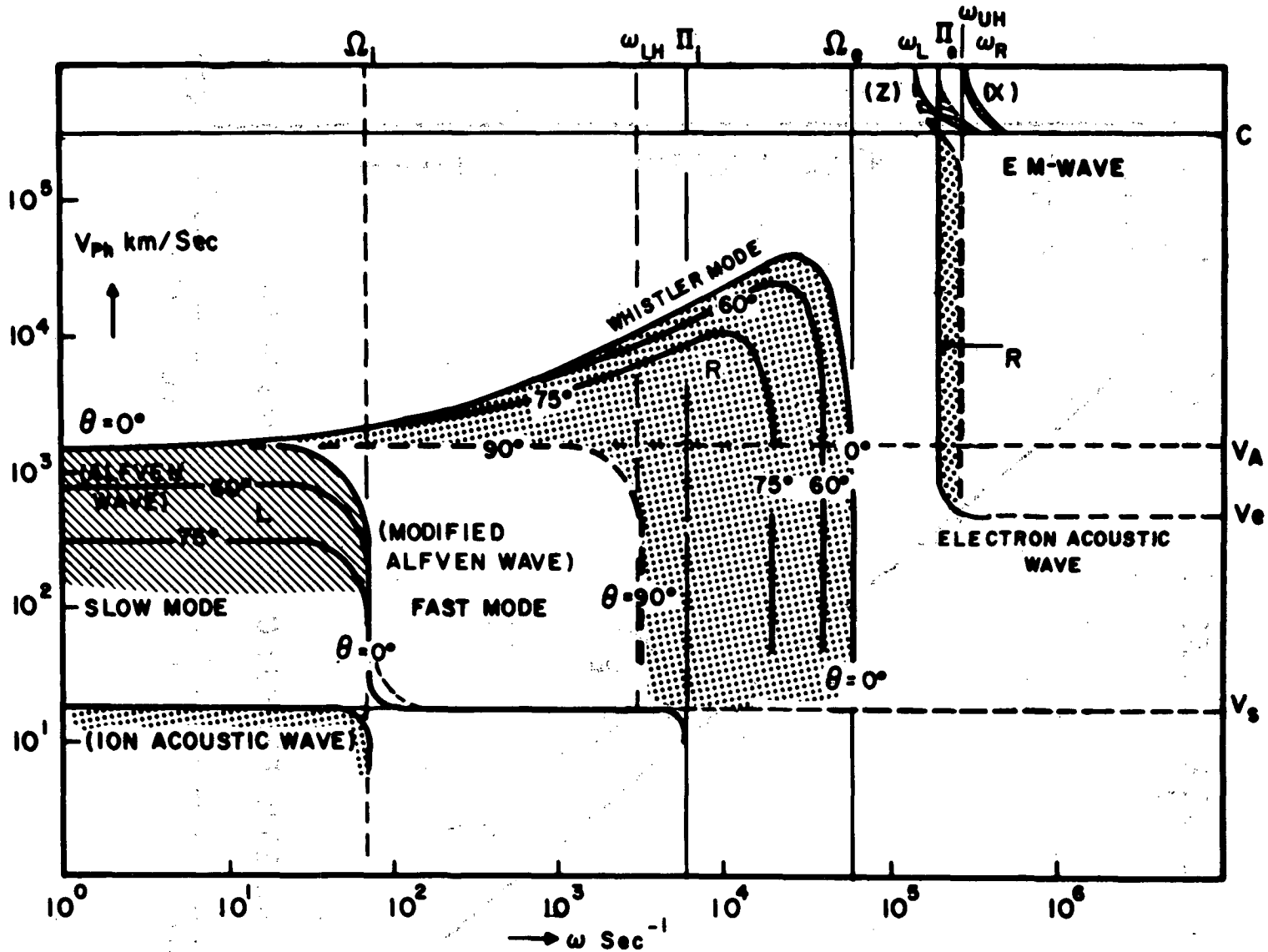
Ω_i
ω_LH
Π_i
Ω_e
ω_L
Π_e
ω_UH
ω_R
(Z)
(X)
C
E M-WAVE
R
V_A
V_e
V_s
ELECTRON ACOUSTIC WAVE
V_Ph km/Sec
WHISTLER MODE
60°
75°
θ=0°
90°
0°
75°
60°
(ELECTRON L WAVE)
60°
L
75°
(MODIFIED ALFVEN WAVE)
FAST MODE
θ=90°
θ=0°
θ=0°
SLOW MODE
(ION ACOUSTIC WAVE)
10^5
10^4
10^3
10^2
10^1
10^0
10^1
10^2
10^3
10^4
10^5
10^6
ω Sec^-1

Fig. 1

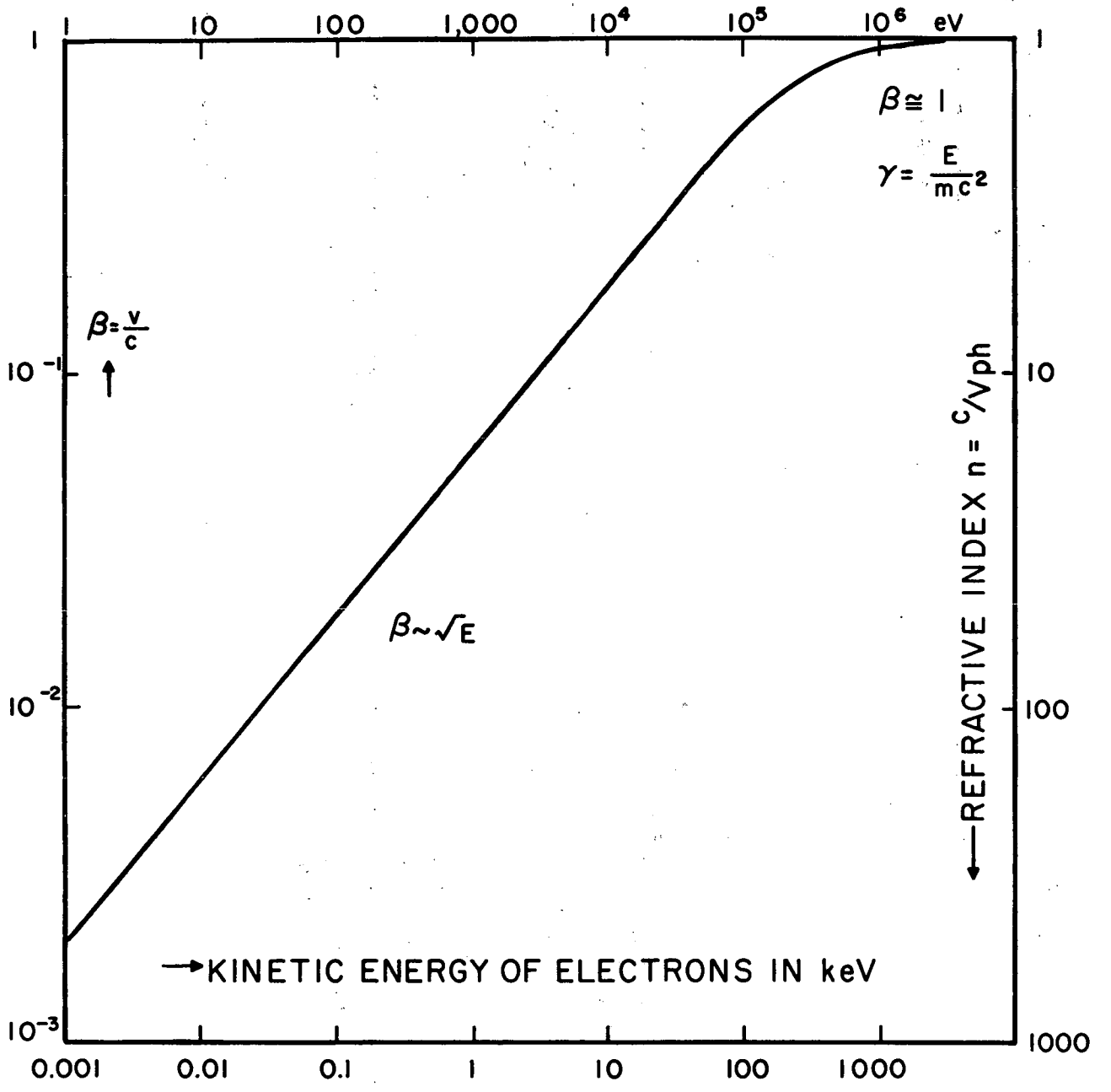
1
10
100
1,000
10^4
10^5
10^6 eV
$\beta \cong 1$
$\gamma = \frac{E}{mc^2}$
$\beta = \frac{v}{c}$
10^{-1}
10^{-2}
10^{-3}
$\beta \sim \sqrt{E}$
REFRACTIVE INDEX $n = c/v_{ph}$
10
100
1000
KINETIC ENERGY OF ELECTRONS IN keV
0.001
0.01
0.1
1
10
100
1000

Fig. 2

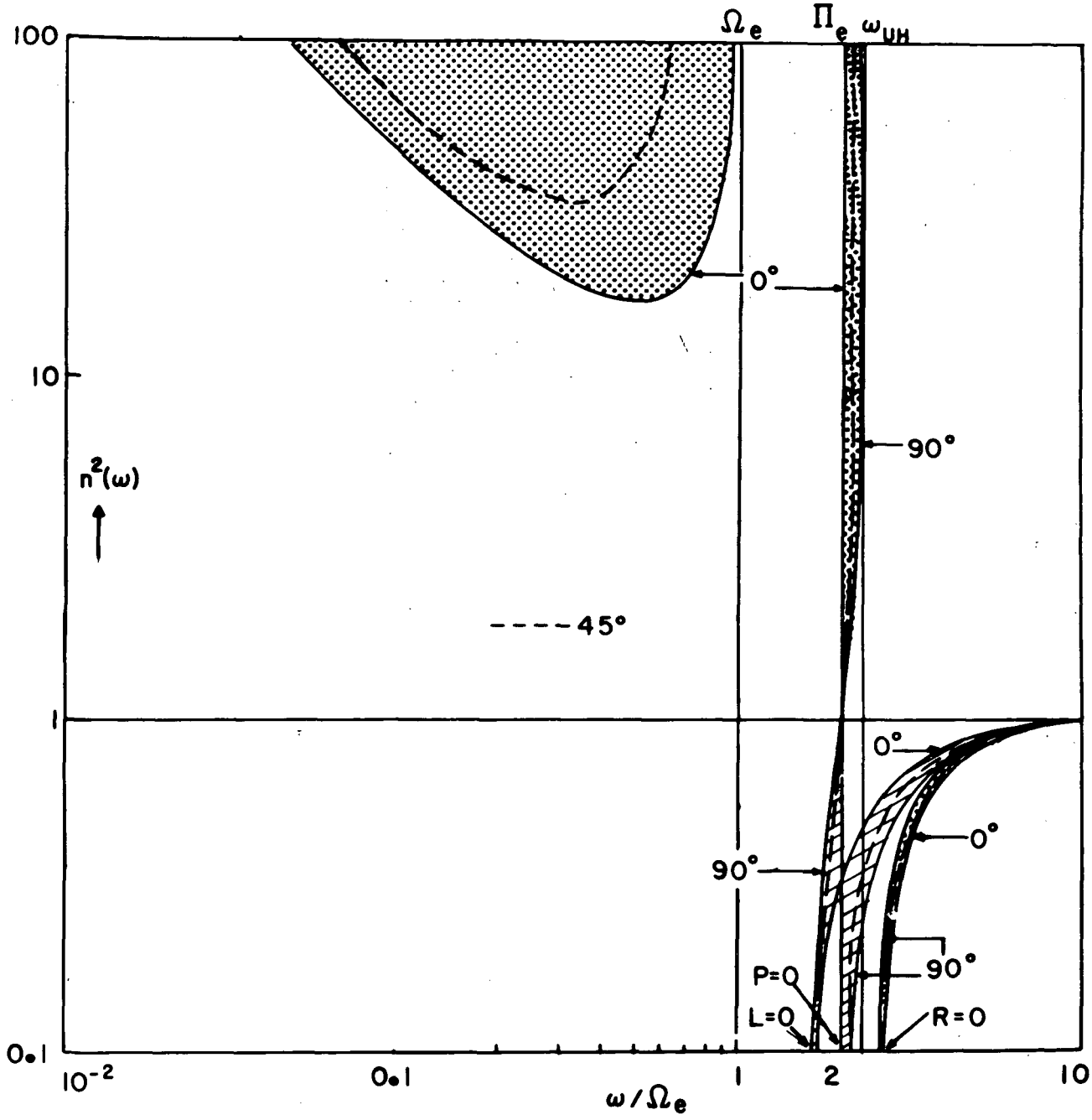
100
10
1
0.1
Ω_e
Π_e
ω_{UH}
0°
90°
$n^2(\omega)$
----45°
0°
0°
90°
90°
P=0
L=0
R=0
10^{-2}
0.1
1
2
10
ω/Ω_e

Fig.3(a)

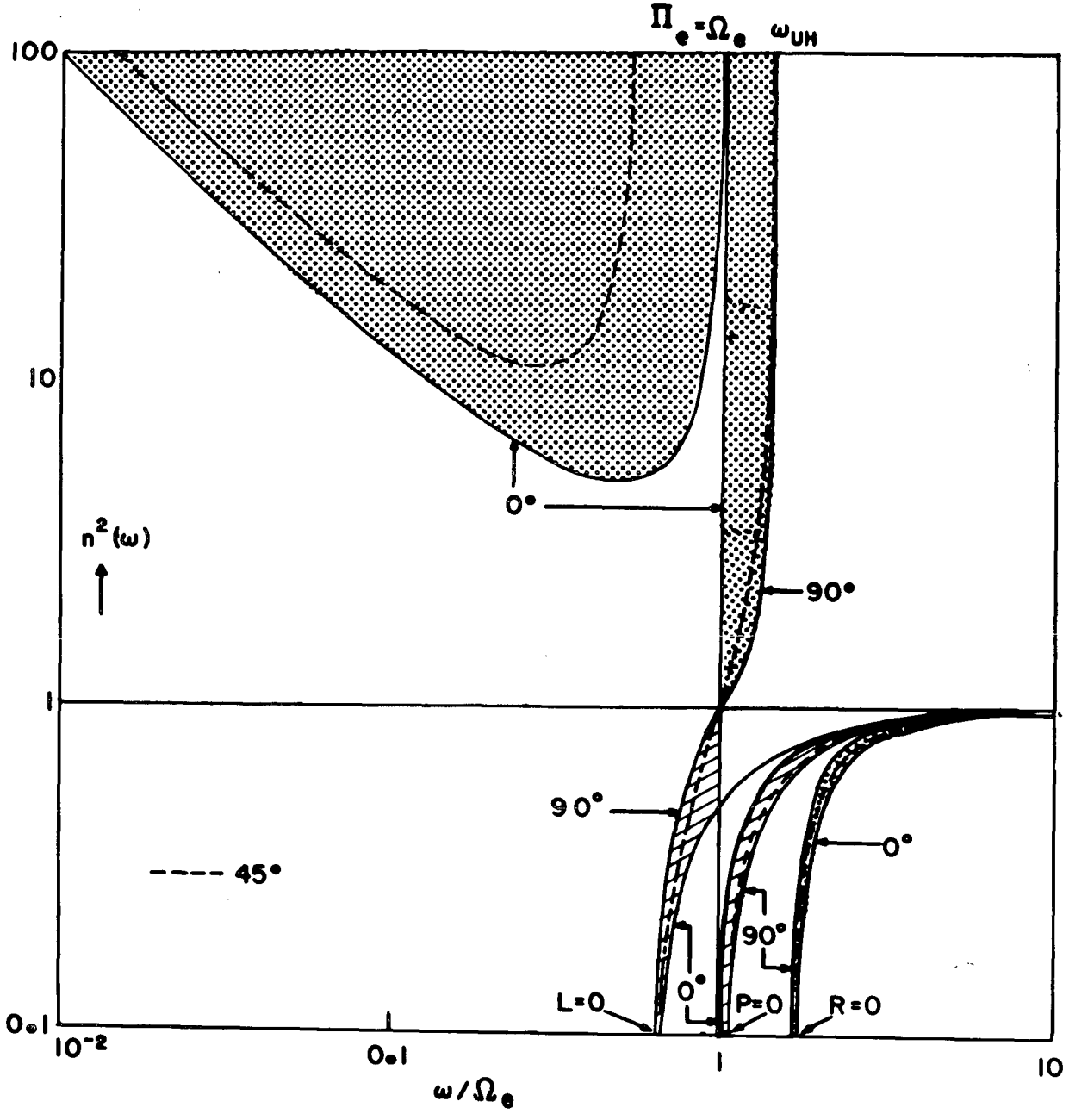
$\Pi_e = \Omega_e$
ω_{UH}
100
10
1
0.1
$n^2(\omega)$
0°
90°
90°
0°
45°
90°
0°
L=0
P=0
R=0
10^{-2}
0.1
1
10
ω/Ω_e

Fig. 3(b)

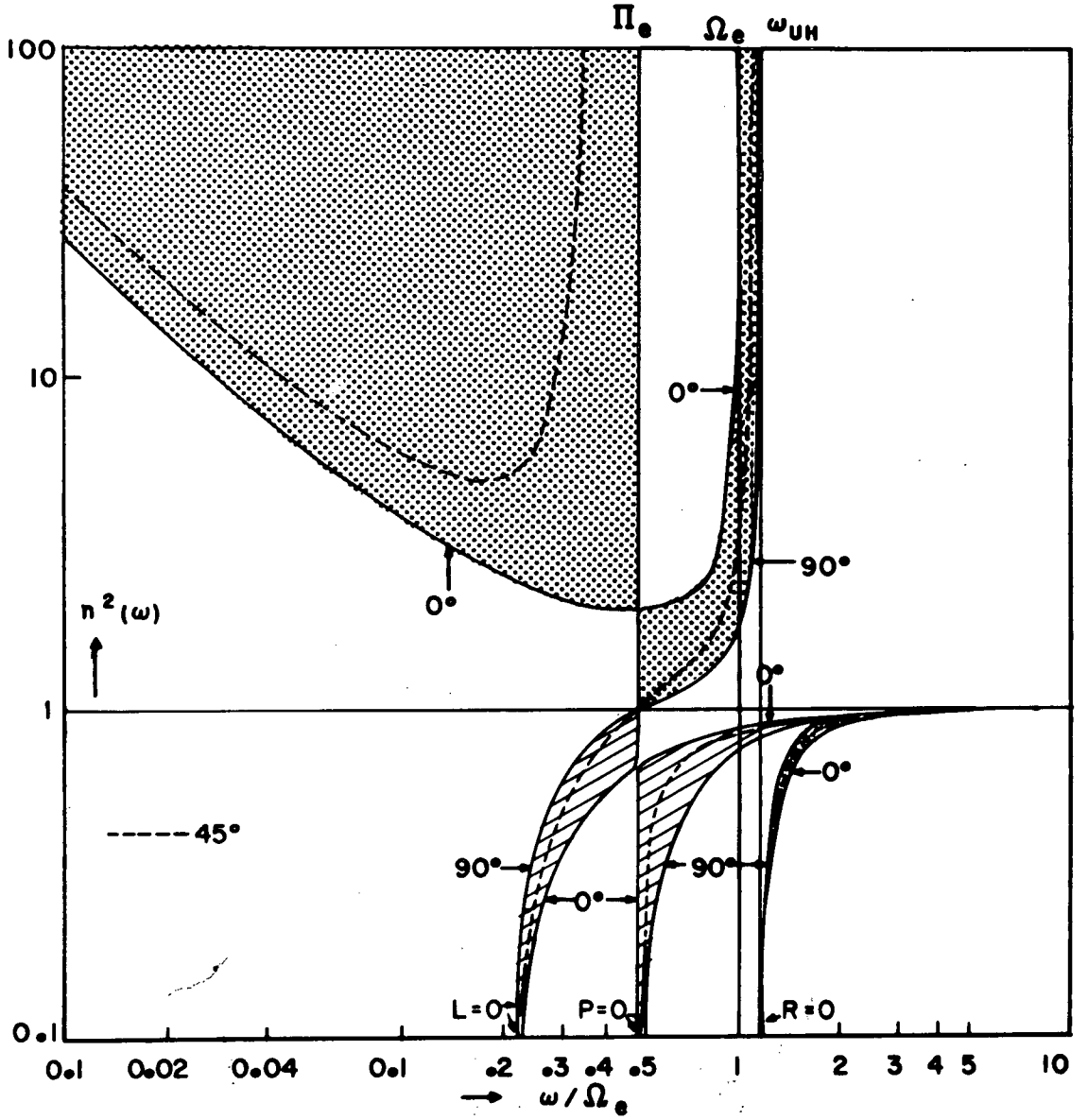
Π_e
Ω_e
ω_UH
100
10
1
0.1
n²(ω)
0°
90°
45°
L=0
P=0
R=0
0.1
0.02
0.04
0.2
0.3
0.4
0.5
2
3
4
5
10
ω/Ω_e

Fig. 3(c)

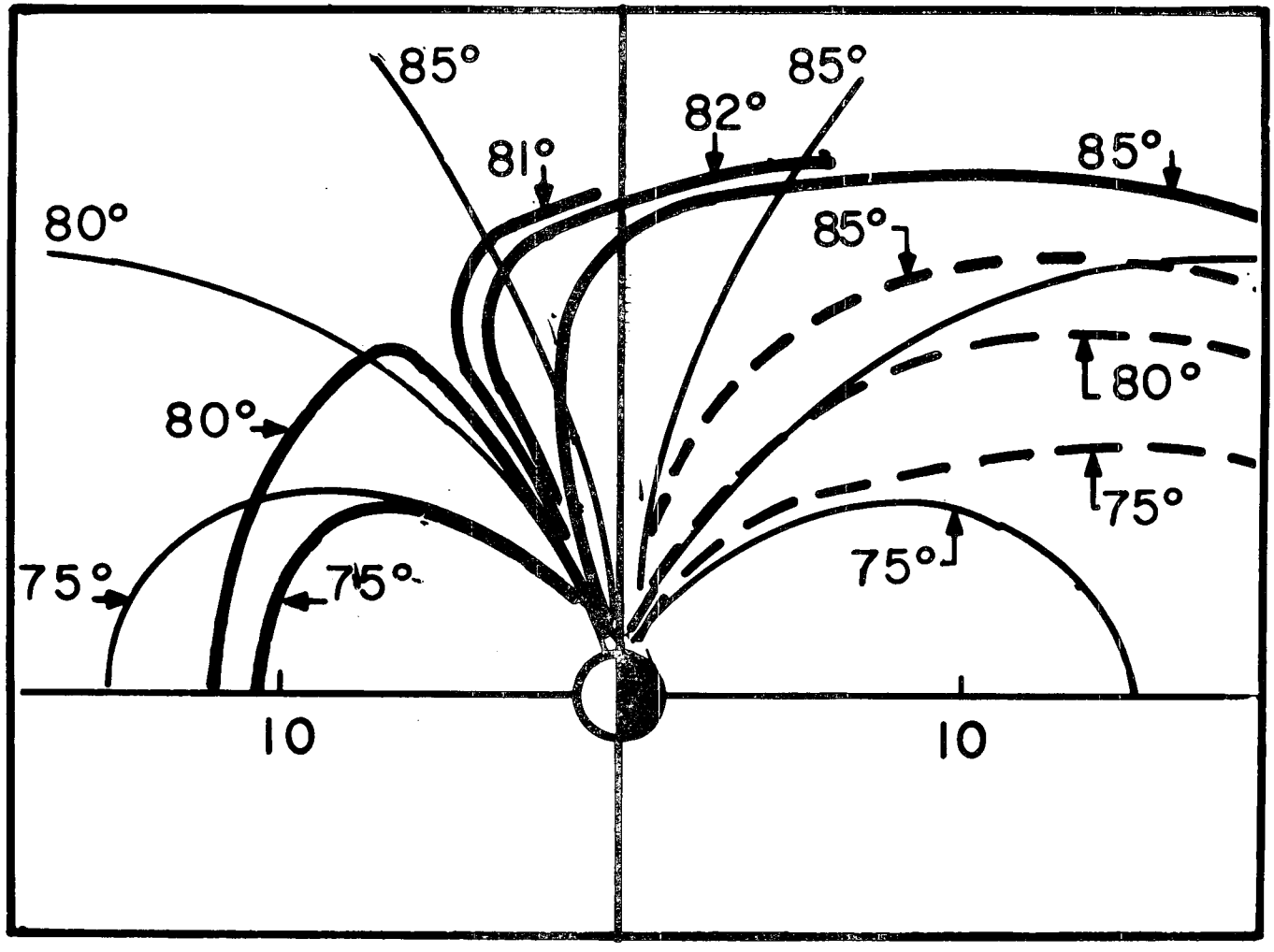

Fig. 4

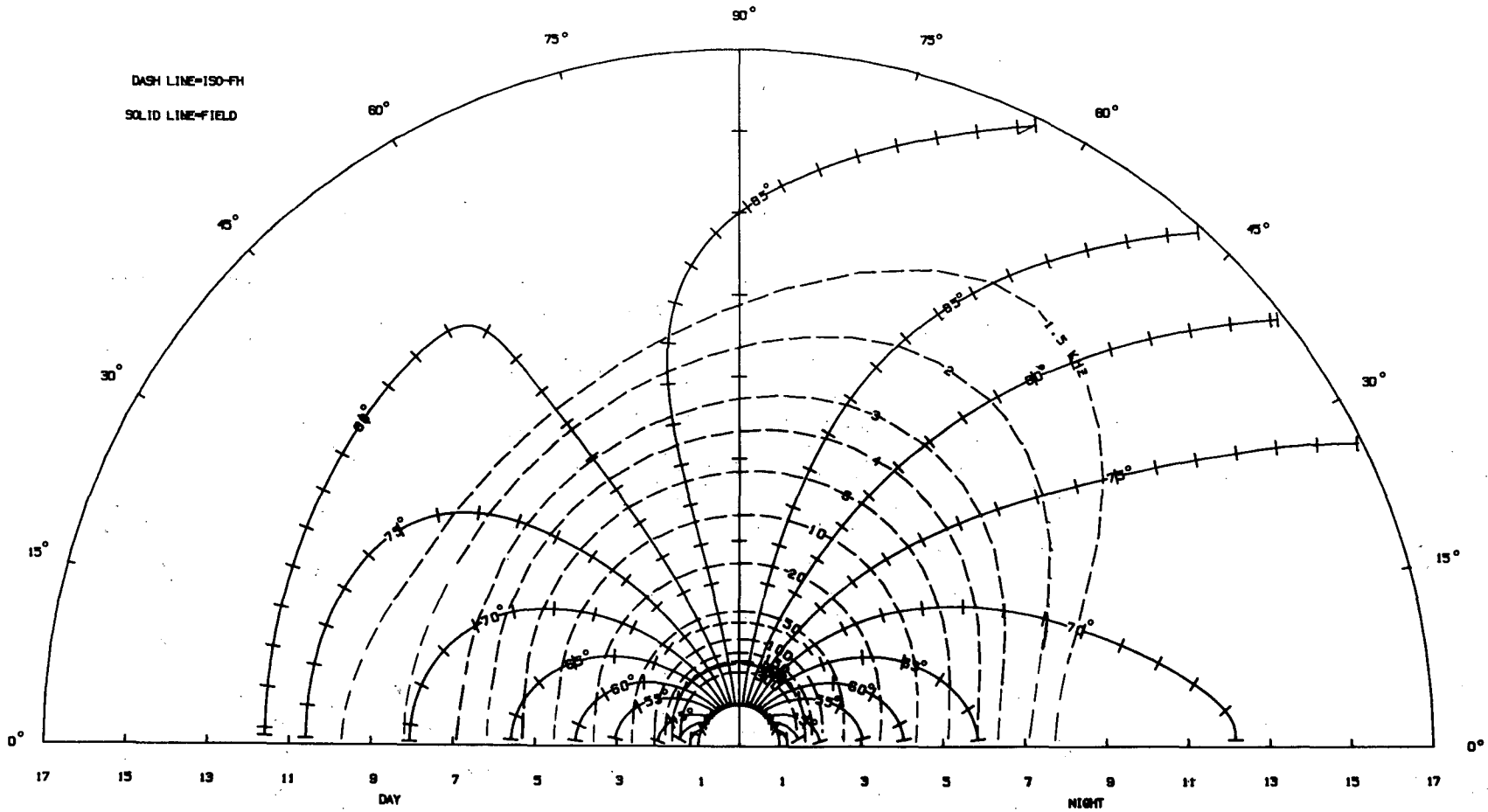
DASH LINE=ISO-FH
SOLID LINE=FIELD
90°
75°
75°
60°
60°
45°
45°
30°
30°
15°
15°
0°
0°
85°
80°
75°
70°
65°
60°
55°
50°
45°
40°
35°
30°
25°
20°
15°
10°
5°
1
2
3
4
6
8
10
20
30
40
50
1.5 FH
17
15
13
11
9
7
5
3
1
1
3
5
7
9
11
13
15
17
DAY
NIGHT

Fig. 5(a)

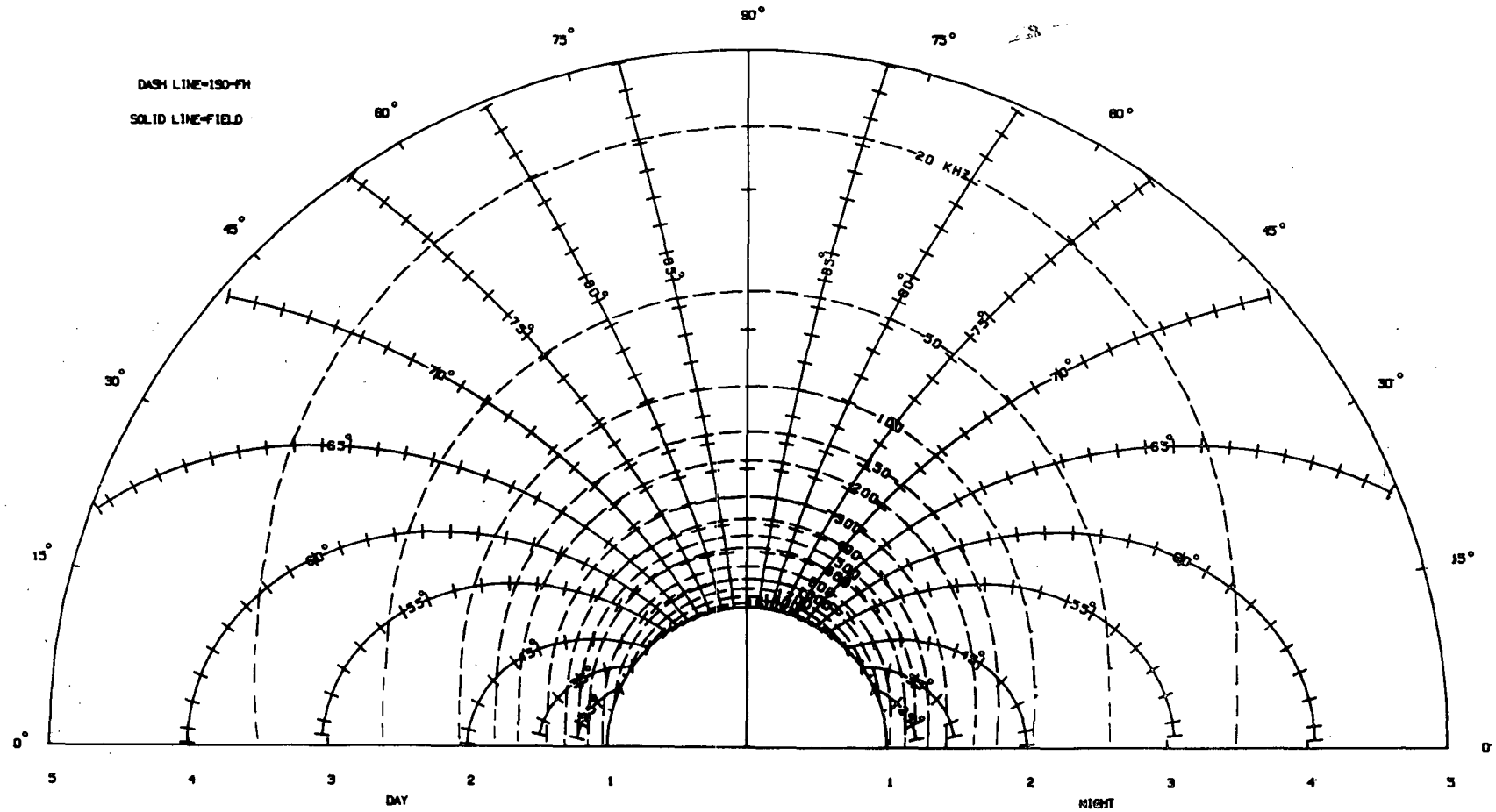
DASH LINE=190-FM
SOLID LINE=FIELD
80°
75°
60°
45°
30°
15°
0°
20 KHz.
30
100
150
200
300
500
1000
65°
55°
DAY
NIGHT
5
4
3
2
1

09

Fig. 5(b)

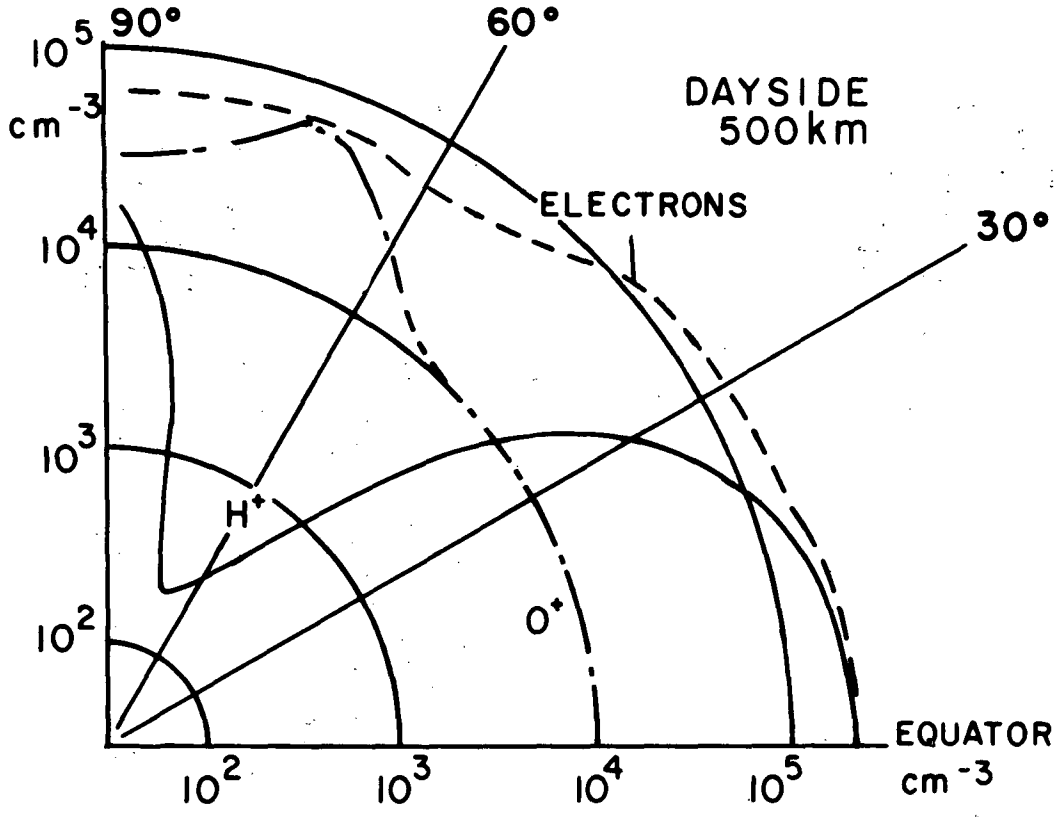
90°
60°
30°
10^5
cm^{-3}
10^4
10^3
10^2
DAYSIDE
500km
ELECTRONS
H^+
O^+
EQUATOR
cm^{-3}
10^2
10^3
10^4
10^5

Fig. 6(a)

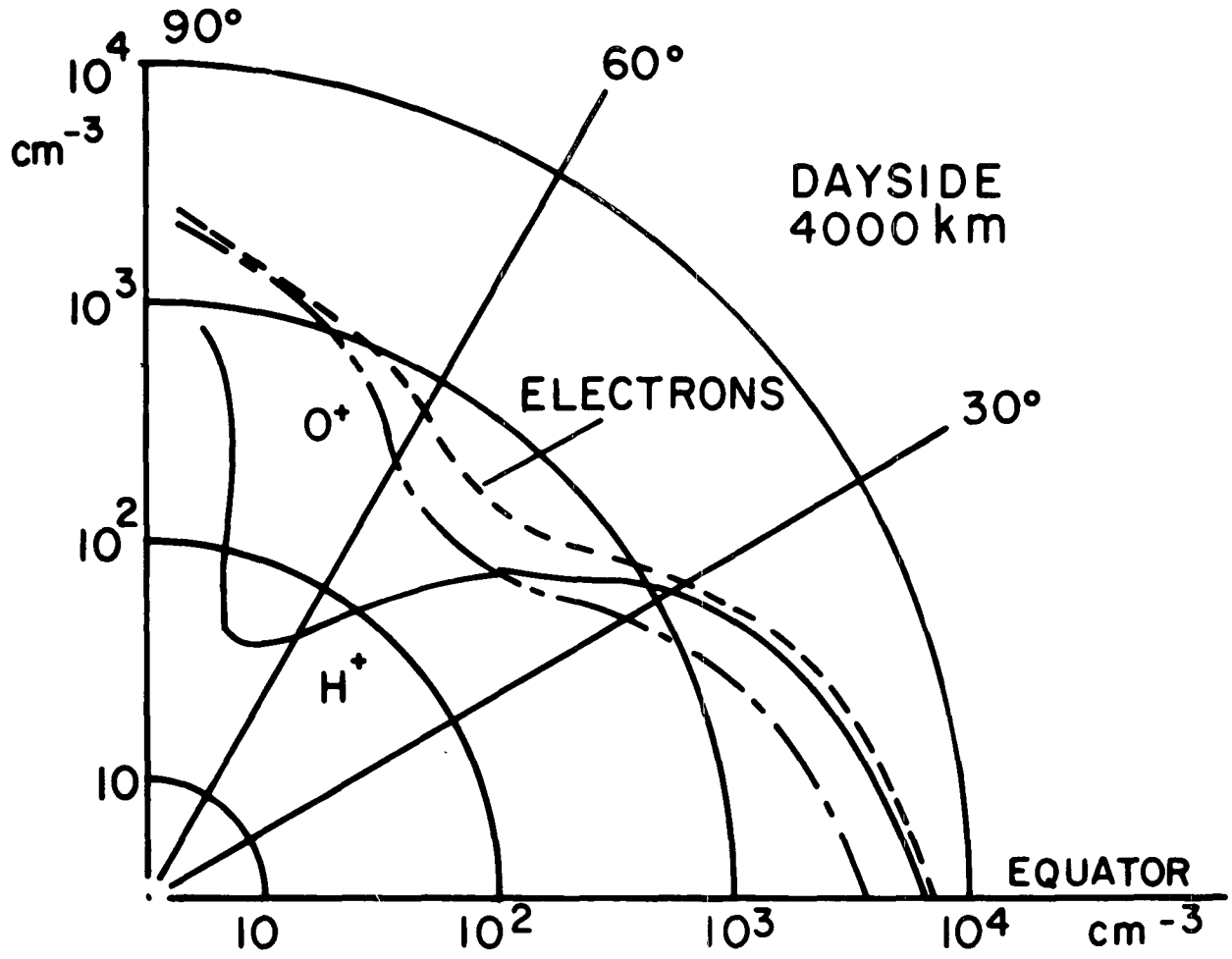
90°
60°
30°
10^4
cm^{-3}
10^3
10^2
10
DAYSIDE
4000 km
ELECTRONS
O^+
H^+
EQUATOR
10
10^2
10^3
10^4
cm^{-3}

Fig. 6(b)

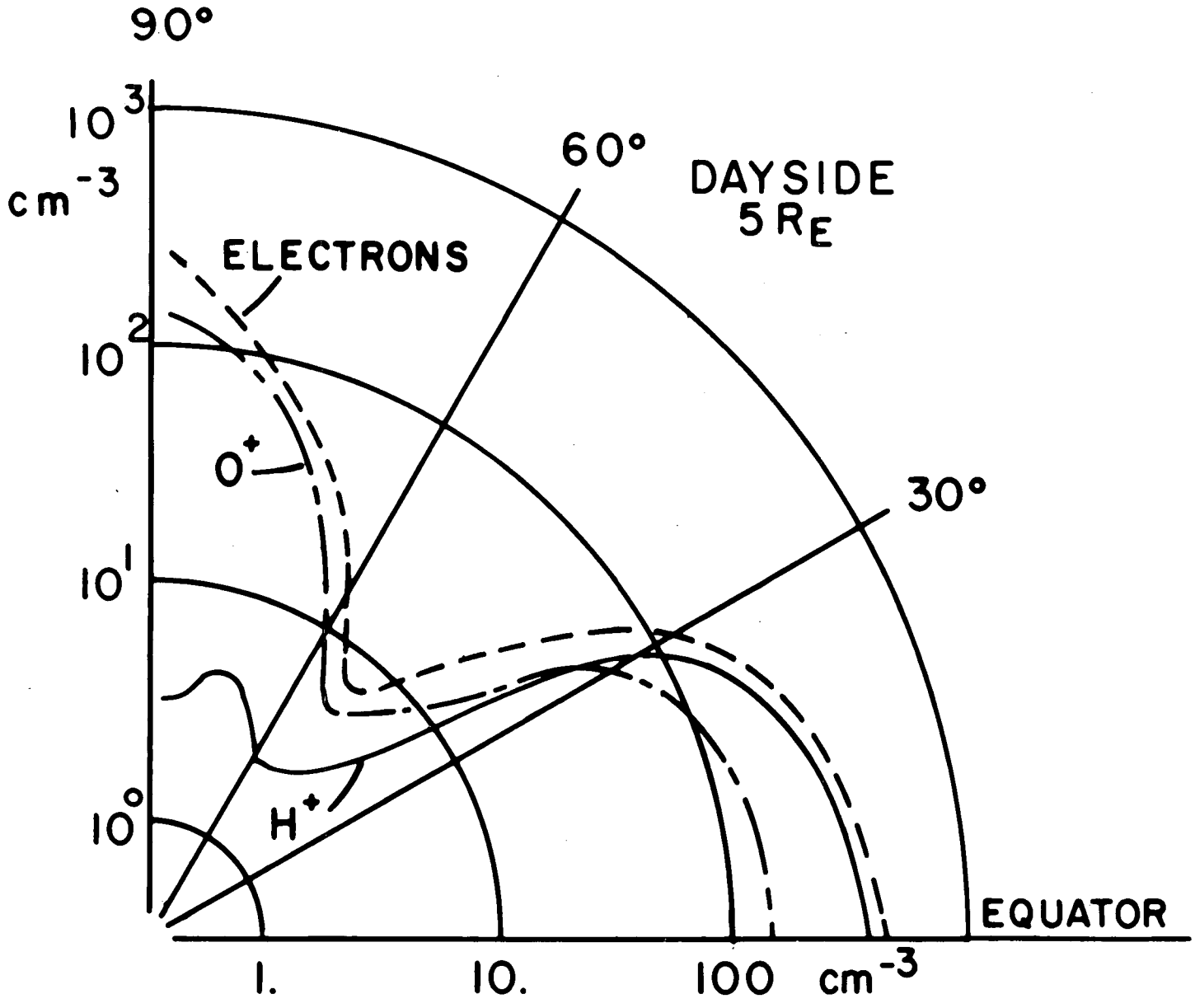
90°
10^3
cm^{-3}
60°
DAYSIDE
$5 R_E$
ELECTRONS
10^2
O^+
30°
10^1
10^0
H^+
EQUATOR
1.
10.
100
cm^{-3}

Fig. 6(c)

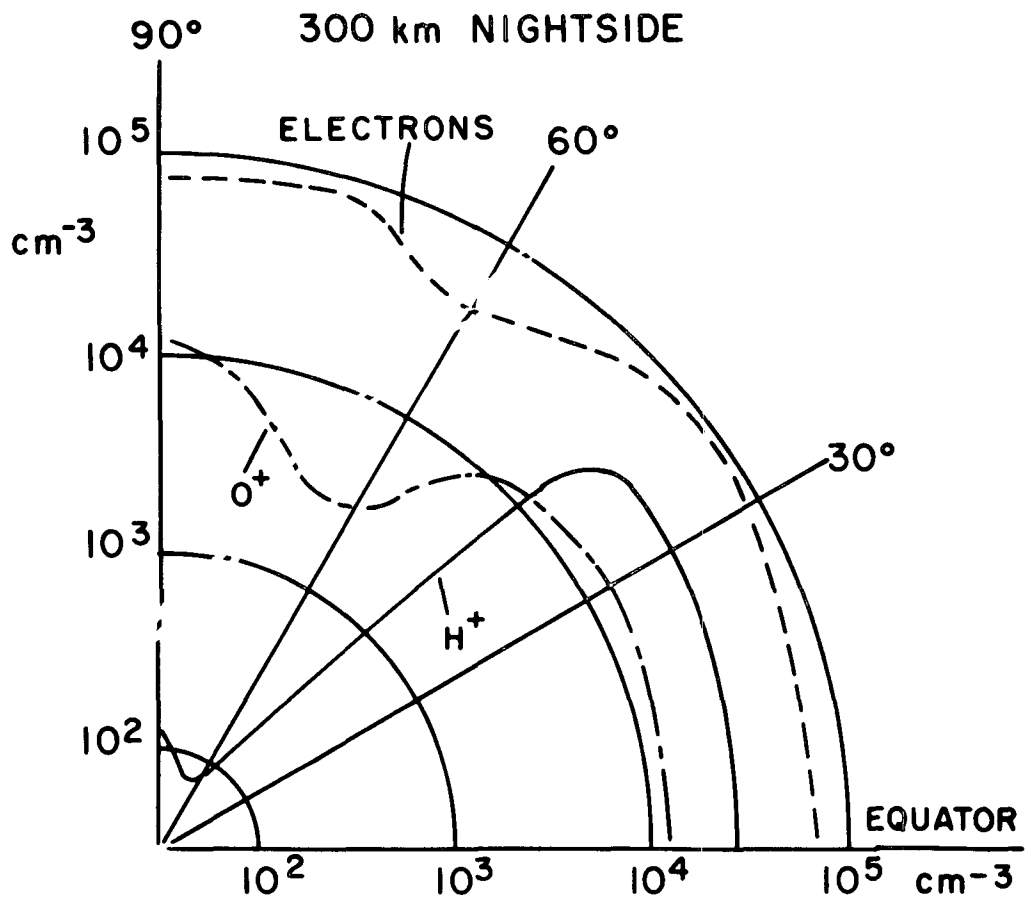
90°
300 km NIGHTSIDE
10^5
ELECTRONS
60°
cm^{-3}
10^4
30°
O^+
10^3
H^+
10^2
EQUATOR
10^2
10^3
10^4
10^5 cm^{-3}

Fig. 7(a)

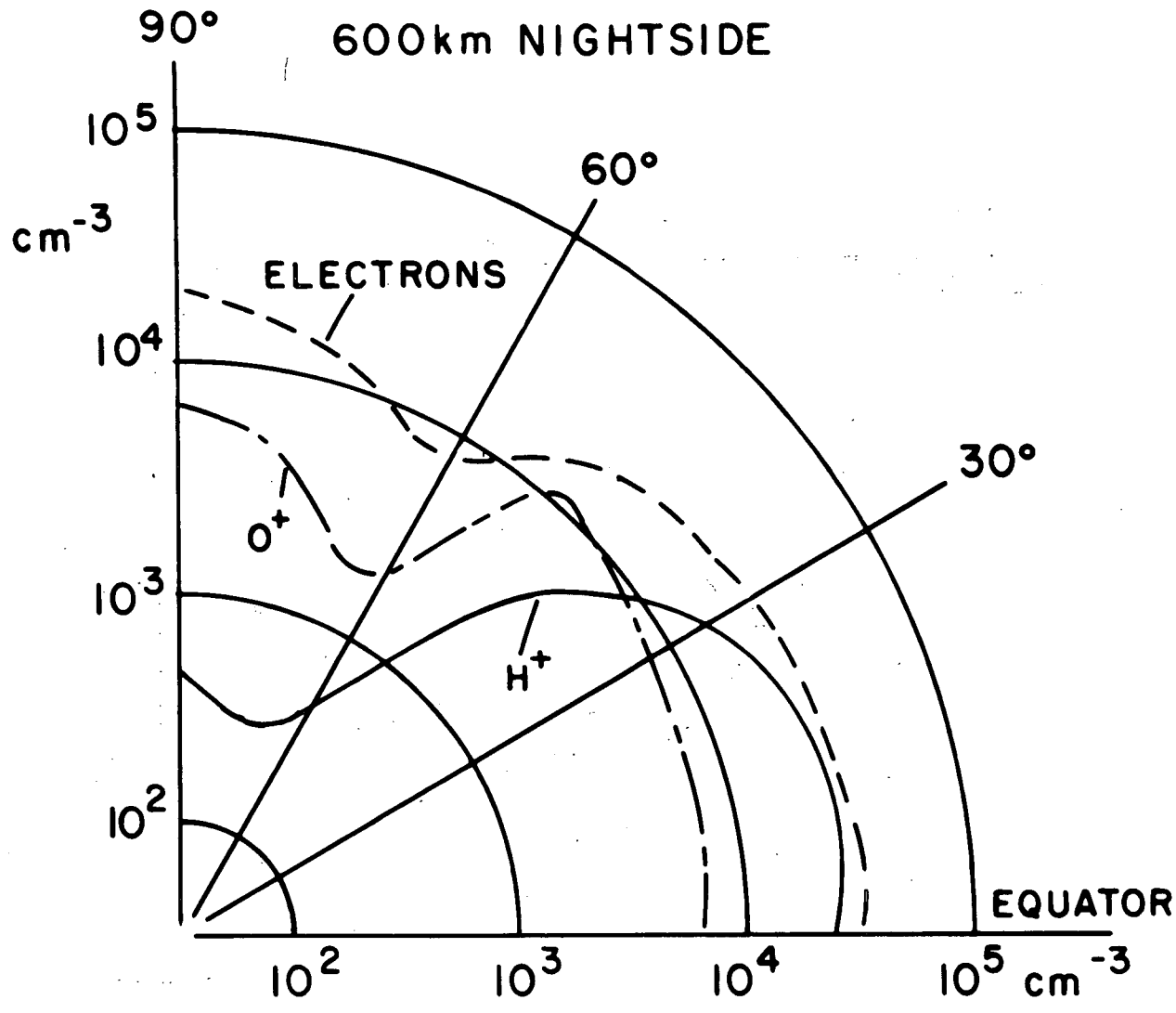
90°
600km NIGHTSIDE
10^5
cm^{-3}
60°
ELECTRONS
10^4
30°
O^+
10^3
H^+
10^2
EQUATOR
10^2
10^3
10^4
10^5 cm^{-3}

Fig. 7(b)

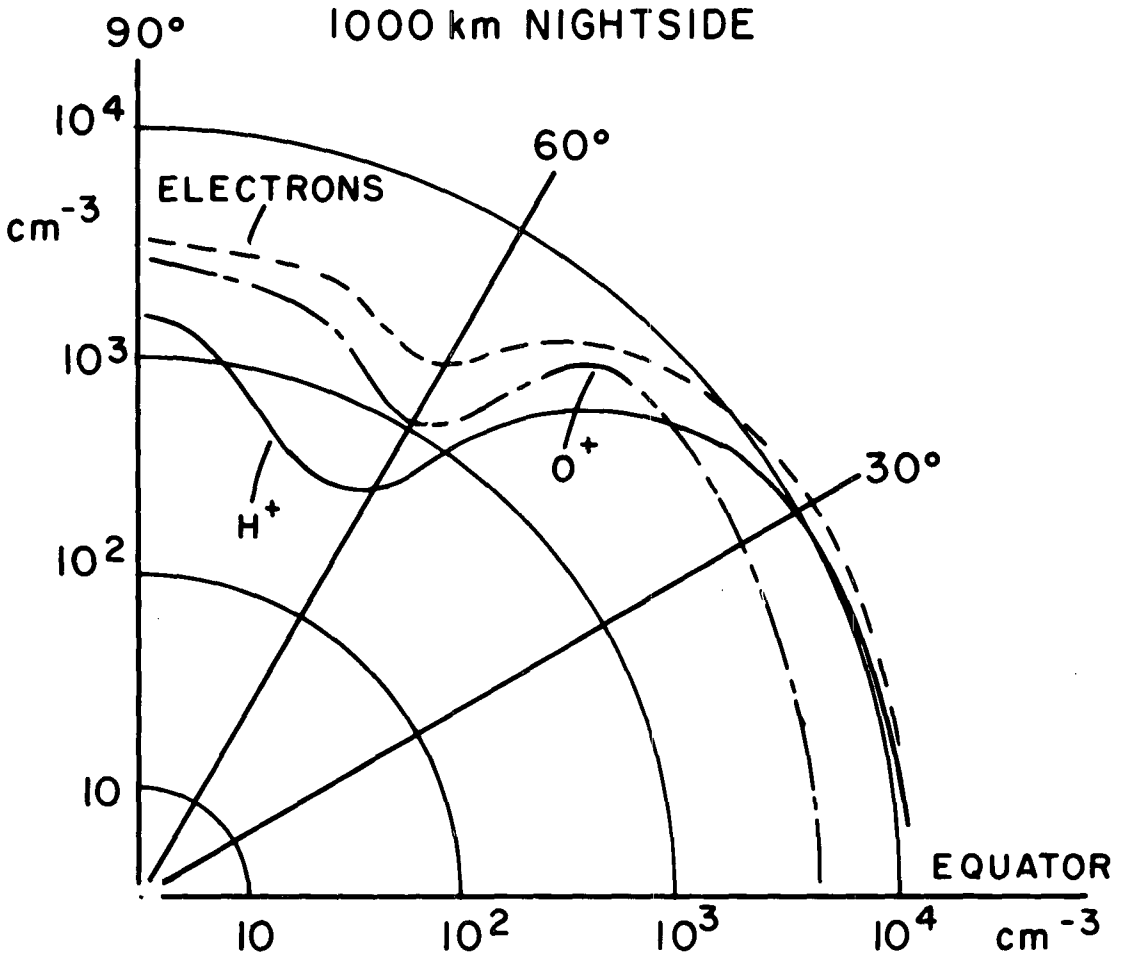
90°
1000 km NIGHTSIDE
10^4
60°
ELECTRONS
cm^{-3}
10^3
O^+
30°
H^+
10^2
10
EQUATOR
10
10^2
10^3
10^4
cm^{-3}

Fig. 7(c)

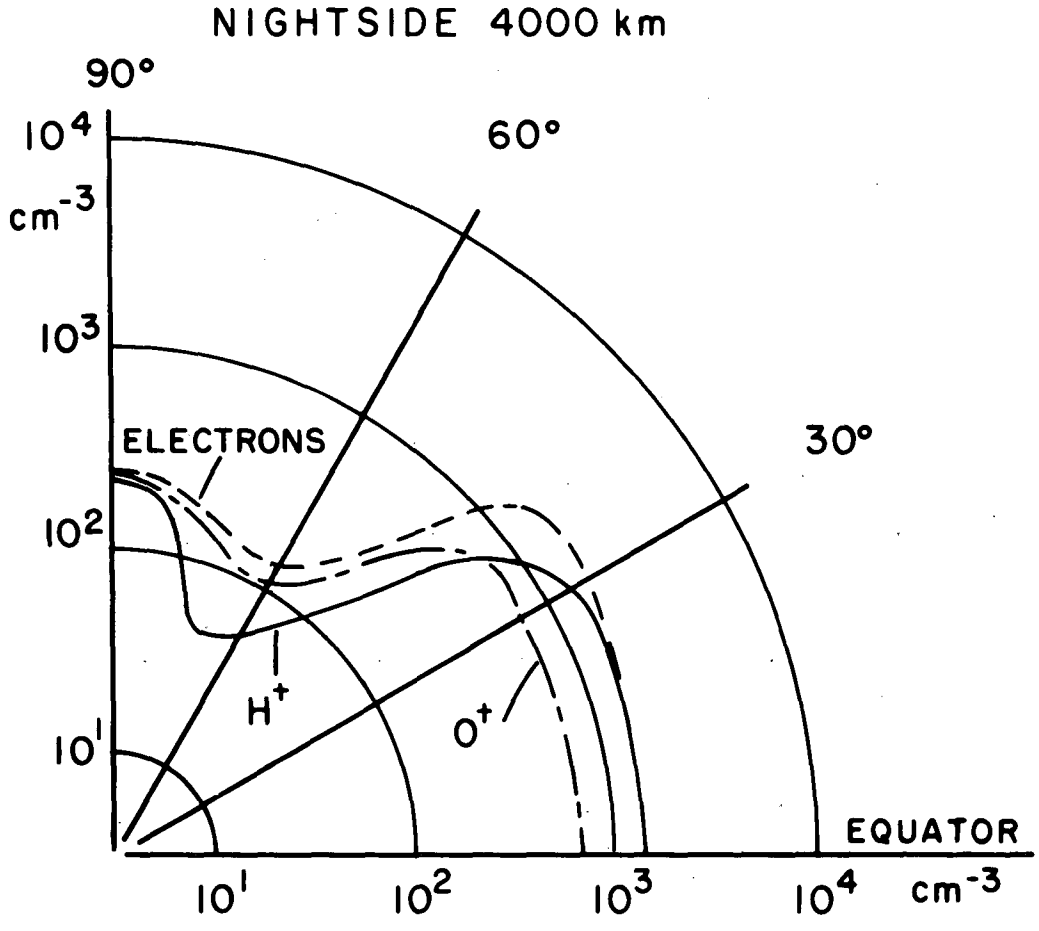
NIGHTSIDE 4000 km
90°
60°
30°
10^4
cm^{-3}
10^3
10^2
10^1
ELECTRONS
H^+
O^+
EQUATOR
10^1
10^2
10^3
10^4
cm^{-3}

Fig. 7(d)

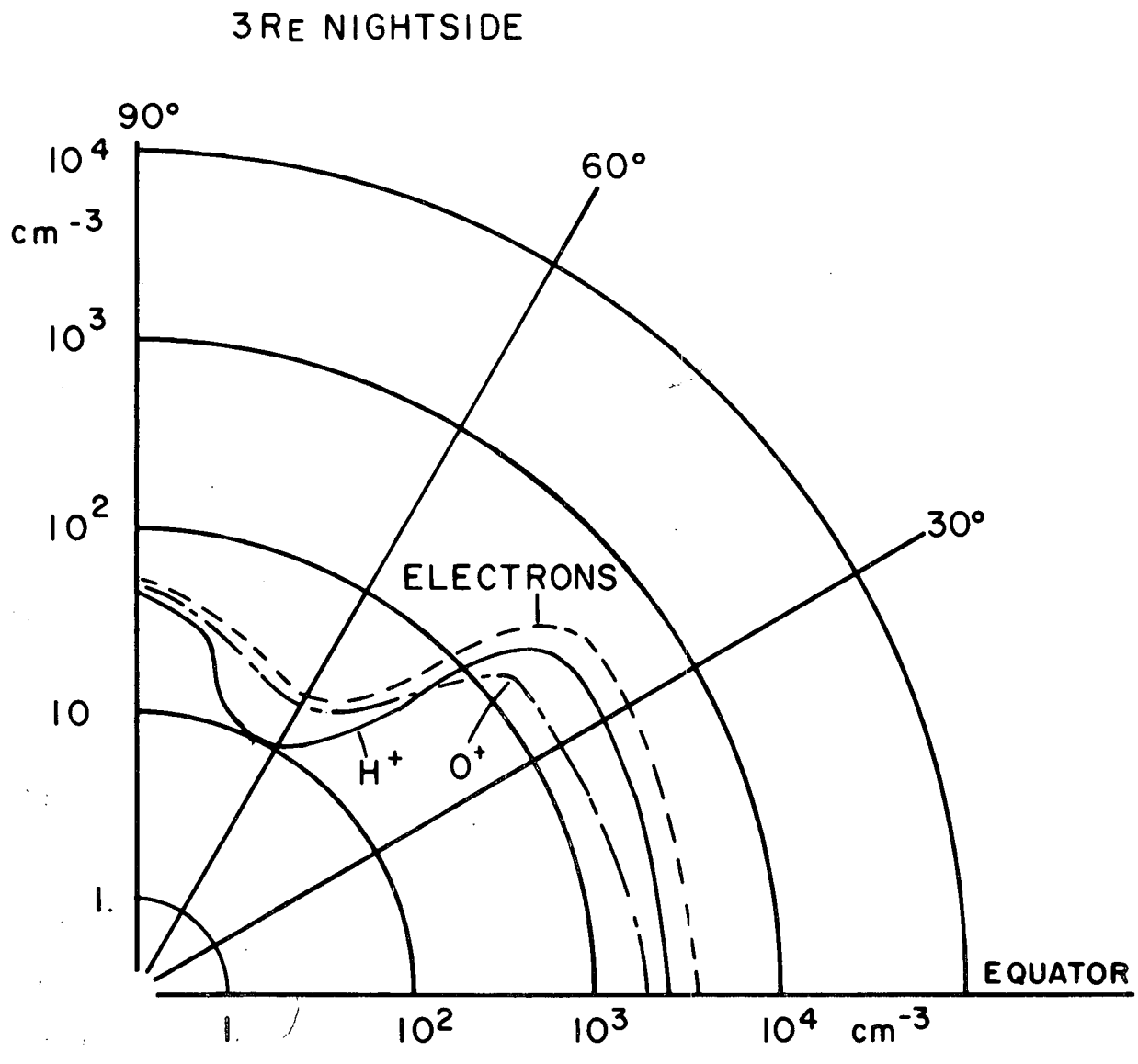
3RE NIGHTSIDE
90°
60°
30°
10^4
cm $^{-3}$
10^3
10^2
10
1.
ELECTRONS
H^+
O^+
EQUATOR
1.
10^2
10^3
10^4 cm^{-3}

Fig. 7(e)

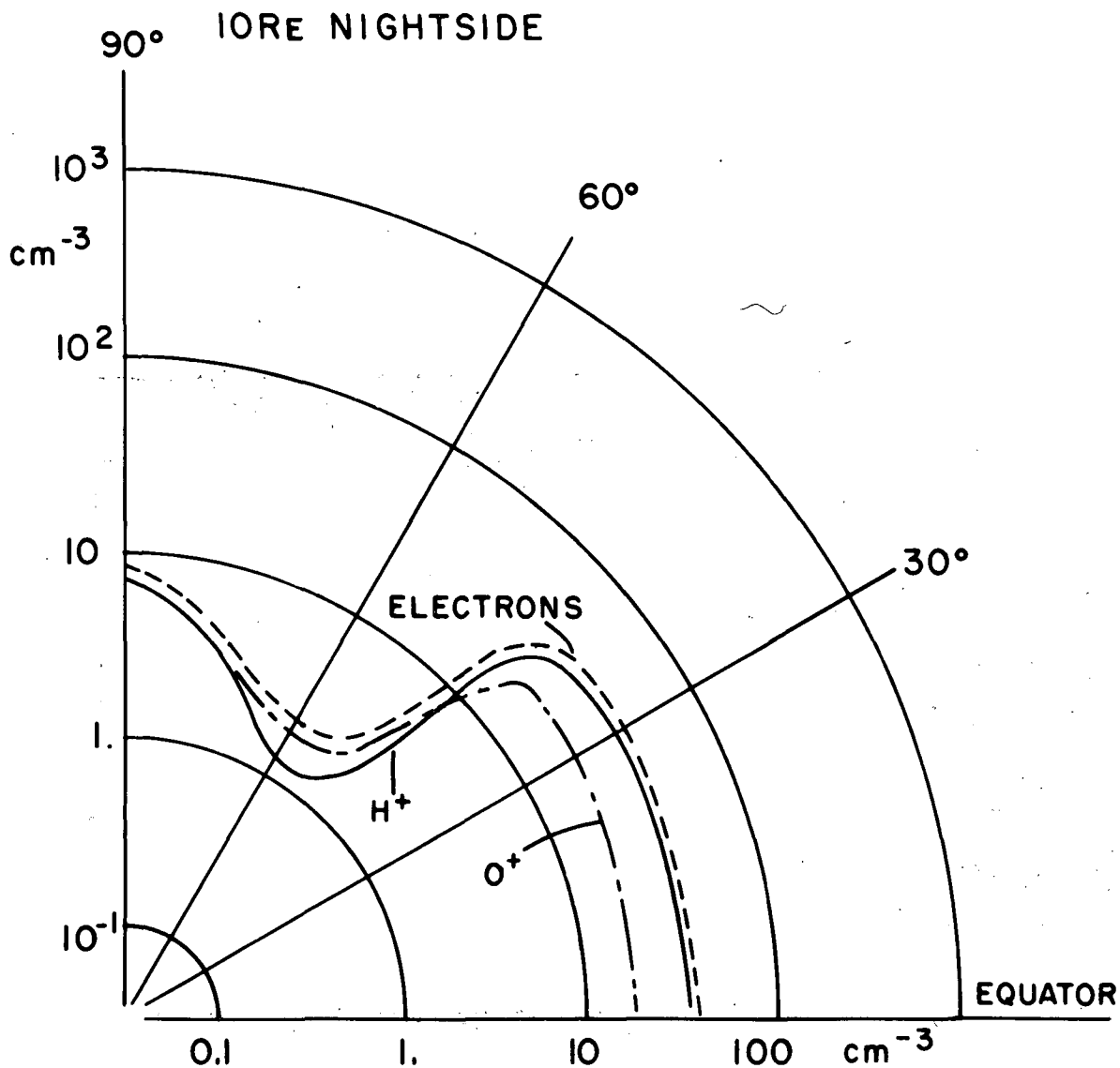
10RE NIGHTSIDE
90°
60°
30°
10^3
cm^{-3}
10^2
10
1.
10^{-1}
ELECTRONS
H^+
O^+
EQUATOR
0.1
1.
10
100
cm^{-3}

Fig. 7(f)

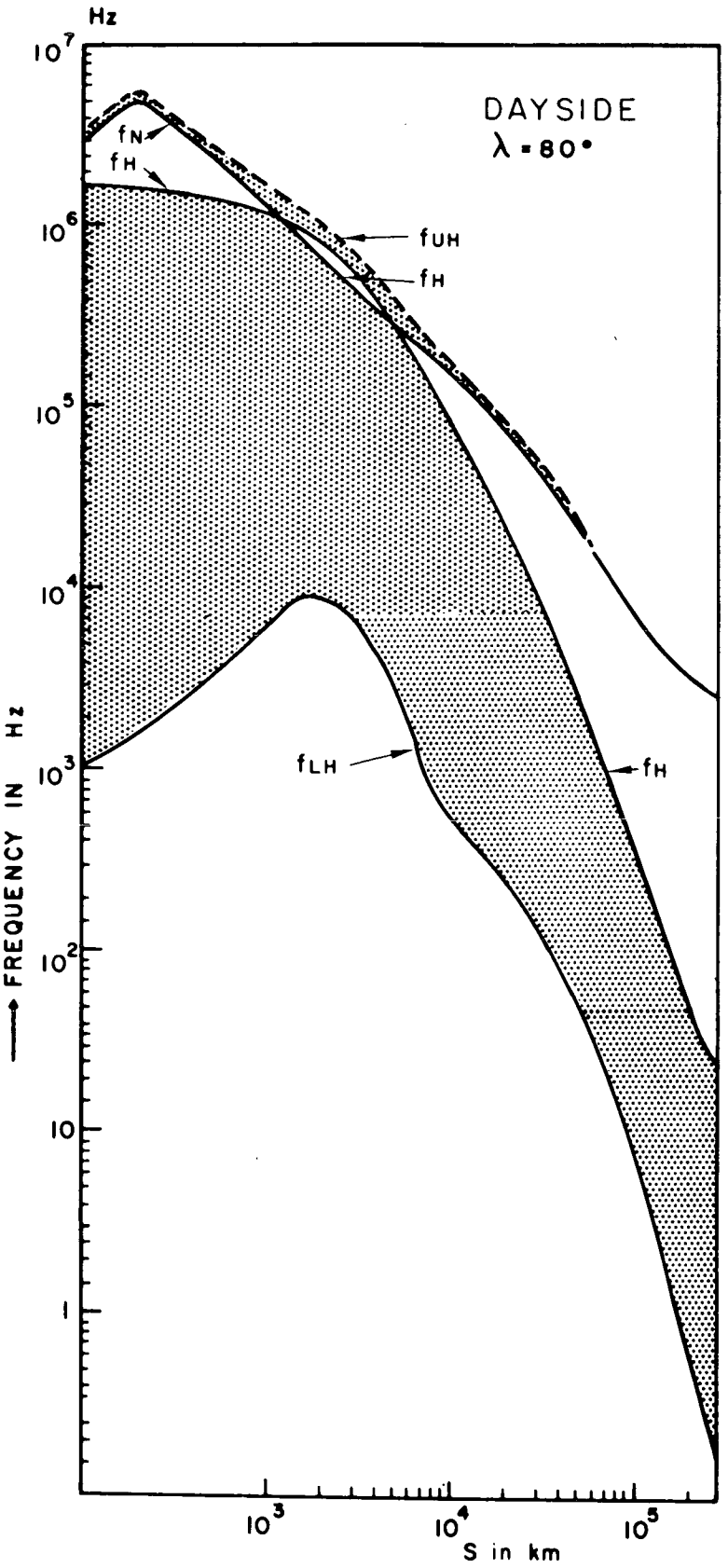

Fig. 8(a)

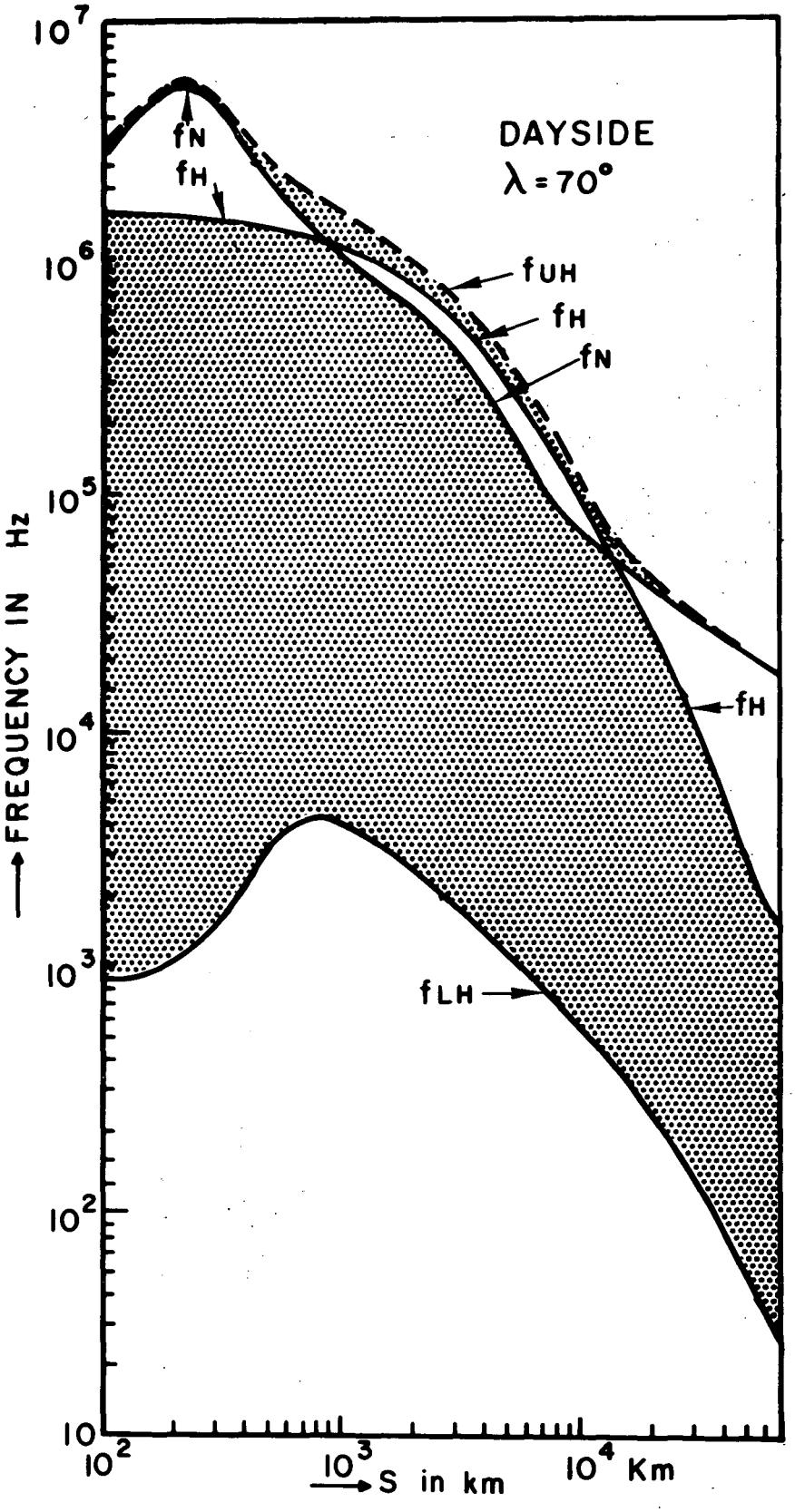
DAYSIDE
λ = 70°
fN
fH
fUH
fH
fN
fH
fLH
FREQUENCY IN Hz
10^7
10^6
10^5
10^4
10^3
10^2
10
10^2
10^3
S in km
10^4 Km

Fig. 8(b)

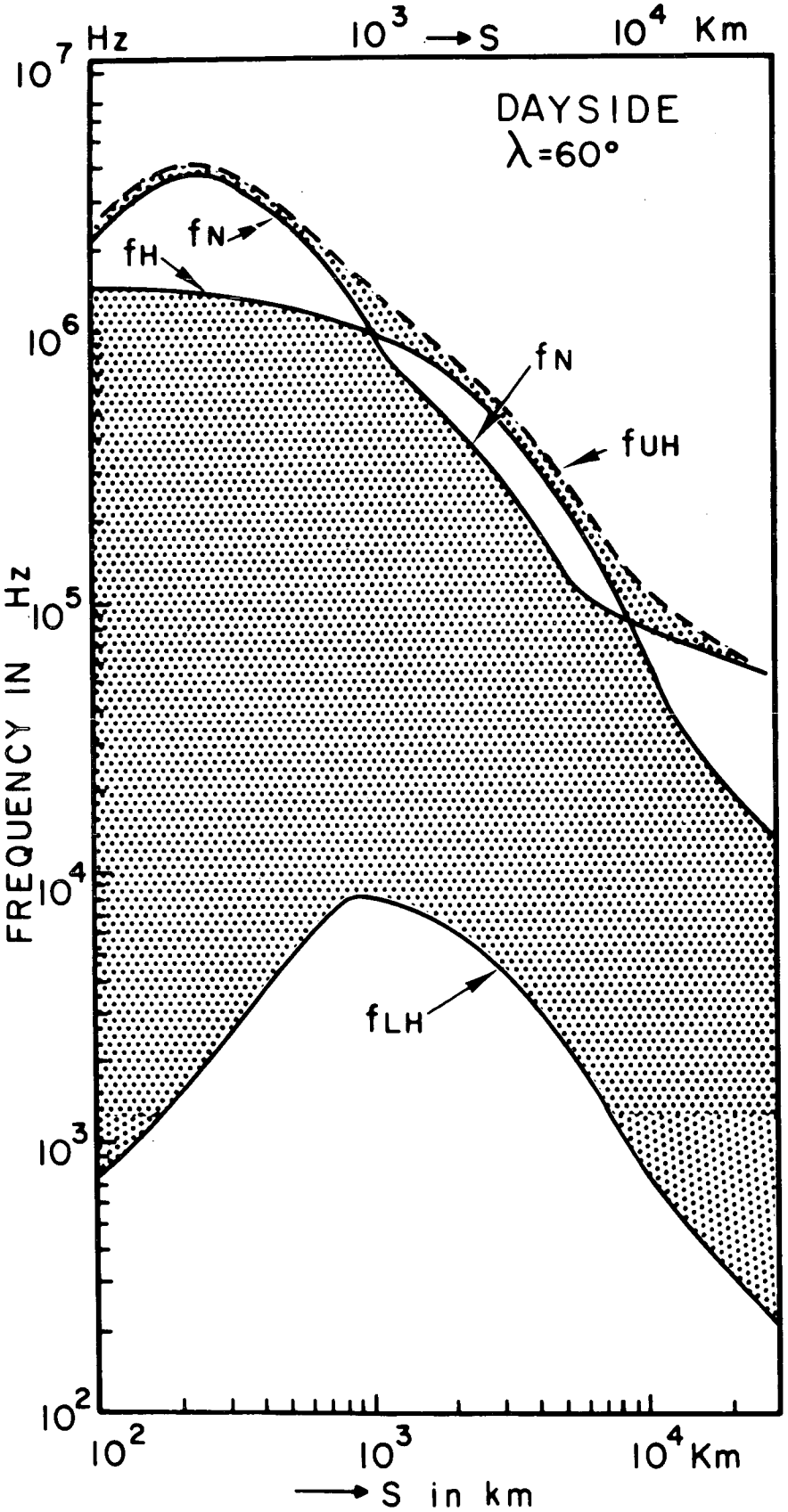
Hz
10^3 → S
10^4 Km
10^7
DAYSIDE
λ=60°
fN
fH
10^6
fN
fUH
10^5
FREQUENCY IN Hz
10^4
fLH
10^3
10^2
10^2
10^3
10^4 Km
→ S in km

Fig. 8(c)

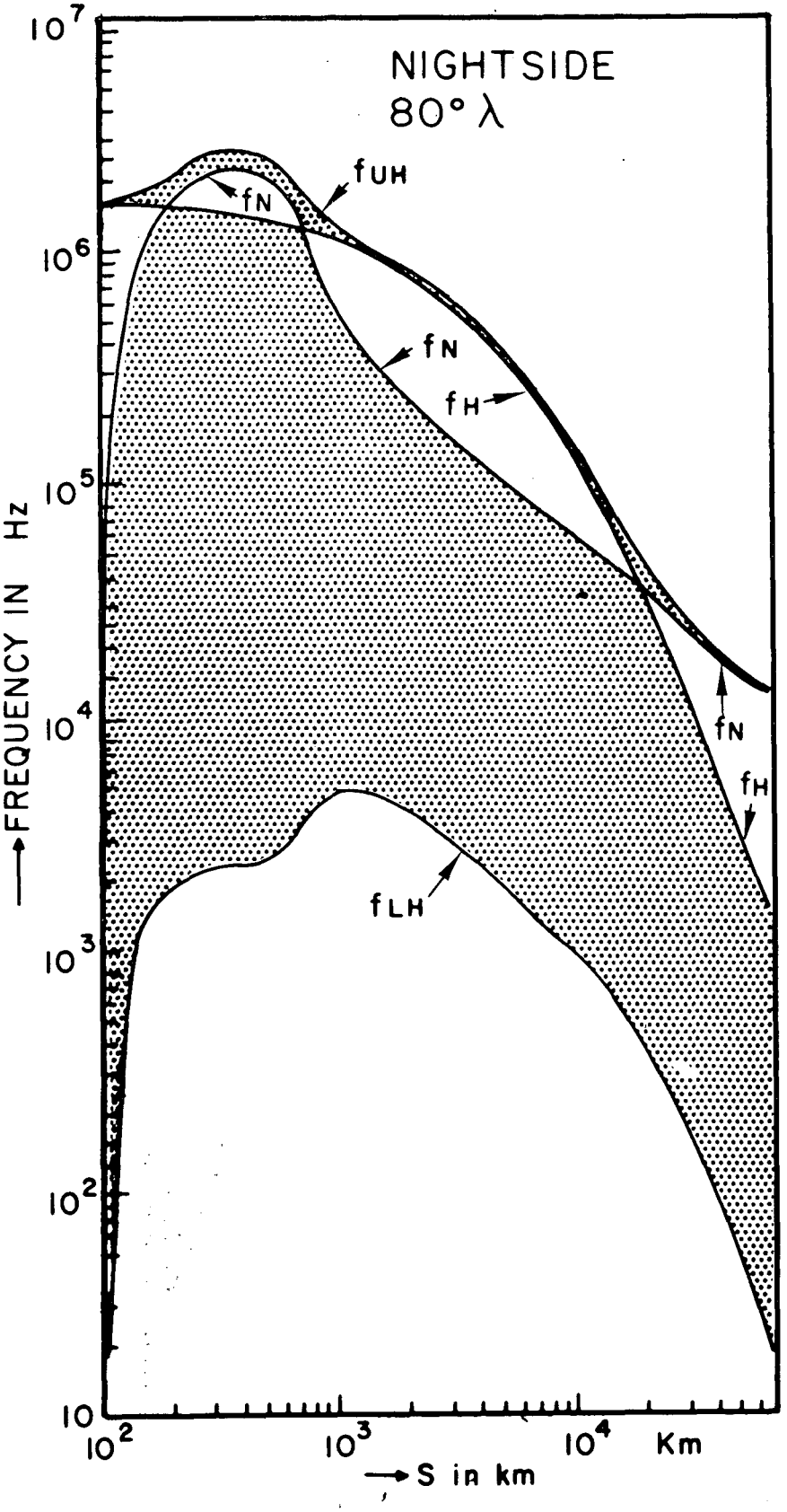
NIGHTSIDE
80° λ
fUH
fN
fN
fH
fN
fH
fLH
FREQUENCY IN Hz
10^7
10^6
10^5
10^4
10^3
10^2
10
10^2
10^3
10^4
Km
S in km

Fig. 9(a)

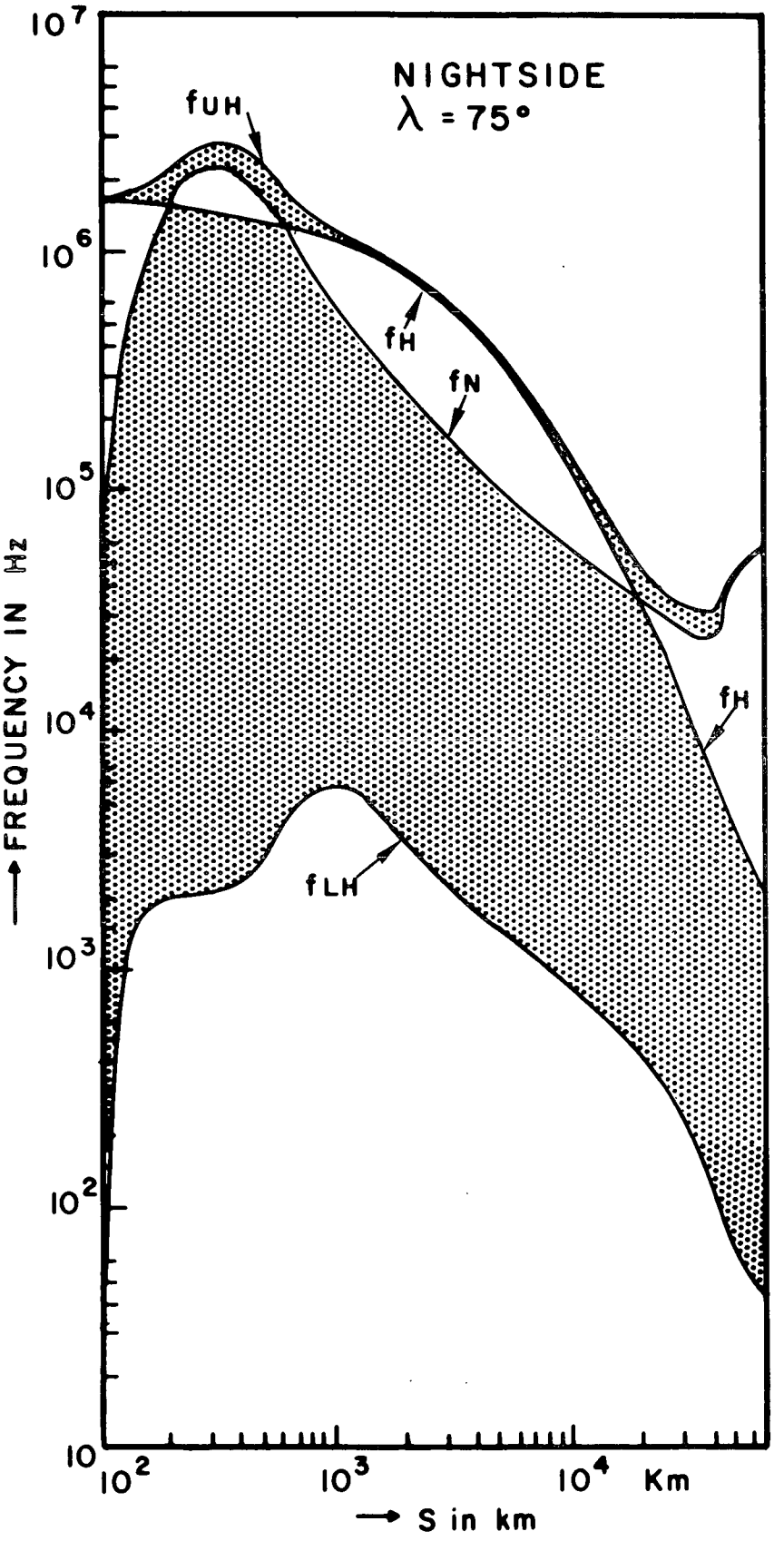
NIGHTSIDE
λ = 75°
fUH
fH
fN
fH
fLH
FREQUENCY IN Hz
10^7
10^6
10^5
10^4
10^3
10^2
10
10^2
10^3
10^4 Km
S in km

Fig. 9(b)

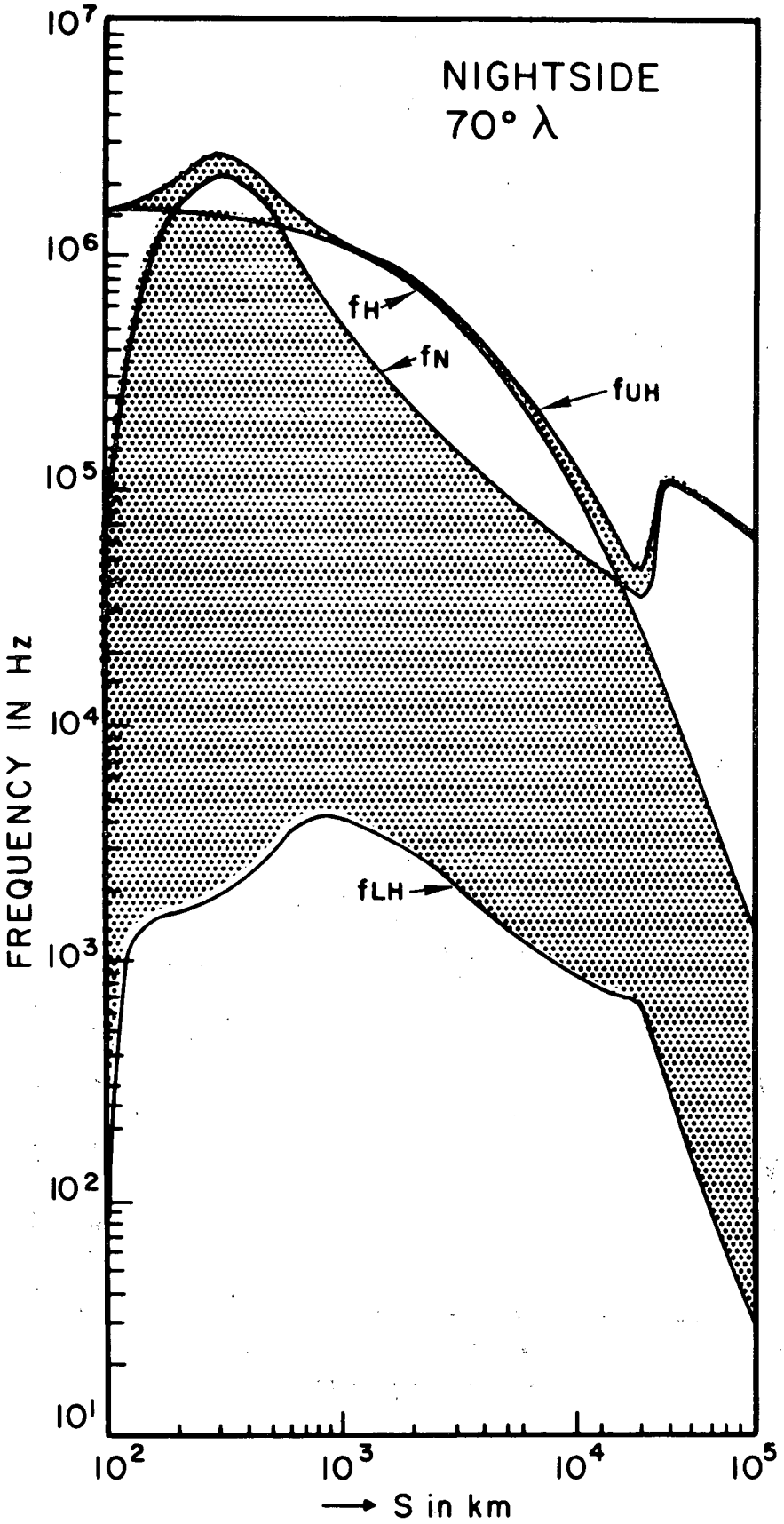
NIGHTSIDE
70° λ
fH
fN
fUH
fLH
FREQUENCY IN Hz
10^7
10^6
10^5
10^4
10^3
10^2
10^1
10^2
10^3
10^4
10^5
S in km

Fig. 9(c)

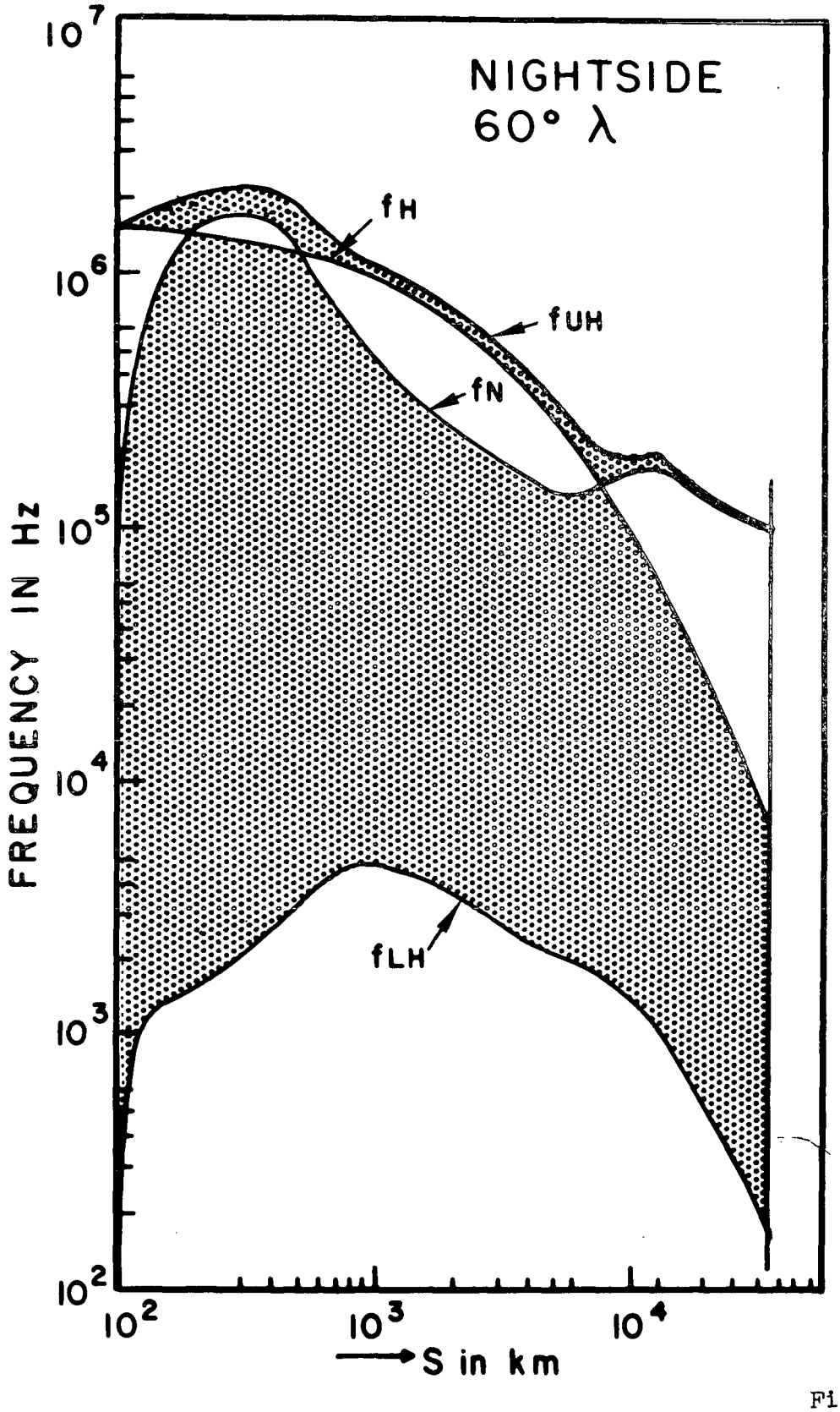
NIGHTSIDE
60° λ
fH
fUH
fN
fLH
FREQUENCY IN Hz
10^7
10^6
10^5
10^4
10^3
10^2
10^2
10^3
10^4
S in km

Fig. 9(d)

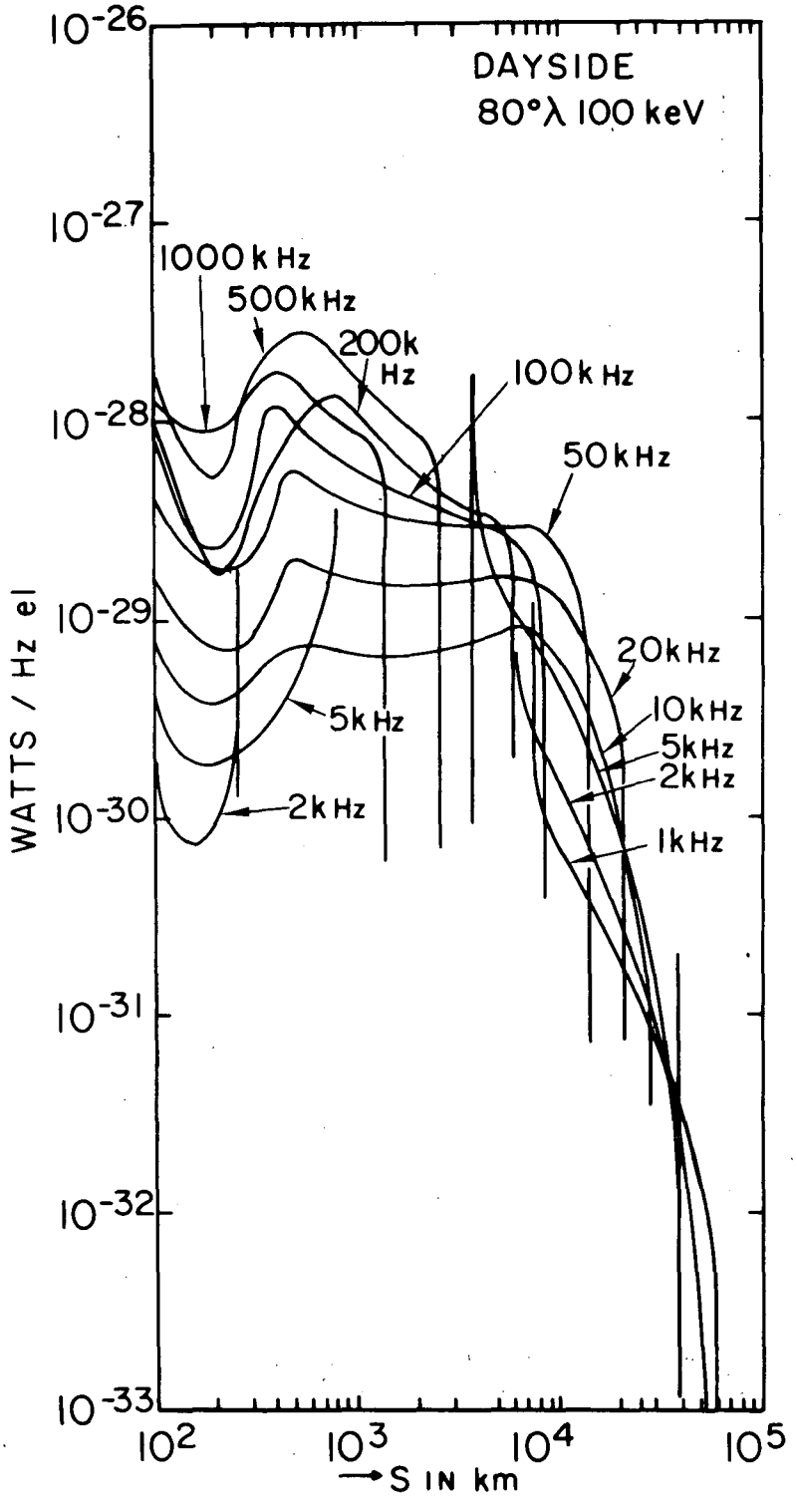
DAYSIDE
80°λ 100 keV
1000 k Hz
500k Hz
200k Hz
100k Hz
50k Hz
20k Hz
10k Hz
5k Hz
2k Hz
1k Hz
5k Hz
2k Hz
WATTS / Hz el
10-26
10-27
10-28
10-29
10-30
10-31
10-32
10-33
10^2
10^3
10^4
10^5
S IN km

Fig. 10(a)

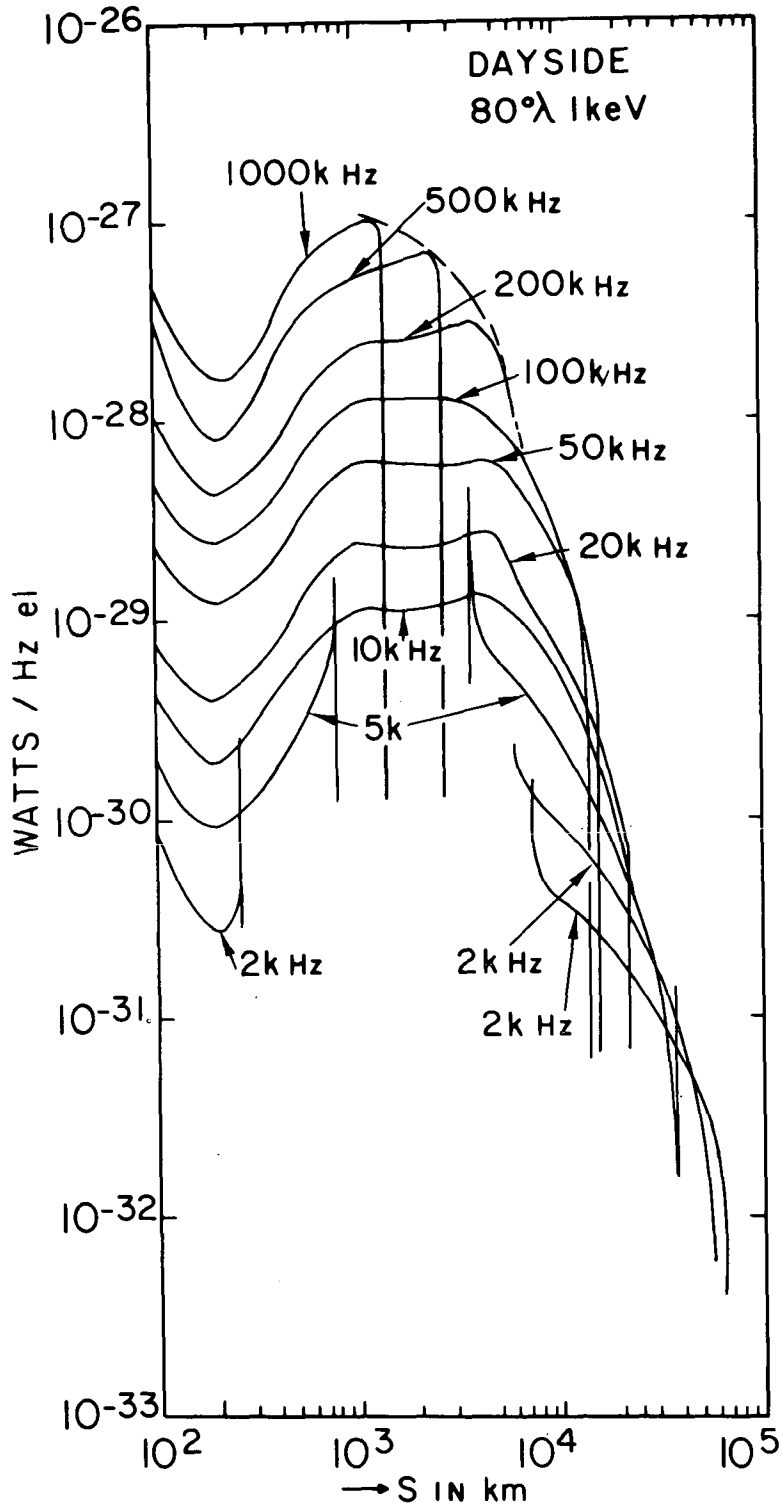
DAYSIDE
80°λ 1keV
1000k Hz
500k Hz
200k Hz
100k Hz
50k Hz
20k Hz
10k Hz
5k
2k Hz
2k Hz
2k Hz
WATTS / Hz el
10-26
10-27
10-28
10-29
10-30
10-31
10-32
10-33
10^2
10^3
10^4
10^5
S IN km

Fig. 10(b)

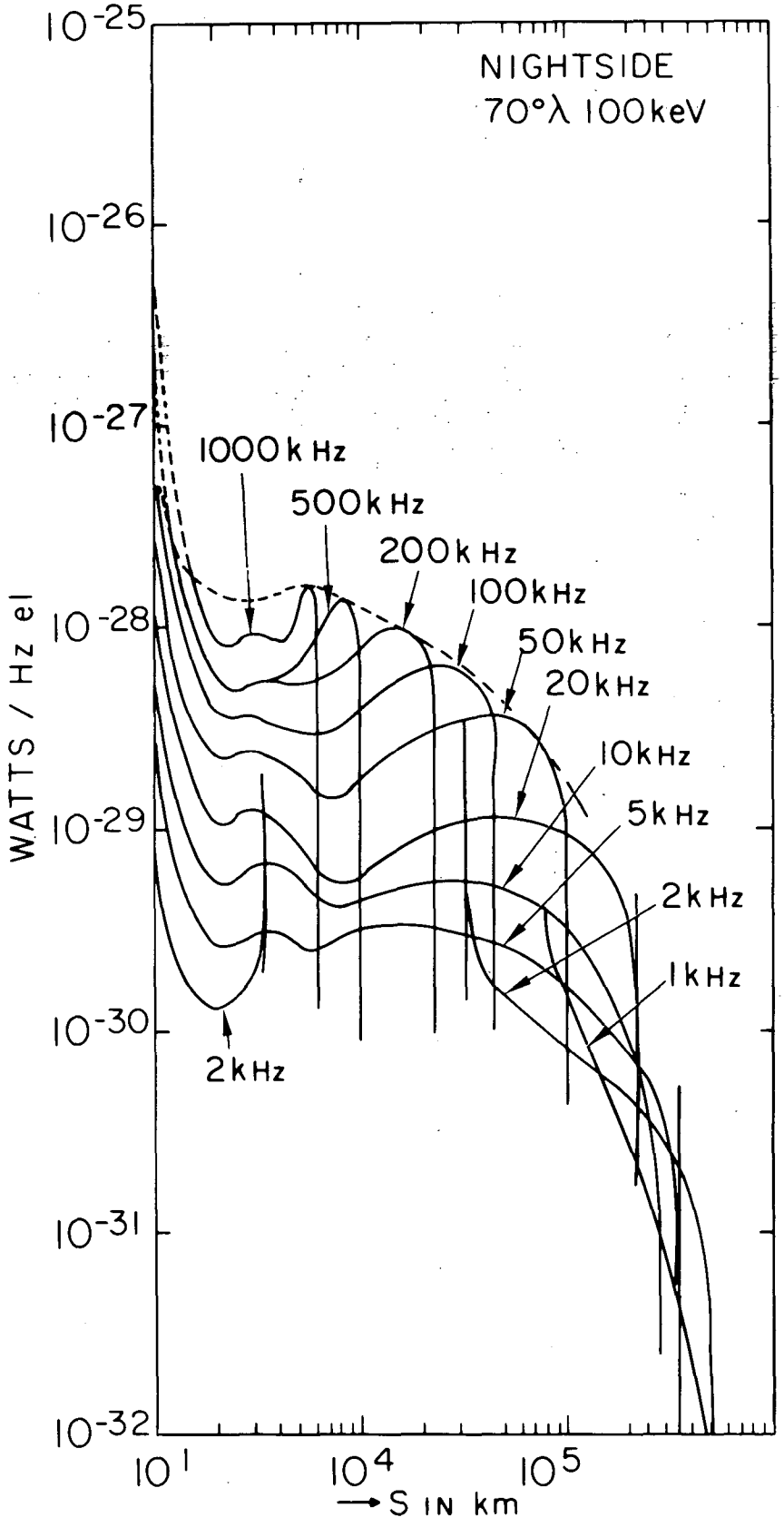
NIGHTSIDE
70°λ 100keV
WATTS / Hz el
10-25
10-26
10-27
10-28
10-29
10-30
10-31
10-32
1000kHz
500kHz
200kHz
100kHz
50kHz
20kHz
10kHz
5kHz
2kHz
1kHz
2kHz
10 1
10 4
10 5
→S IN km

Fig. 11(a)

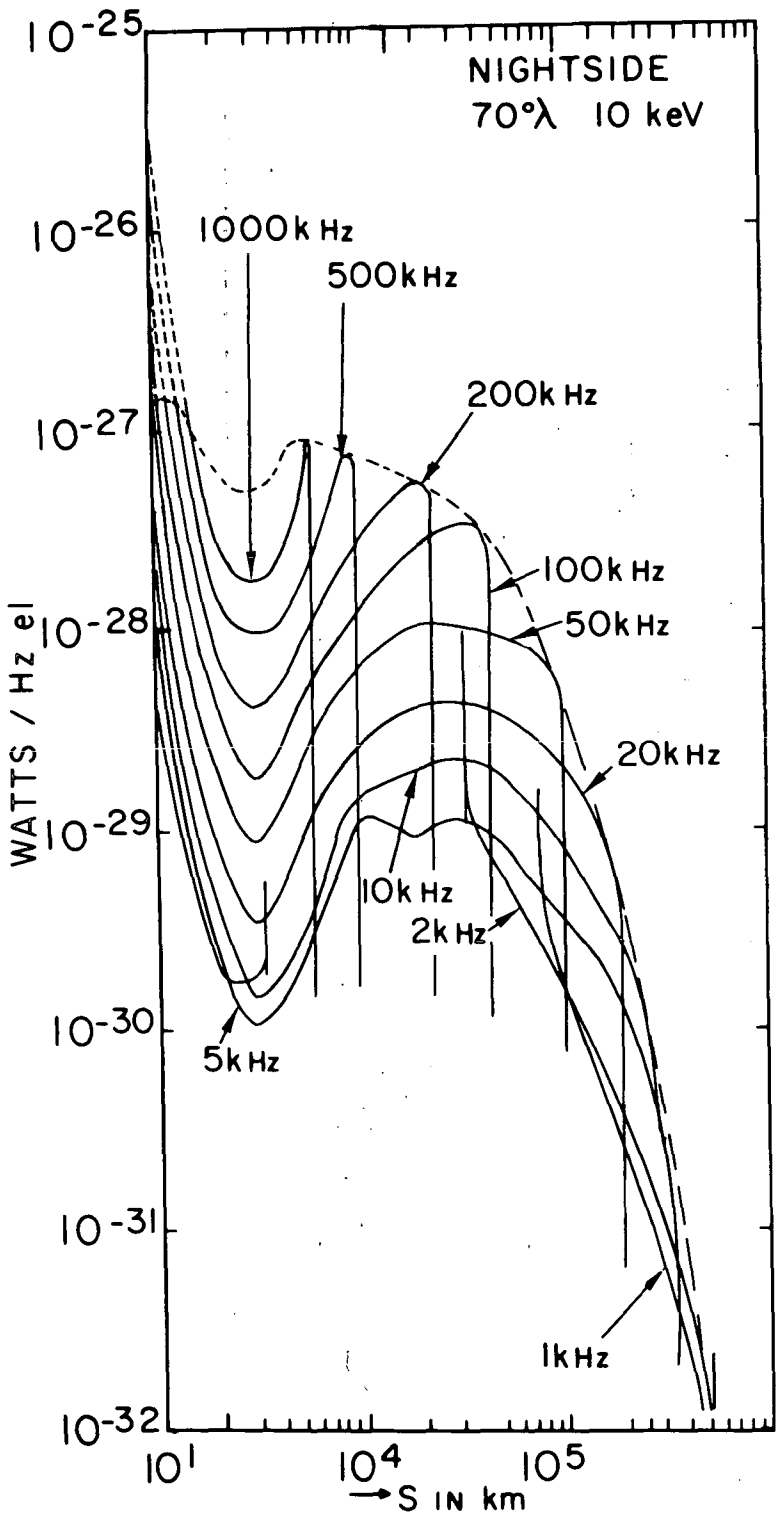
NIGHTSIDE
70°λ 10 keV
1000k Hz
500k Hz
200k Hz
100k Hz
50k Hz
20k Hz
10k Hz
2k Hz
5k Hz
1k Hz
WATTS / Hz el
10-25
10-26
10-27
10-28
10-29
10-30
10-31
10-32
10¹
10⁴
10⁵
S IN km

Fig. 11(b)

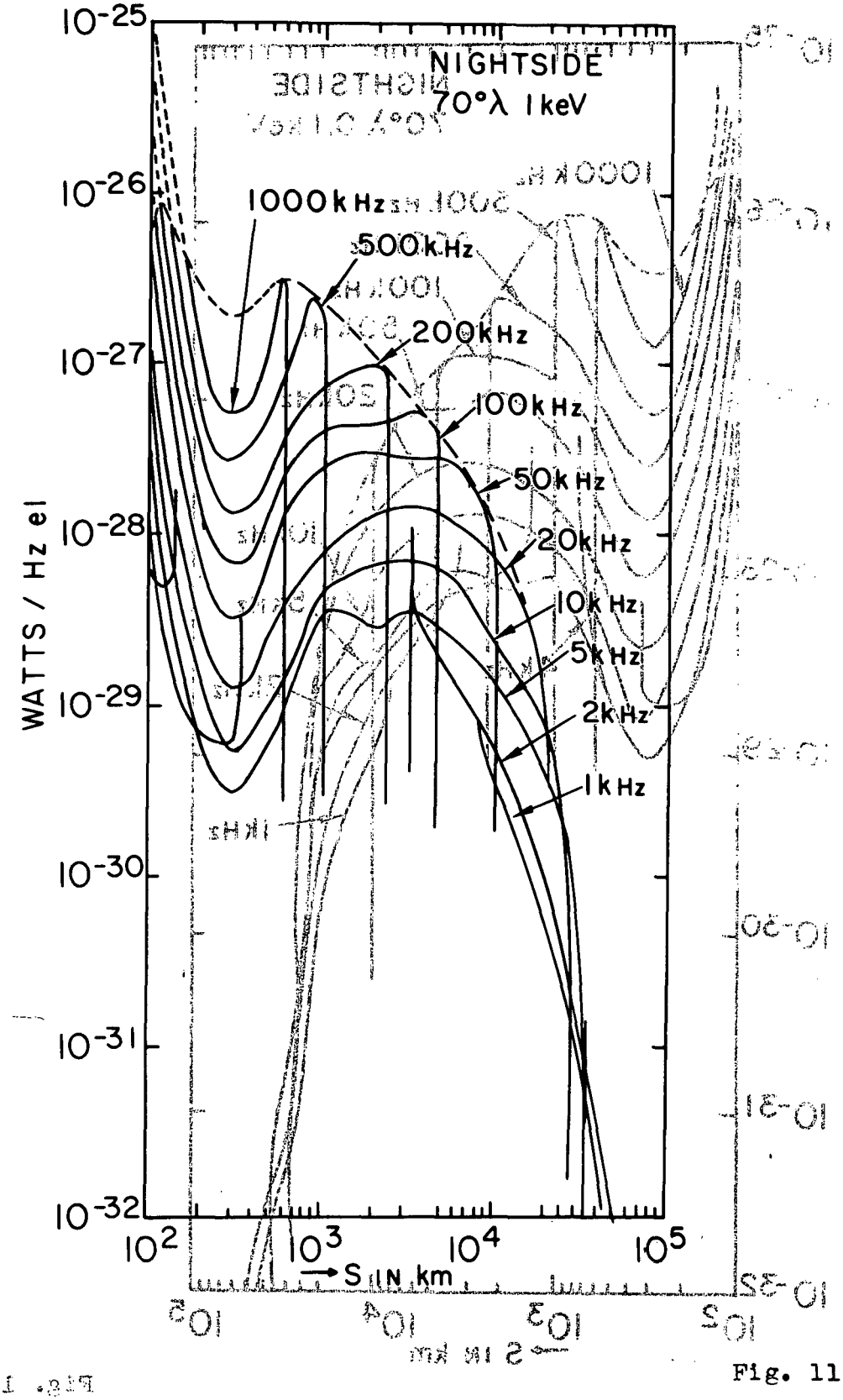
NIGHTSIDE
70°λ 1keV
1000kHz
500kHz
200kHz
100kHz
50kHz
20kHz
10kHz
5kHz
2kHz
1kHz
WATTS / Hz el
10-25
10-26
10-27
10-28
10-29
10-30
10-31
10-32
10²
10³
10⁴
10⁵
S in km

Fig. 11(c)

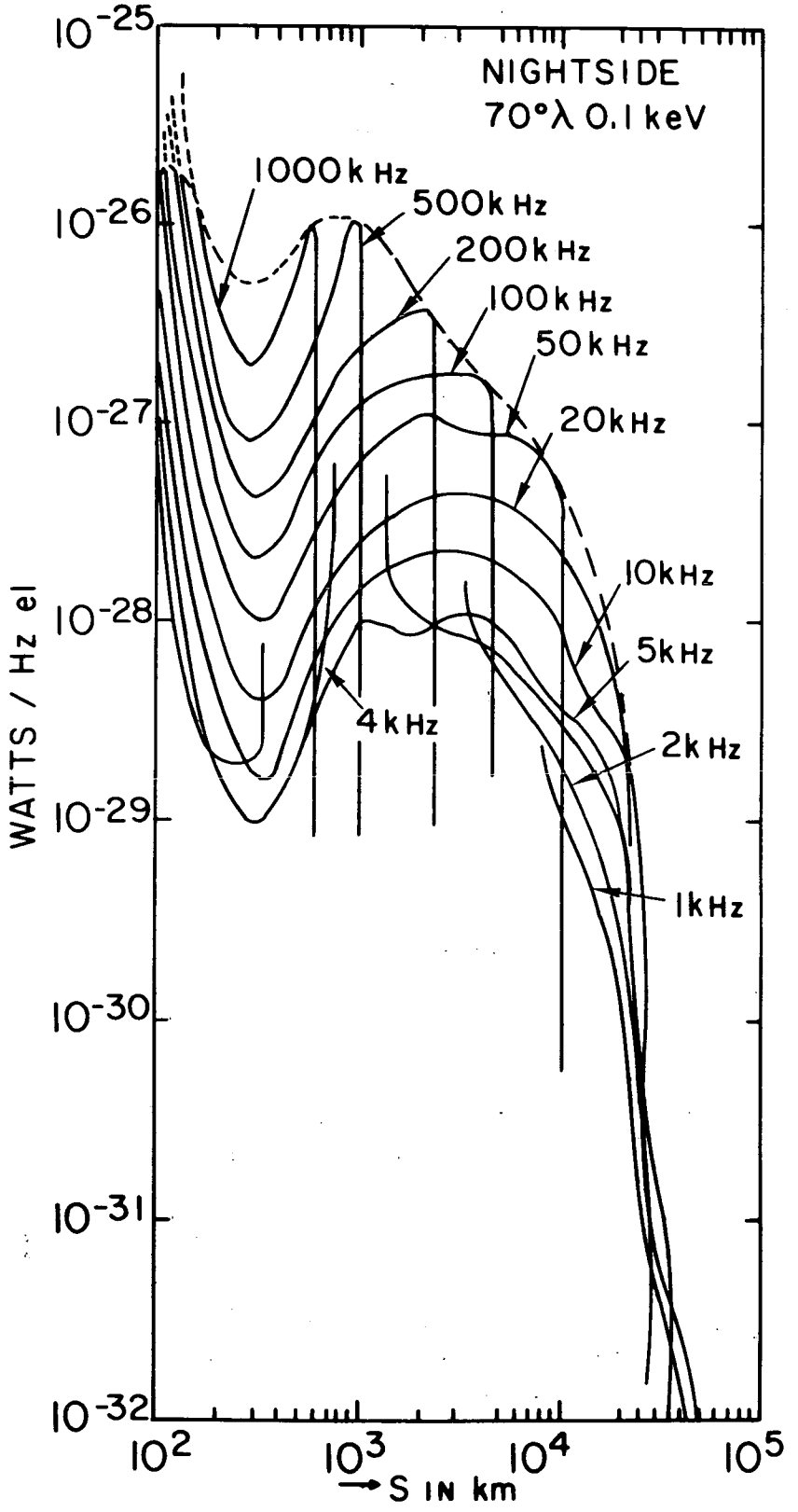
NIGHTSIDE
70°λ 0.1 keV
1000 k Hz
500k Hz
200k Hz
100k Hz
50k Hz
20k Hz
10k Hz
5k Hz
2k Hz
1k Hz
4k Hz
WATTS / Hz el
10-25
10-26
10-27
10-28
10-29
10-30
10-31
10-32
10²
10³
10⁴
10⁵
S IN km

Fig. 11(d)

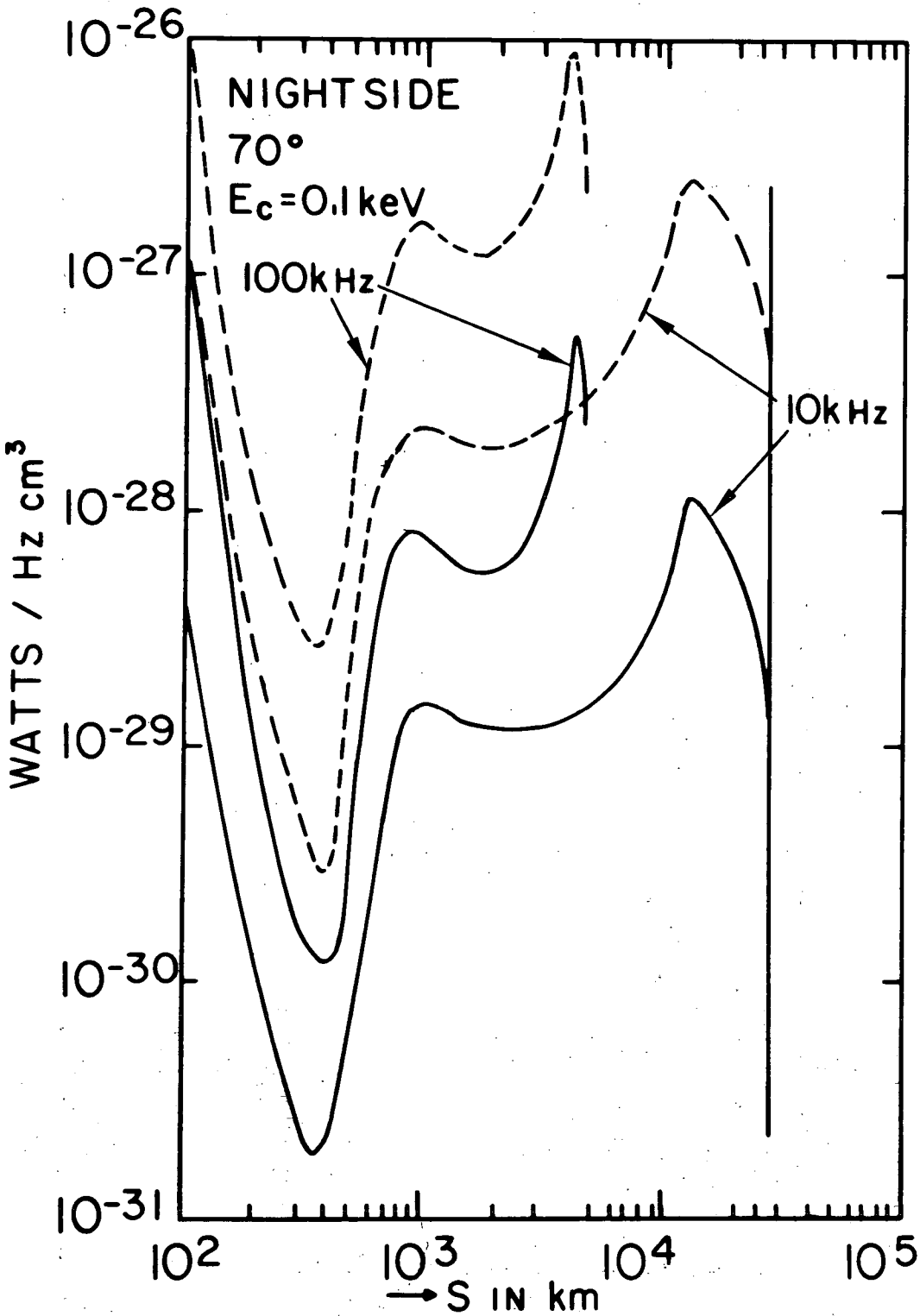
NIGHT SIDE
70°
E_c = 0.1 keV
100k Hz
10k Hz
WATTS / Hz cm^3
10^{-26}
10^{-27}
10^{-28}
10^{-29}
10^{-30}
10^{-31}
10^2
10^3
10^4
10^5
S IN km

Fig. 12(a)

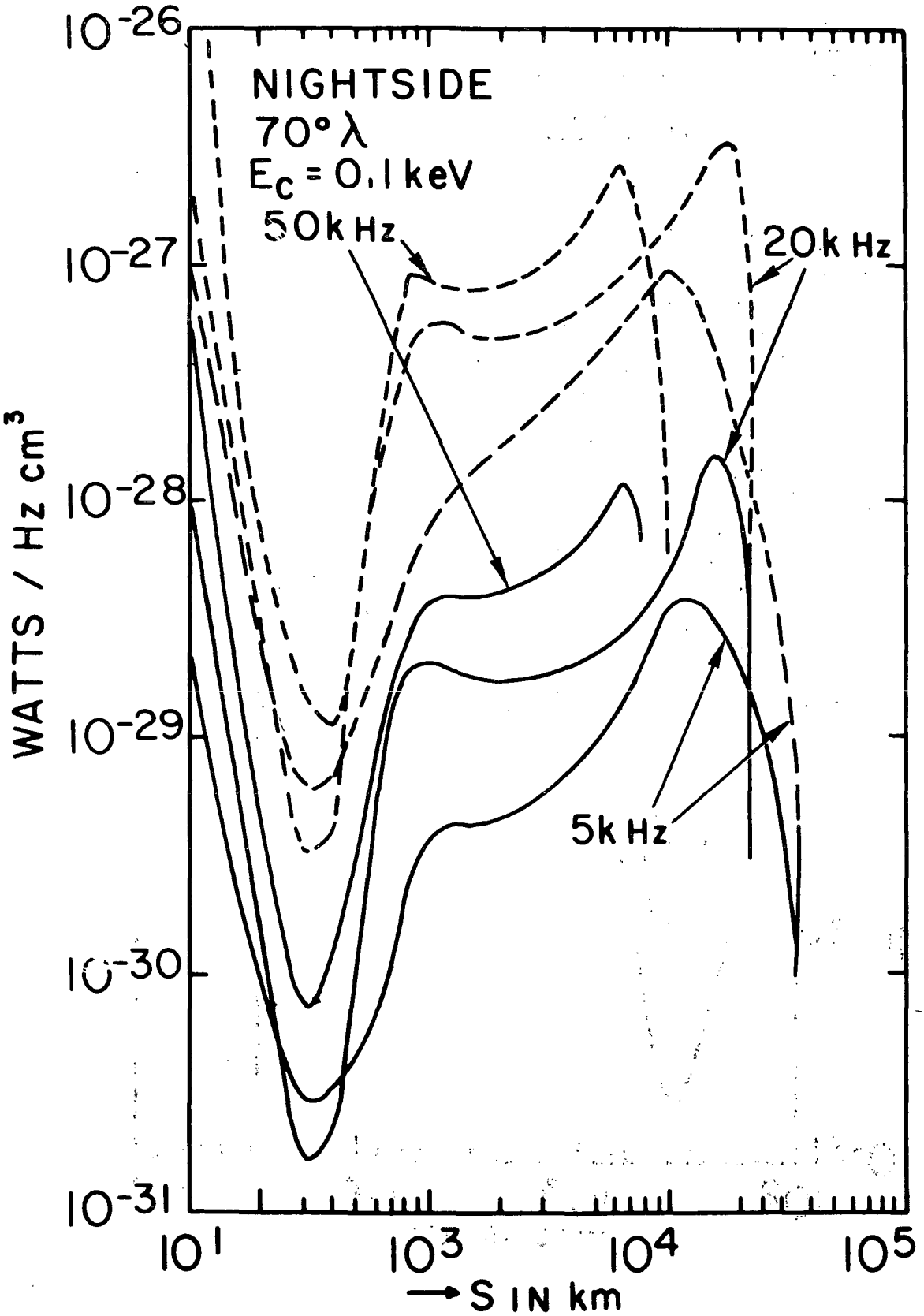
NIGHTSIDE
70° λ
E_c = 0.1 keV
50k Hz
20k Hz
5k Hz
WATTS / Hz cm^3
10^{-26}
10^{-27}
10^{-28}
10^{-29}
10^{-30}
10^{-31}
10^1
10^3
10^4
10^5
→ S IN km

Fig. 12(b)

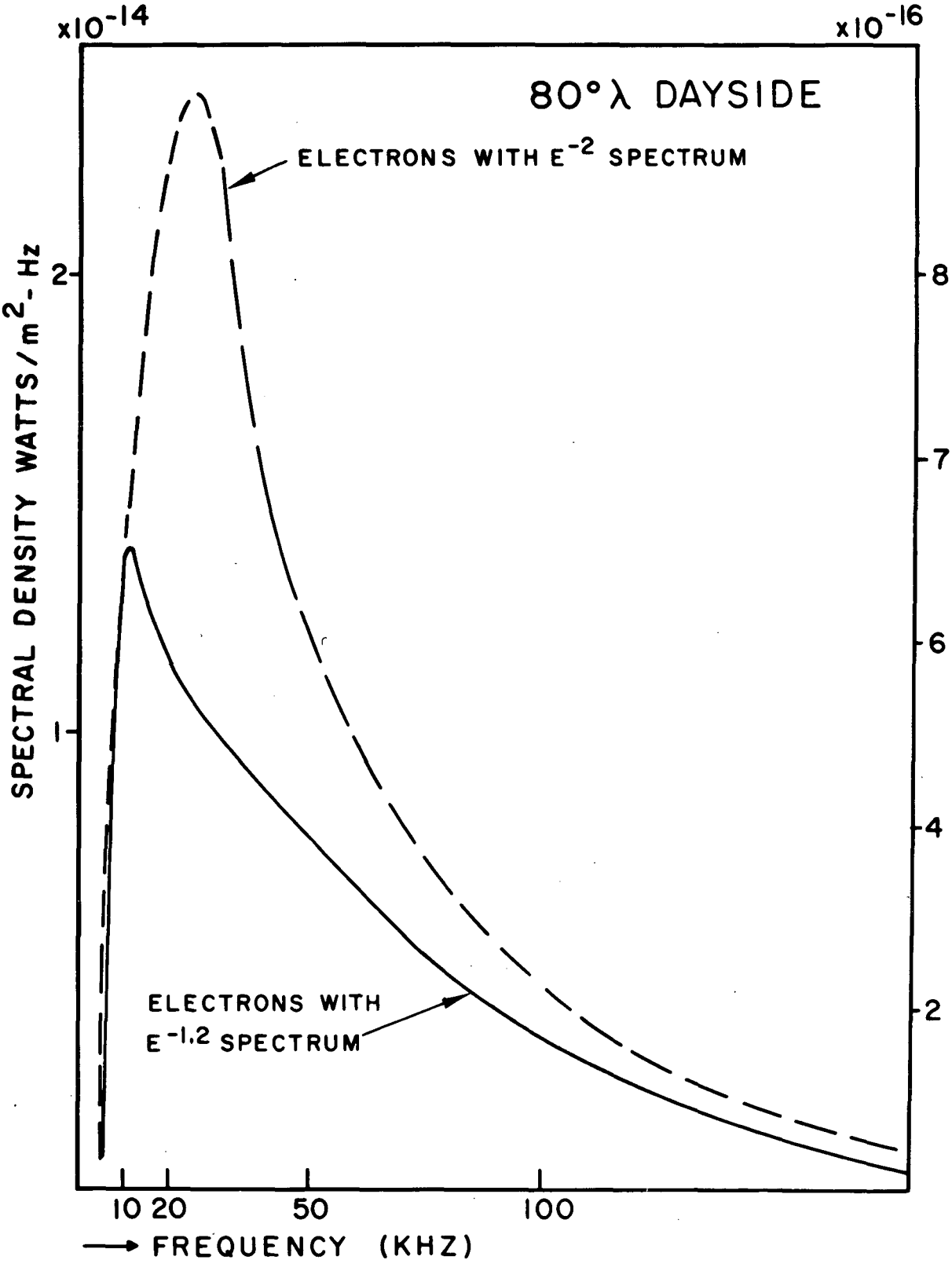
x10-14
x10-16
80° λ DAYSIDE
ELECTRONS WITH E-2 SPECTRUM
SPECTRAL DENSITY WATTS/m2-Hz
2
1
8
7
6
4
2
ELECTRONS WITH
E-1.2 SPECTRUM
10 20
50
100
FREQUENCY (KHZ)

Fig. 13(a)

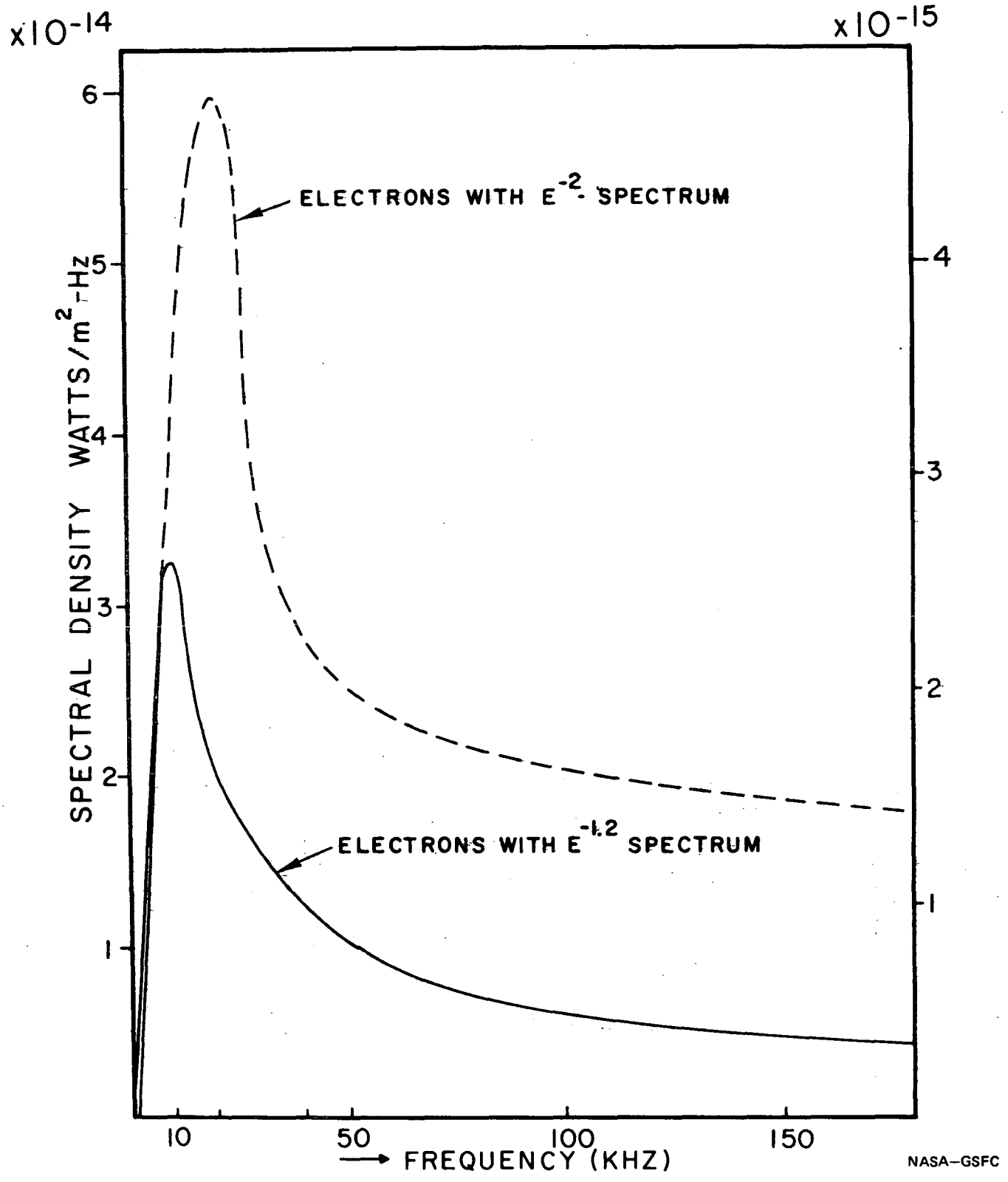
x10-14
x10-15
6
5
4
3
2
1
4
3
2
1
SPECTRAL DENSITY WATTS/m2-Hz
ELECTRONS WITH E-2 SPECTRUM
ELECTRONS WITH E-1.2 SPECTRUM
10
50
100
150
FREQUENCY (KHZ)
NASA-GSFC

Fig. 13(b)